The role of thioredoxin in the redox regulation of the Tpx1/Pap1 pathway in *Schizosaccharomyces pombe*

By

Kelisa C. Naidoo

BSc. (*Hons*) Genetics

Submitted in fulfilment of the academic requirements for the degree of Master of Science in the Discipline of Genetics, School of Life Sciences, College of Agriculture, Engineering and Science, University of KwaZulu-Natal, Pietermaritzburg, South Africa

As the candidate's supervisor I, have approved this dissertation for submission

Supervisor: Dr C. S. Pillay

Signature: [redacted]

Date: 2022/03/17

Preface

The research contained in this dissertation was completed by the candidate from Januray 2019 to December 2021 while based in the discipline of Genetics, School of Life Sciences of the College of Agriculture, Engineering and Science, University of KwaZulu-Natal, Pietermaritzburg, South Africa under the supervision of Dr C. S. Pillay.

These studies represent original work by the candidate and have not otherwise been submitted in any form to another University. Where use has been made of the work by other authors it has been duly acknowledged in the text.

Supervisor: Dr C. S. Pillay

Signature: [redacted]

Date: 2022/03/17

College of Agriculture, Engineering, and Science

Declaration of Plagiarism

I, Kelisa C. Naidoo, declare that:

(i) the research reported in this dissertation, except where otherwise indicated or acknowledged, is my original work;

(ii) this dissertation has not been submitted in full or in part for any degree or examination to any other university;

(iii) this dissertation does not contain other persons' data, pictures, graphs or other information, unless specifically acknowledged as being sourced from other persons;

(iv) this dissertation does not contain other persons' writing, unless specifically acknowledged as being sourced from other researchers. Where other written sources have been quoted, then:

(a) their words have been re-written but the general information attributed to them has been referenced;

(b) where their exact words have been used, their writing has been placed inside quotation marks, and referenced;

(c) where I have used material for which publications followed, I have indicated in detail my role in the work;

(v) this dissertation is primarily a collection of material, prepared by myself, published as journal articles or presented as a poster and oral presentations at conferences. In some cases, additional material has been included;

(vi) this dissertation does not contain text, graphics or tables copied and pasted from the Internet, unless specifically acknowledged, and the source being detailed in the dissertation and in the References sections.

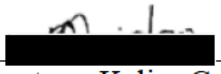

Signature: Kelisa C. Naidoo

Date: _13/12/2021_____

Declaration Plagiarism 22/05/08 FHDR Approved

Abstract

Reactive oxygen species (ROS) can damage cellular components leading to dysfunction and cell death. Paradoxically, ROS, such as hydrogen peroxide, are also essential for a range of metabolic and signalling functions within cells. Given these opposing functions, cells have developed several redox signalling mechanisms to manage ROS within specific homeostatic limits. In bacterial cells, thiol-peroxidases (peroxiredoxins) and other enzymes detoxify ROS, while the antioxidant transcriptional response is induced by transcription factors directly oxidized by ROS. In many eukaryotes, these functions are combined with peroxiredoxins detoxifying ROS as well as activating redox-sensitive transcription factors. The relative benefits and disadvantages of such sensor-mediated redox signalling systems are unknown, and we aimed to understand the logic underlying this signalling mechanism using the *Schizosaccharomyces pombe* Tpx1/Pap1 pathway. In this pathway, the peroxiredoxin Tpx1 reduces hydrogen peroxide and oxidizes the redox transcription factor Pap1. Following a hydrogen peroxide perturbation, the Pap1 signal profile revealed a biphasic profile with a rapid initial increase followed by a relatively prolonged decrease in Pap1 oxidation. These dynamics were suggestive of an incoherent feedforward loop, and we hypothesized that the Trx1 protein was responsible for the incoherence as it could both dampen and increase the signal by reducing Pap1 and Tpx1, respectively. To test this hypothesis, we analyzed the effect of several oxidants (hydrogen peroxide, tert-butyl hydroperoxide, and diamide) on Pap1 activation to determine if we could selectively modulate signal duration. However, we could not quantitatively delineate the effects of these oxidants on the signal profiles obtained. We, therefore, utilized computational modelling to analyze the Tpx1/Pap1 pathway and found that excess Trx1 reduced Tpx1 faster, preventing the association of Tpx1 and Pap1. On the other hand, insufficient Trx1 allowed for Pap1 to be oxidized over a longer interval which increased the signal duration. Thus, our analysis showed that, in contrast to our hypothesis, Trx1 limitation, rather than incoherence, was responsible for the Pap1 oxidation profile. These results indicate that in the presence of ROS, Trx1 plays a vital role in determining the signal profile of Pap1.

Acknowledgements

Firstly, to my supervisor, Dr Ché Pillay, thank you for your guidance, patience and understanding over the past few years. Thank you for allowing me to be a part of your lab and constantly challenging me, which has made me a better scientist.

To the National Research Foundation (NRF), thank you for the bursary which allowed me to pursue my MSc degree.

Thank you to Diane and Nolyn for welcoming me into Lab B23 and always helping me with any science-related questions over the years. To Diane, Nolyn, Tejal and Limpho, thank you for all the laughs and engaging conversations. A special thank you to Diane and Tejal for allowing me to use your research in my dissertation, which allowed me to formulate my hypothesis (Chapter 1) and support my computational modelling results about Trx1 (Chapter 3), respectively.

To my parents, Julie and Wallace, thank you for your unwavering support through this degree and for always believing in me. I would not be the person I am today without you, so thank you for everything. To my brothers, Eldon and Kimen, thank you for being the best older brothers a girl could ask for. Another special thank you to Eldon for our late-night chats, your constant motivation, and your most-appreciated help for as long as I can remember. Thank you for constantly reminding me that I am capable of so much more and always pushing me to strive for excellence. I love you all, and I'm so grateful you are my family!

To Keziah, thank you for being the perfect definition of a best friend. I sincerely appreciate your encouragement and support through every journey of mine so far. Thank you for all our jokes, fun moments and especially for our rants. You're the sister I never had and didn't know I needed. I love you forever.

Last but not least, Nav. Thank you for your support and for always believing in me even when I didn't believe in myself. Thank you for taking the time to understand all my science-related talk so you could weigh in while I celebrated the little victories or complained. Thank you for always making me happy, dealing with my moods, taking me on adventures and most importantly, treating me like I can conquer the world with just a click of my fingers. For all those reasons and so much more, you're my favourite human Nav.

List of Abbreviations

AhpC	Alkyl hydroperoxide reductase C
ALS	Amyotrophic lateral sclerosis
AP-1	Activating protein -1
APS	Ammonium persulfate
ATP	Adenosine triphosphate
a.u	Absorbance units
BCA	Bicinchoninic acid
BSA	Bovine serum albumin
CRP	cAMP receptor protein
Ctt	Catalase
Cys	Cysteine
DNA	Deoxyribonucleic acid
DNTP	5, 5'-dithiobis (2-nitrobenzoic acid)
DTT	Dithiothreitol
ECL	Enhanced Chemiluminescence
EDTA	Ethylenediaminetetraacetic acid
EMM	Edinburgh Minimal Medium
ERO1	Endoplasmic reticulum oxidoreductase 1
ETC	Electron transport chain
GPx	Glutathione peroxidases
GR	Glutathione reductase
Grx1	Glutaredoxin 1
GSSG	Glutathione disulfide
GSH	Glutathione
H_2O_2	Hydrogen peroxide
HCl	Hydrochloric acid
HNO_2	Nitrous acid
HOCl	Hypochlorous acid

HSF1	Heat shock transcription factor
IAA	Iodoacetic acid
IgG	Immunoglobulin G
KatG	Hydroperoxidase I
KatE	Hydroperoxidase II
LysR	Family of transcriptional regulators
$MgCl_2$	Magnesium chloride
NaCl	Sodium chloride
NADPH	ß-nicotinamide adenine dinucleotide phosphate
NADH	Nicotinamide adenine dinucleotide
NaOH	Sodium hydroxide
NES	Nuclear export signal
NF-κB	Nuclear factor kappa B
NO	Nitric oxide
NOX	NADPH oxidase
NRF2	Nuclear factor erythroid 2-related factor 2
NTC	No template control
O_2^-	Superoxide
OD	Optical density
ODE	Ordinary differential equation
·OH	Hydroxyl radical
OxyR	Hydrogen peroxide-inducible genes activator
PCR	Polymerase chain reaction
PDI	Protein disulfide isomerase
Prx	Peroxiredoxin
PySCeS	Python Simulator of Cellular Systems
ROS	Reactive oxygen species
SDS	Sodium dodecyl sulfate
SDS-PAGE	Sodium dodecyl sulfate-polyacrylamide gel electrophoresis
SOD	Superoxide dismutase
Srx1	Sulfiredoxin

Sty1	Mitogen-activated protein kinase sty1
TAE	Tris-base, acetic acid and EDTA
tBOOH	Tert-butyl hydroperoxide
TBST	Tris Buffered Saline with Tween
TCA	Trichloroacetic acid
TE	Tris-EDTA buffer solution
TEMED	N,N,N', N'-tetramethylethylenediamine
Tpx1	Thioredoxin peroxidase
Trr1	Thioredoxin reductase
Trx1/2	Thioredoxin
Tsa1	Thiol-specific antioxidant
Txl1	Thioredoxin-like protein
Ura4	orotidine 5'-phosphate decaroxylase
UV	Ultraviolet radiation
Yap1	Yeast activating protein 1
Ybp1	Yeast binding protein 1
YE5S	Yeast extract supplemented with 5 amino acids

Contents

List of Tables

List of Figures

Chapter 1: Literature review

1.1. Introduction

Reactive oxygen species (ROS) are a range of chemically reactive oxygen-containing molecules consisting of unpaired valence electrons (free radicals). They were first discovered by Henry Fenton (1894), who exposed biomolecules to a combination of hydrogen peroxide (H_2O_2) and ferrous iron, subsequently resulting in their oxidation (Fenton, 1894). Although Fenton and later Gomberg (1900) proved the existence of ROS, these experiments gave no indication that ROS also existed within organisms. However, the discovery of free radicals within the skeletal muscle by Commoner and colleagues (Commoner *et al.*, 1954) was the first evidence of ROS within biological organisms. Shortly after this, Harman proposed the "free radical theory of ageing", which suggested free radicals exuded no positive roles and were responsible for biological damage, disease, and ageing (Harman, 1956). Ultimately, the discovery of superoxide dismutase (SOD), an enzyme responsible for breaking down superoxide into either oxygen or hydrogen peroxide, by McCord and Fridovich, led to the acceptance of ROS as essential aspects in biological systems (Mccord and Fridovich, 1969). Following the discovery of the SOD enzyme, the study of how ROS and oxidative stress negatively affect organisms became significant (Roy *et al.*, 2017).

ROS have different effects on a cell, the most well-known being the irreversible damage to nucleic acids, carbohydrates, lipids, and proteins (Brieger *et al.*, 2012; Roy *et al.*, 2017). The damage they cause to these biomolecules can contribute to the pathogenesis and progression of multiple diseases (Figure 1.1) (Zuo *et al.*, 2015). For example, increased ROS causes an imbalance between relaxing and contracting factors responsible for vascular tone, thereby contributing to hypertension (Chen *et al.*, 2018a). Besides hypertension, ROS have been implicated in a range of cardiovascular diseases, including atherosclerosis, restenosis, and ischemia (Brieger *et al.*, 2012; Panth *et al.*, 2016; Chen *et al.*, 2018a). In addition, increased ROS in the brain can account for neuronal damage associated with multiple neurological diseases, such as schizophrenia, amyotrophic lateral sclerosis (ALS), Alzheimer's, and Parkinson's disease (Brieger *et al.*, 2012; Kausar *et al.*, 2018). An increase in ROS has also been linked to aging and a multitude of other

diseases that include but are not limited to pulmonary, inflammatory, autoimmune, and fibrotic diseases and cancers (Brieger *et al.*, 2012).

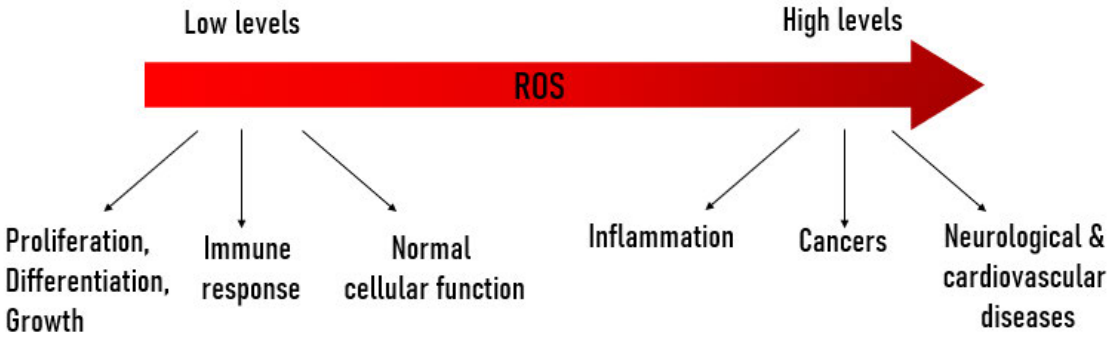

Figure 1.1: The paradoxical implications of reactive oxygen species. Low levels of ROS allow for maintenance of life compared to high levels of ROS that can result in damage and disease. This figure was developed from Roy *et al.*, 2017.

Although ROS were initially implicated in only negative roles, later evidence showed they played pivotal roles in homeostasis and maintained life (Figure 1.1). Lower ROS levels are required for normal cellular processes such as migration, differentiation, proliferation, growth, and antioxidant gene expression (Brieger *et al.*, 2012; Veal *et al.*, 2014). For example, ROS are important in long-term potentiation within the hippocampus of the brain as it strengthens synaptic plasticity, which helps learning and memory functions (Massaad and Klann, 2011; Beckhauser *et al.*, 2016). ROS also play a significate role in numerous aspects of immune system function (Sies and Jones, 2020). An example is the proliferation of naïve T-cells, and differentiation of multiple other T-cells is accomplished by ROS involvement (Yarosz and Chang, 2018). Besides the nervous and immune systems, ROS also plays multiple positive roles in skeletal muscles, the cardiovascular system, and metabolic regulation such as allowing for skeletal muscle regeneration, the production of new capillaries, and metabolic adaptation to the ever-changing cellular environment, respectively (Sies and Jones, 2020). The literature discussed above shows that ROS play positive roles at low levels and negative roles at high levels. Therefore, ROS have a dose-dependent function and a complex role within living organisms.

1.2. The generation of ROS

ROS can be divided into two subgroups, namely non-radicals and free radicals. Non-radicals like hydrogen peroxide, nitrous acid (HNO_2), and hypochlorous acid (HOCl) contain paired

electrons in their outer orbital but still have the ability to oxidize biological material (Phaniendra *et al.*, 2015; Sies and Jones, 2020). Free radicals are those which have unpaired electrons and include superoxide (O_2^-), hydroxyl radical ($^{\cdot}OH$), and nitric oxide (NO), amongst others (Phaniendra *et al.*, 2015; Sies and Jones, 2020).

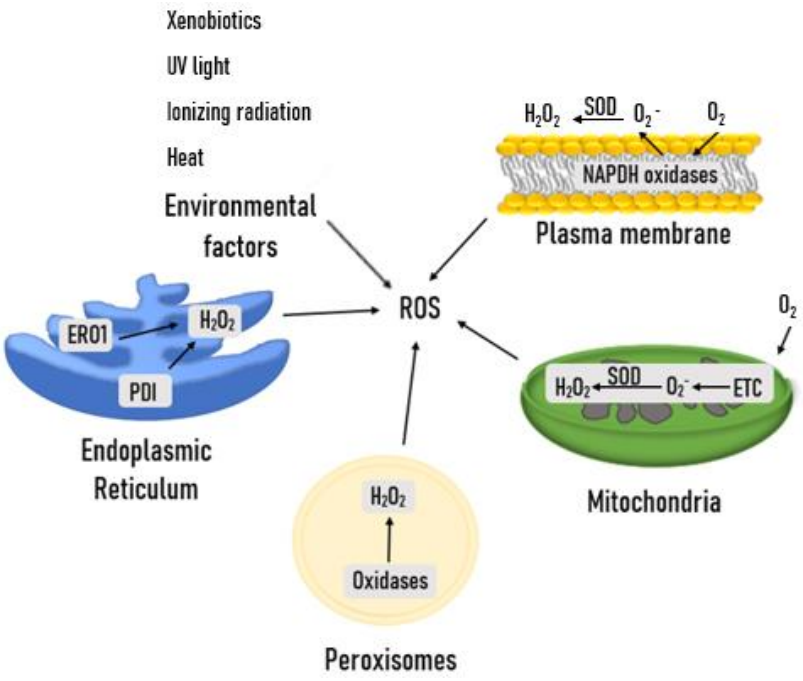

Figure 1.2: ROS arise from different endogenous and exogenous sources. Multiple normal cellular activities throughout the cell and exposure to environmental factors are responsible for ROS production. This figure was developed from literature sources (Cao and Kaufman, 2014; Forrester *et al.*, 2018; Sies and Jones, 2020). (ERO1, endoplasmic reticulum oxidoreductin 1; ETC, electron transport chain; H2O2, hydrogen peroxide; NADPH, Nicotinamide adenine dinucleotide phosphate; O2-, superoxide; O2, oxygen; PDI, protein disulfide isomerase, SOD, superoxide dismutase; UV light, ultraviolet light).

ROS can be produced via multiple endogenous or exogenous sources (Figure 1.2). The most common endogenous producer of ROS is the mitochondrial electron transport chain (ETC) during oxidative phosphorylation required for ATP production. The reactions taking place at complexes I, II, and III produce mainly superoxide, which is quickly dismutated to hydrogen peroxide by superoxide dismutase (Forrester *et al.*, 2018; Mailloux, 2020). Pyruvate dehydrogenase and α-ketoglutarate dehydrogenase in the mitochondria also produce ROS during their reactions in the Krebs cycle via forward and reverse electron transfer (Forrester *et al.*, 2018; Mailloux, 2020). Forward electron transfer occurs when electrons are transferred from coenzymes to a substrate, therefore oxidizing the coenzyme (NADH to NAD^+) (Onukwufor *et al.*, 2019). In contrast, reverse

electron transfer is the opposite, and the coenzyme is reduced (Onukwufor *et al.,* 2019). Peroxisomes are the second significant producers of ROS, and reactions taking place in the peroxisome mainly result in hydrogen peroxide and, to a lesser extent, superoxide molecules (Forrester *et al.*, 2018). Here, multiple enzymes, like D-amino acid oxidase and xanthine oxidase, found in the peroxisome create hydrogen peroxide as a byproduct of their reactions due to the addition of free electrons to water molecules (Forrester *et al.*, 2018; Sies and Jones, 2020). A third producer of ROS is the endoplasmic reticulum. Protein folding occurs within the endoplasmic reticulum and includes disulfide bridge additions to nascent proteins. Disulfide bridges are added via the endoplasmic reticulum oxidoreductin 1 (ERO1) and protein disulfide isomerase (PDI) pathways, and for every disulfide bridge created, a molecule of hydrogen peroxide is released (Cao and Kaufman, 2014; Forrester *et al.*, 2018). In addition to the above, the plasma membrane is also capable of generating ROS by NADPH oxidase (NOX) enzymes (Sies and Jones, 2020).

Exogenous sources of ROS include UV light, heat, ionizing radiation, microbial infections, and xenobiotic substances, including drugs and environmental pollutants (Brieger *et al.*, 2012; Sies and Jones, 2020). Different ROS can be produced depending on the type of pollutant the cell is exposed to. For example, quinones promote superoxide formation, whereas paraquat can react to form ozone (O_3) (Krumova and Cosa, 2016). In addition, the exogenous factors mentioned above result in ROS through multiple different mechanisms. For example, ionizing radiation can produce ROS through the dissociation of water molecules, while antibiotics and chemotherapy drugs produce ROS through indirect mechanisms that can lead to cell death (Krumova and Cosa, 2016).

1.3. ROS detoxification by non-enzymatic and enzymatic antioxidants

When ROS are present at lower intracellular levels (around 100 nM), eukaryotic cells are in a balanced state, allowing for positive cellular responses like growth (Sies and Jones, 2020). An increase in intracellular ROS disturbs this state as oxidative stress occurs, and therefore excessive ROS needs to be removed. The discovery of superoxide dismutase in 1969 showed that this imbalance was constrained by a cellular antioxidant defence network. An antioxidant is an endogenous or exogenous molecule that has the ability to neutralize ROS and any adverse effects it may have on a cell (Mirończuk-Chodakowska *et al.*, 2018). Cells have developed a wide range of non-enzymatic and enzymatic antioxidants that function cooperatively for this purpose.

Antioxidants react in three fundamental ways. They can neutralize ROS before they can cause harm, prevent the formation of further ROS and repair any damage caused by ROS (Mirończuk-Chodakowska *et al.*, 2018; Neha *et al.*, 2019). Consequently, antioxidant action can be divided into three lines of defence. The first line includes both enzymatic and non-enzymatic antioxidants, the second line consists of only non-enzymatic antioxidants, and the last line of defence comprises those antioxidants that repair damage caused by free radicals (Mirończuk-Chodakowska *et al.*, 2018).

Some non-enzymatic antioxidants include glutathione (GSH), uric acid, metal-binding proteins, melatonin, vitamins A, C, and E, polyphenols, and carotenoids (Mirończuk-Chodakowska *et al.*, 2018). These antioxidants function by scavenging free radicals, preventing them from interacting with cellular components and causing damage. For example, intracellular uric acid is produced through purine metabolism and can scavenge multiple free radicals, including hydroxyl radicals and singlet oxygen (Nimse and Pal, 2015; Mirończuk-Chodakowska *et al.*, 2018). Uric acid is also essential in the blood as it protects erythrocyte membranes from lipid peroxidation (Pisoschi and Pop, 2015). Another critical antioxidant is glutathione which is involved in numerous reactions under normoxic and hyperoxic conditions. GSH is an abundant tri-peptide containing a thiol group that allows it to scavenge free radicals, protect the thiol groups on other proteins, and plays a role in repair processes (Nimse and Pal, 2015; Mirończuk-Chodakowska *et al.*, 2018).

Enzymatic antioxidants function by decomposing ROS to prevent them from causing any harm to the cell. One of the most efficient enzymatic antioxidants is catalase, which breaks down two hydrogen peroxide molecules via a two-step process into oxygen and two water molecules (Aslani and Ghobadi, 2016; He *et al.*, 2017a). Superoxide dismutase contains metal ions, can exist in different isoforms, and functions by catalyzing the dismutation reaction of superoxide into hydrogen peroxide and water (Aslani and Ghobadi, 2016). Glutathione peroxidase (GPx) can exist in two forms (i.e., selenium-dependent and selenium-independent) and catalyze the breakdown of hydrogen peroxide and other organic hydroperoxides into either water or alcohol with the help of GSH (He *et al.*, 2017a). During these reactions, GSH becomes oxidized into glutathione disulfide (GSSG) and requires glutathione reductase (GR) and NADPH to be reduced (Aslani and Ghobadi, 2016). Peroxiredoxins are thiol-based peroxidases responsible for reducing most peroxides found

within a cell. Therefore, they play a vital role in antioxidant defence redox signalling and will be discussed in greater detail below.

1.3.1. Peroxiredoxins

There are six types of peroxiredoxins that are divided into three subgroups based on the presence and position of their cysteine residues. The three subgroups are 1-cysteine peroxiredoxins (peroxiredoxin VI), typical 2-cysteine peroxiredoxins (peroxiredoxin I, II, III, and IV), and lastly, atypical 2-cysteine peroxiredoxins (peroxiredoxin V) (Rhee, 2016; Cao and Lindsay, 2017). Here we will focus specifically on typical 2-cysteine peroxiredoxins. They are the most abundant peroxiredoxin type and contain resolving and peroxidatic cysteines in their active sites. The 2-cysteine peroxiredoxins exist as decameric structures made of five dimers (Rhee and Woo, 2020). Each dimer consists of two subunits arranged antiparallel to each other, therefore the peroxidatic cysteine of one peroxiredoxin is in contact with the resolving cysteine of another peroxiredoxin (Rhee and Woo, 2020). Peroxiredoxins reduce a single peroxide molecule via a peroxidatic cysteine, forming a sulfenic acid (SOH) which causes a conformational change that triggers the dissociation of the decameric structure into dimers (Cao and Lindsay, 2017; Rhee and Woo, 2020). The resolving cysteine on another peroxiredoxin subunit reacts with the sulfenic acid and creates a homodimer via an intermolecular disulfide bond (S-S) (Figure 1.3) (Rhee, 2016; Cao and Lindsay, 2017). The homodimer is then reduced by thioredoxin (Trx), breaking the disulfide bond and returning both peroxiredoxins to their original form, which will allow the dimers to reassociate into a decamer (Cao and Lindsay, 2017; Rhee and Woo, 2020). Thioredoxin becomes oxidized through this reaction and is reduced by thioredoxin reductase (Trr) and NADPH (Veal *et al.*, 2014). When peroxide concentrations increase, the sulfenylated peroxiredoxin can reduce another peroxide molecule resulting in hyperoxidation (sulfenic acid becomes a sulfinic acid) (Cao and Lindsay, 2017). Hyperoxidized peroxiredoxins are considered catalytically inactivated but can be reduced to a sulfenic acid again by sulfiredoxin (Srx) and ATP (Figure 1.3) (Cao and Lindsay, 2017; Veal *et al.*, 2018). Thioredoxin peroxidase (Tpx1), the fission yeast peroxiredoxin, follows a similar catalytic cycle as described above. Tpx1 is a part of the hydrogen peroxide detoxification system in *Schizosaccharomyces pombe* (Day *et al.*, 2012; Veal *et al.*, 2014), which was the focus of this dissertation.

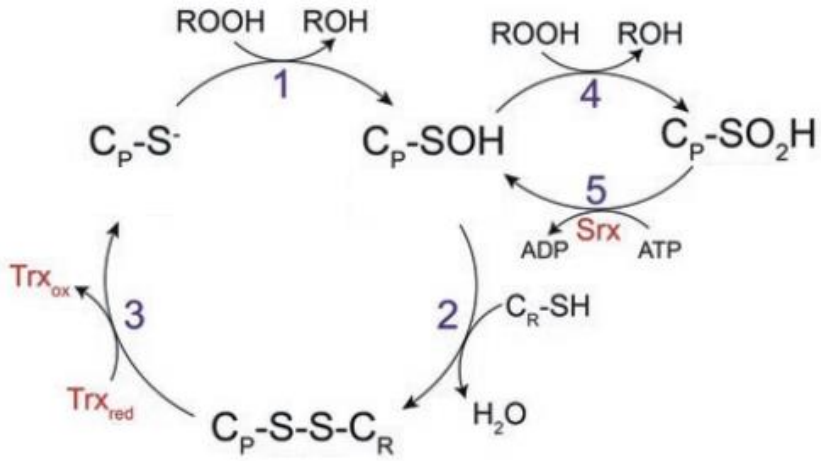

Figure 1.3: Schematic representation of the peroxiredoxin catalytic cycle when reducing peroxides. The peroxidatic cysteine (C_P) reduces a peroxide (1), then forms a disulfide bond with the resolving cysteine (C_R) of another peroxiredoxin (2), which is reduced by Trx (3). Peroxiredoxins can also reduce a second peroxide (4), and the resultant sulfinic acid is reduced by Srx (5) (Adapted from Cao and Lindsay, 2017). Copyright permission to reproduce this image was obtained from Springer.

1.4. ROS as signalling molecules

Hydrogen peroxide is an important signalling molecule in cells (Garcia-Santamarina *et al.*, 2014). Of all the ROS, hydrogen peroxide appears to be the most used for signalling, even under normoxic conditions. Consequently, several hydrogen peroxide sensing mechanisms have evolved in different cells (Garcia-Santamarina *et al.*, 2014). These sensory mechanisms convert the hydrogen peroxide input into a transcriptional response. It is essential for this to occur so that cells can elicit an adaptive response against oxidative stress.

1.4.1. Direct sensors

Some cells have transcription factors that directly interact with hydrogen peroxide resulting in their activation. An example is the OxyR transcription factor in *Escherichia coli* which belongs to the LysR family of transcriptional regulators found in prokaryotic cells (Zheng *et al.*, 1998). Although OxyR contains six cysteine residues, mutational studies have shown that only cysteine 199 and cysteine 208 are responsible for its activation (Zheng *et al.*, 1998). OxyR exists as a homotetramer, and it becomes rapidly oxidized (activated) by hydrogen peroxide (Zheng *et al.*, 1998). During this time, OxyR undergoes a conformational change, allowing for transcriptional activation of multiple genes to overcome oxidative stress (Figure 1.4) (Garcia-Santamarina *et al.*,

2014). OxyR is then recycled back to its reduced form by glutaredoxin 1 (Grx1), which is reduced by GSH. While oxidized, OxyR activates the transcription of genes needed to reduce hydrogen peroxide, such as alkyl hydroperoxide reductase C (*ahpC*) and the catalases, hydroperoxidase I (*katG*) and hydroperoxidase II (*katE*) (Zheng *et al.*, 1998; Åslund *et al.*, 1999; Garcia-Santamarina *et al.*, 2014). The OxyR cycle is autoregulated as it also induces transcription of *grxA* and *gorA*, which code for glutaredoxin 1 and glutathione reductase, respectively (Zheng *et al.*, 1998; Åslund *et al.*, 1999).

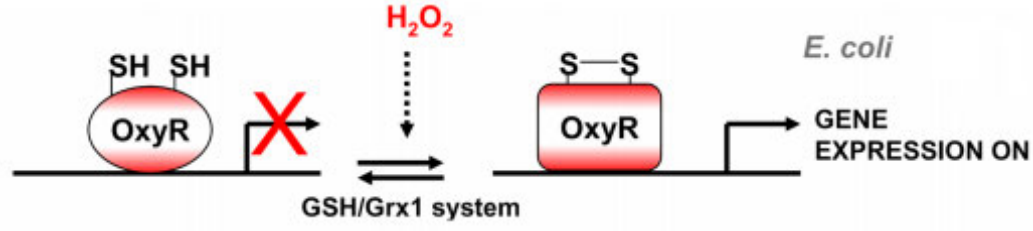

Figure 1.4: OxyR in *E.coli* is activated through direct interaction with hydrogen peroxide. When activated, OxyR undergoes a conformational change allowing for gene expression. OxyR is then reduced by the glutathione/glutaredoxin (GSH/Grx1) system (Adapted from Garcia-Santamarina *et al.*, 2014). Copyright permission to reproduce this figure was obtained from American Chemical Society.

Currently, two models are proposed for activating OxyR by hydrogen peroxide (Garcia-Santamarina *et al.*, 2014). The first is the conformational switch model, where OxyR forms a disulfide bond. This model suggests that cysteine 199 interacts with hydrogen peroxide transforming its thiol group into a SOH, resulting in the cysteine turning to expose the SOH group as its current position can no longer accommodate it (Choi *et al.*, 2001; Garcia-Santamarina *et al.*, 2014). Once exposed, the SOH group on cysteine 199 is closer to the cysteine 208, promoting disulfide bond formation (Choi *et al.*, 2001). The disulfide bonds cause changes to the homotetramer conformation, allowing for DNA binding to occur. The second model is known as molecular code, and it proposes that the oxidation of cysteine 199 alone by hydrogen peroxide and other oxidants is sufficient to activate OxyR, and therefore, the disulfide bond isn't necessary (Garcia-Santamarina *et al.*, 2014).

1.4.2. Indirect sensors

Eukaryotic cells can also use an indirect method to activate their transcription in response to hydrogen peroxide. This mechanism involves an intermediate protein interacting with hydrogen

peroxide and then transferring the signal onto the transcription factor. An example of the indirect sensor is the Yap1 transcription factor found in *Saccharomyces cerevisiae* (Figure 1.5) (Marinho *et al.*, 2014).

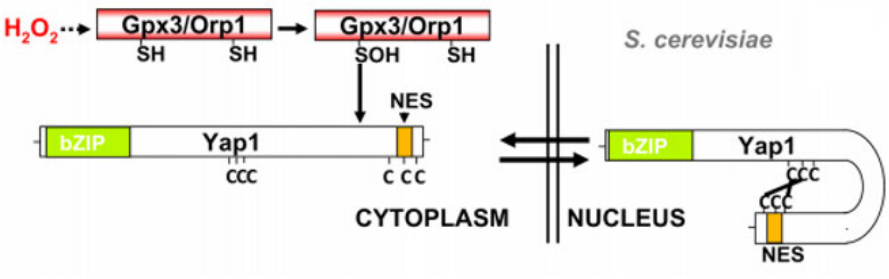

Figure 1.5: Budding yeast transcription factor Yap1 indirectly senses hydrogen peroxide via an intermediate protein. In *S. cerevisiae* Orp1 activates Yap1 after interacting with hydrogen peroxide. The transcription factor can enter the nucleus after forming disulfide bonds as it allows for conformational change that blocks the nuclear export signal (NES) on the protein (Adapted from Garcia-Santamarina *et al.*, 2014). Copyright permission to reproduce this figure was obtained from American Chemical Society.

Hydrogen peroxide oxidizes Orp1 at cysteine 36, forming a sulfenic acid (Orp1-SOH) which can then react with Yap1 at cysteine 598, resulting in an intermolecular disulfide bond (Orp1-S-S-Yap1) which is mediated by Ybp1 (Garcia-Santamarina *et al.*, 2014; Marinho *et al.*, 2014; Bersweiler *et al.*, 2017). Cysteine 303 on Yap1 initiates the reaction with cysteine 598, producing an intramolecular disulfide bond while simultaneously dissociating Orp1 and Yap1 (Bersweiler *et al.*, 2017). Although Yap1 contains one disulfide bond through this interaction, it is still considered partially active and is only fully activated when other disulfide bonds form via more oxidized Orp1 molecules (Garcia-Santamarina *et al.*, 2014; Bersweiler *et al.*, 2017). Yap1 can also be activated by another peroxiredoxin, Tsa1, in Δ*YPB1* cells (Tachibana *et al.*, 2009). Under non-stressed conditions, Yap1 is localized to the cytosol due to its association with the Crm1 exporter because of its nuclear export signal (NES) region (Figure 1.5). Under peroxide stress, Yap1 quickly accumulates in the nucleus after being oxidized, as the resultant disulfide bond blocks the nuclear export signal, preventing nuclear export via Crm1 (Marinho *et al.*, 2014). However, the nuclear export of Yap1 resumes when the disulfide bonds on Yap1 are reduced by Trx2 (Garcia-Santamarina *et al.*, 2014; Marinho *et al.*, 2014). While bound to DNA, Yap1 can induce the transcription of multiple genes, including the glutaredoxin (*glr1* and *gsh1*) and thioredoxin (*trx2* and *trr1*) systems (Delaunay *et al.*, 2000).

Another example of an indirect sensing system is the transcription factor Pap1 found in *S. pombe* (Figure 1.6) which is a homologue and functions similarly to Yap1 in *S. cerevisiae*. While the hydrogen peroxide sensor in *S. cerevisiae* is a glutathione peroxidase-like protein (Orp1), in *S. pombe*, it is the peroxiredoxin Tpx1 that oxidizes Pap1 (Garcia-Santamarina *et al.*, 2014). In *S. pombe*, Pap1 is activated by Tpx1 and undergoes a conformational change which requires cysteines 278, 285, 501, and 532 (Day *et al.*, 2012; Garcia-Santamarina *et al.*, 2014). As with Yap1, Pap1 requires multiple disulfide bridges for full activation and is also translocated to the nucleus when oxidized, where the disulfide bond masks its nuclear export signal (Garcia-Santamarina *et al.*, 2014). Once activated, Pap1 binds to DNA and upregulates the transcription of multiple genes, including thioredoxin genes (*trx1* and *trr1*) and those needed to overcome oxidative stress like catalase (*ctt1*) and superoxide dismutase (*sod1*) (Veal *et al.*, 2002; Veal *et al.*, 2014). Pap1 is inactivated by reduced Trx1.

1.5. The logic of the Tpx1/Pap1 pathway

The Tpx1/Pap1 pathway is found in *S. pombe* and is essential for the cellular response to different oxidants, including hydrogen peroxide (Figure 1.6). When hydrogen peroxide is at or below physiological levels (<70µM), Tpx1 reduces hydrogen peroxide to water resulting in a sulfenic acid (Tpx1-SOH) (Day *et al.*, 2012; Veal *et al.*, 2014). This form of Tpx1 is later reduced by thioredoxin 1 (Trx1) and thioredoxin reductase (Trr1) (Day *et al.*, 2012). Just like the homologous Tsa1 and Orp1 proteins, it is most likely that Tpx1 transfers a SOH to Pap1 instead of a disulfide bond (Bersweiler *et al.*, 2017). As the hydrogen peroxide concentration increases to a medium-range (70µM-200µM), Tpx1-SOH transfers the sulfenic to Pap1 so the cell can adapt to the oxidative stress by inducing the transcription of multiple genes, as mentioned above (Veal *et al.*, 2014; Domènech *et al.*, 2018). Pap1 is then reduced by Trx1 and Trr1, which are the same proteins that also reduce Tpx1 (Veal *et al.*, 2014; Papadakis and Workman, 2015). Thioredoxin like 1 (Txl1) is also considered to have a redundant role with Trx1 in reducing Pap1 and Tpx1. When the concentration of hydrogen peroxide exceeds 200µM, Tpx1-SOH breaks down another molecule of hydrogen peroxide resulting in hyperoxidation of the sulfenic group (Tpx1-SOOH) (Veal *et al.*, 2014). This reaction helps preserve the thioredoxin pool for repair processes (Day *et al.*, 2012). Hyperoxidized Tpx1 cannot oxidize Pap1 and therefore only becomes reactive again once reduced by sulfiredoxin (Srx1) in an ATP-mediated reaction (Domènech *et al.*, 2018).

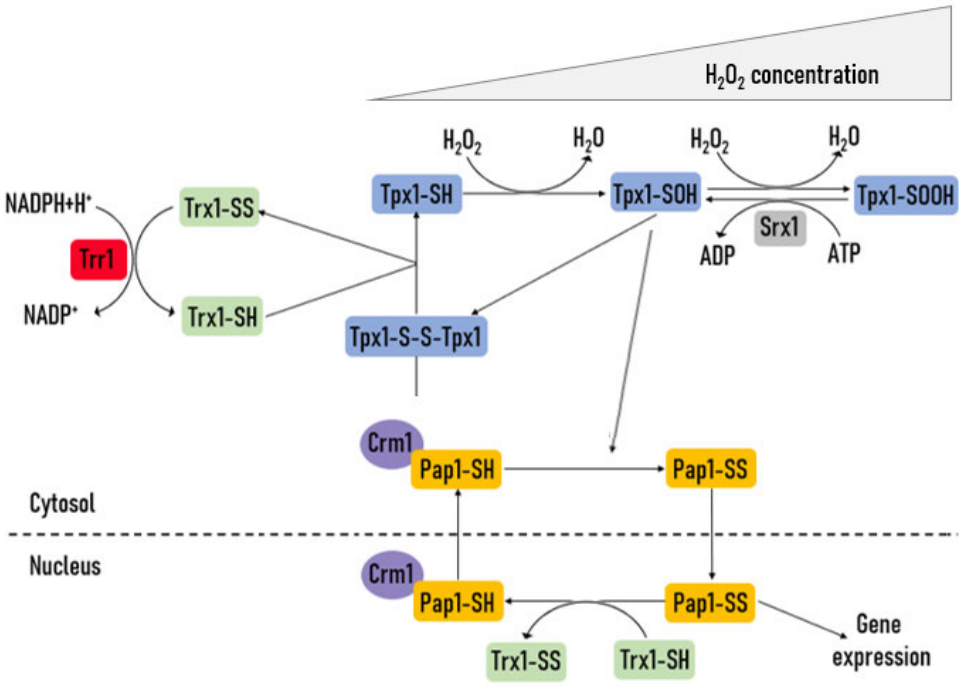

Figure 1.6: Functionality of the Tpx1/Pap1 pathway involved in hydrogen peroxide reduction and antioxidant gene expression. During low physiological hydrogen peroxide levels, Tpx1 breaks down hydrogen peroxide, ultimately forming a disulfide bond that is reduced by the thioredoxin system (Trx1 and Trr1). During intermediate hydrogen peroxide levels, sulfenylated Tpx1 activates Pap1, which dissociates from Crm1 and enters the nucleus for antioxidant gene expression. The thioredoxin system also reduces Pap1. Under high hydrogen peroxide levels, sulfenylated Tpx1 becomes hyperoxidized, which is reversed by sulfiredoxin. This figure was developed from (Veal *et al.*, 2014).

The Tpx1/Pap1 pathway has been well studied using multiple methods. For example, gene knockout technology has been widely used to determine protein function and interactions, and mutational studies have been used to determine the active sites on proteins. In addition, northern blotting has provided insight into which genes are transcribed during Pap1 activation (Veal *et al.*, 2002), and western blotting has helped elucidate protein function in addition to the activation range of the Tpx1/Pap1 pathway (Domènech *et al.*, 2018). However, there have been no studies about what controls the dynamics of the Pap1 redox signal.

1.5.1. Incoherent feedforward loop

There are multiple complex cellular networks within cells, like transcription networks, which are made up of smaller common patterns known as network motifs (Milo *et al.*, 2002; Mangan and Alon, 2003). Network motifs consist of nodes and edges where nodes represent cellular components like proteins, and edges represent the interactions with each other (Milo *et al.*, 2002; Mangan and Alon, 2003). The first-ever biological network motifs were defined in *E. coli* (Shen-

Orr *et al.*, 2002), consisting of four different categories of network motifs: simple regulation, single-input modules, dense overlapping regulons, and feedforward loops (Shen-Orr *et al.*, 2002; Alon, 2007). Each network motif is suggested to perform a particular dynamical function (Shen-Orr *et al.*, 2002). For this review, we will focus on feedforward loops.

Feedforward loops can be divided into two sub-categories, namely coherent and incoherent. These motifs consist of three components, X, Y, and Z, which form two interaction pathways where X regulates Z directly (X→Z), and X regulates Z indirectly via Y (X→Y→Z) (Shen-Orr *et al.*, 2002). If both these pathways have a positive (activation) or negative (repression) effect on Z, the feedforward loop is coherent, but if the pathways have opposing effects on Z, the feedforward loop is incoherent (Shen-Orr *et al.*, 2002; Kim *et al.*, 2008). As the three edges in this motif can exist in different combinations of activation and repression, there are four types of both coherent and incoherent feedforward loops, respectively (Mangan and Alon, 2003; Alon, 2007). Examples of incoherent feedforward loops can be found in Figure 1.7 (Alon, 2007).

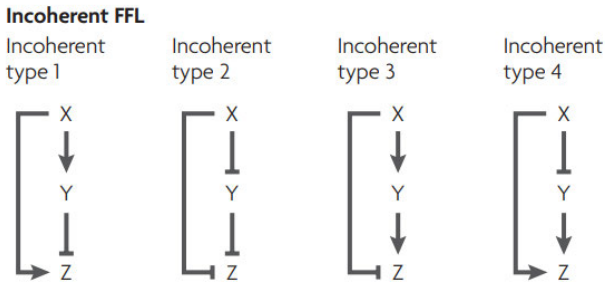

Figure 1.7: The different types of incoherent feedforward loops. X affects Z via two pathways in feedforward loops, either by activation (→) or inactivation (⊥) and incoherent feedforward loops occur when the paths have opposing effects (Adapted from Alon, 2007). Permission to reproduce this figure was obtained from Springer.

Incoherent feedforward loops are frequently observed in cellular networks and have been identified in multiple organisms from bacteria to yeast and mammalian cells. These motifs offer a transient dynamic function, i.e., fast activation and delayed inhibition to the system (Kim *et al.*, 2008). An example of an incoherent feedforward loop is the CRP-*galS*-*galE* galactose network found in *E. coli* (Mangan *et al.*, 2006). Here the transcription factor CRP positively regulates *galS* and *galE* during glucose starvation, but galS also represses the *galE* promoter (Mangan *et al.*, 2006). Another more complex example is the nitrogen utilization network in *S. cerevisiae* that

contains four interconnected incoherent feedforward loops (Hong *et al.*, 2018). One includes Gat1 that directly activates transcription of multiple nitrogen catabolite repression targets while activating another protein, Dal80, that represses their transcription (Hong *et al.*, 2018). In *S. pombe*, the Tpx1/Pap1 pathway appears to have characteristics of an incoherent feedforward loop due to the Trx1 protein. Trx1 reduces oxidized Pap1 and increases the availability of Tpx1 to break down further hydrogen peroxide and oxidize Pap1. However, Trx1 also reduces Pap1, which limits signal propagation.

1.5.2. Dynamics of the Pap1 and OxyR transcription factors

We use three quantitative measures to quantify signalling pathways, viz. signalling time, signalling duration, and signal amplitude (Heinrich *et al.*, 2002). Signalling time refers to the average time taken to activate a target protein; signalling duration refers to the average time that the target protein is active and signal amplitude refers to the average concentration of the active target protein over a specific signal interval (Heinrich *et al.*, 2002). The quantitative parameters can be obtained from western blotting time course data and allow for comparing different signals and pathways.

Western blotting time course data of the OxyR transcription factor in *E. coli* treated with 200 µM hydrogen peroxide was obtained from a previous study (Åslund *et al.*, 1999). The data revealed that OxyR reached its peak oxidation level after one minute and its reduction began soon after, resulting in complete reduction at ten minutes (Åslund *et al.*, 1999). Therefore OxyR has a rapid increase and rapid decrease oxidation profile. In previous experiments done by our group, Pap1 was also treated with 200 µM hydrogen peroxide, and quantitative analysis of western blotting time course data was carried out (Diane Lind, unpublished data). Here, we showed that Pap1 was also quickly oxidized, reaching peak oxidation around two minutes, but was only completely reduced around 60 minutes. Therefore, in contrast to OxyR, the oxidation profile of Pap1 showed a rapid increase and slow decrease pattern (Figure 1.8) which is a characteristic of incoherent feedforward loops.

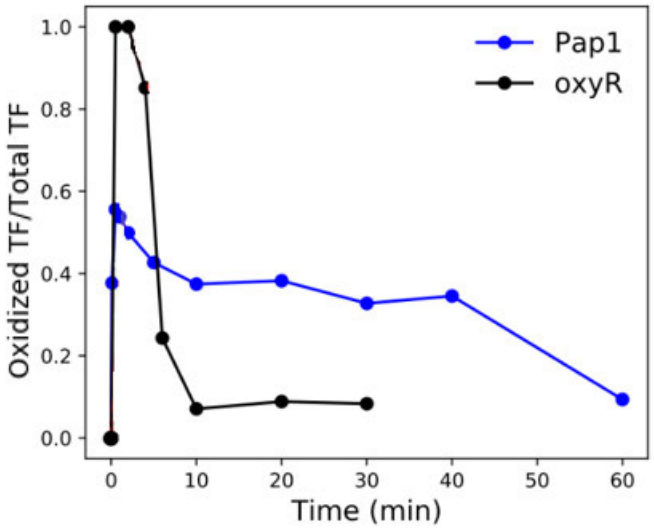

Figure 1.8: Oxidation profiles of the transcription factors OxyR and Pap1 from *E.coli* and *S. pombe*, respectively. When treated with 200 µM hydrogen peroxide, OxyR displays a quick increase and quick decrease in its oxidation, but Pap1 has a rapid increase and a prolonged reduction (Diane Lind, unpublished data).

1.6. Can quantitative signal parameters provide a deeper understanding of the Tpx1/Pap1 pathway?

Earlier work revealed differences between the oxidation profiles of OxyR and Pap1 (Figure 1.8), but the mechanism underlying these differences remained unclear. We hypothesized that the Tpx1/Pap1 pathway was an incoherent system and aimed to perturb the incoherence within the system *in vivo* and *in silico*. The resultant oxidation profiles and signalling data could then be used to develop a mechanistic understanding of the pathway and reveal the design principles of indirect redox signalling systems.

Chapter 2: Chemical perturbation of the Tpx1/Pap1 pathway *in vivo*

2.1. Introduction

S. pombe has become a model cell for understanding redox biology for several reasons. First, a useful characteristic of *S. pombe* is that it contains a single 2-Cys peroxiredoxin, Tpx1, in contrast to the budding yeast *S. cerevisiae* which has five peroxiredoxins (Veal *et al.*, 2014; Rhee, 2016). This makes the redox network of *S. pombe* simpler to understand and manipulate. Second, studying this cell's redox pathways have been made easier because several strains are available with epitope tags, such as Pk-tags or Flag-tags, on key redox proteins (Gadaleta *et al.*, 2013). These tags are used to identify the protein it is attached to by use of antibodies that recognise the tag in western blot analysis, eliminating the need to produce specific antibodies for each protein. Third, the hydrogen peroxide sensitivity of *S. pombe* has been extensively studied and characterized, which aids experimental design (Bozonet *et al.*, 2005; Day *et al.*, 2012; Veal *et al.*, 2014; Papadakis and Workman, 2015; Domènech *et al.*, 2018).

At lower hydrogen peroxide concentrations (~70 µM), Tpx1 is oxidized by hydrogen peroxide. In turn, oxidized Tpx1 can be reduced by Trx1 or can oxidize Pap1, allowing activation of the transcription factor (Figure 2.2) (Garcia-Santamarina *et al.*, 2014; Veal *et al.*, 2014). This is considered an adaptive response as the cells can still actively divide, but there is a change in their transcriptome (Vivancos *et al.*, 2005; Chen *et al.*, 2008; Veal *et al.*, 2014). During this period, antioxidant genes required to overcome oxidative stress, such as *trx1* (thioredoxin reductase), are upregulated (Toone *et al.*, 1998; Brown *et al.*, 2013). The second type of response noted in *S. pombe* due to oxidative stress is the survival response observed at much higher concentrations of hydrogen peroxide (~6 mM) (Figure 2.2) (Vivancos *et al.*, 2005; Veal *et al.*, 2014). During this time, the Pap1-induced antioxidant gene response is switched off as hyperoxidized Tpx1 cannot transmit the signal to Pap1, and the generalized Sty1 stress-response pathway is activated (Vivancos *et al.*, 2006; He *et al.*, 2017b). A further consequence of Tpx1 hyperoxidation is that reduced Trx1 is now available to support damage repair pathways (Day *et al.*, 2012; Veal *et al.*, 2014).

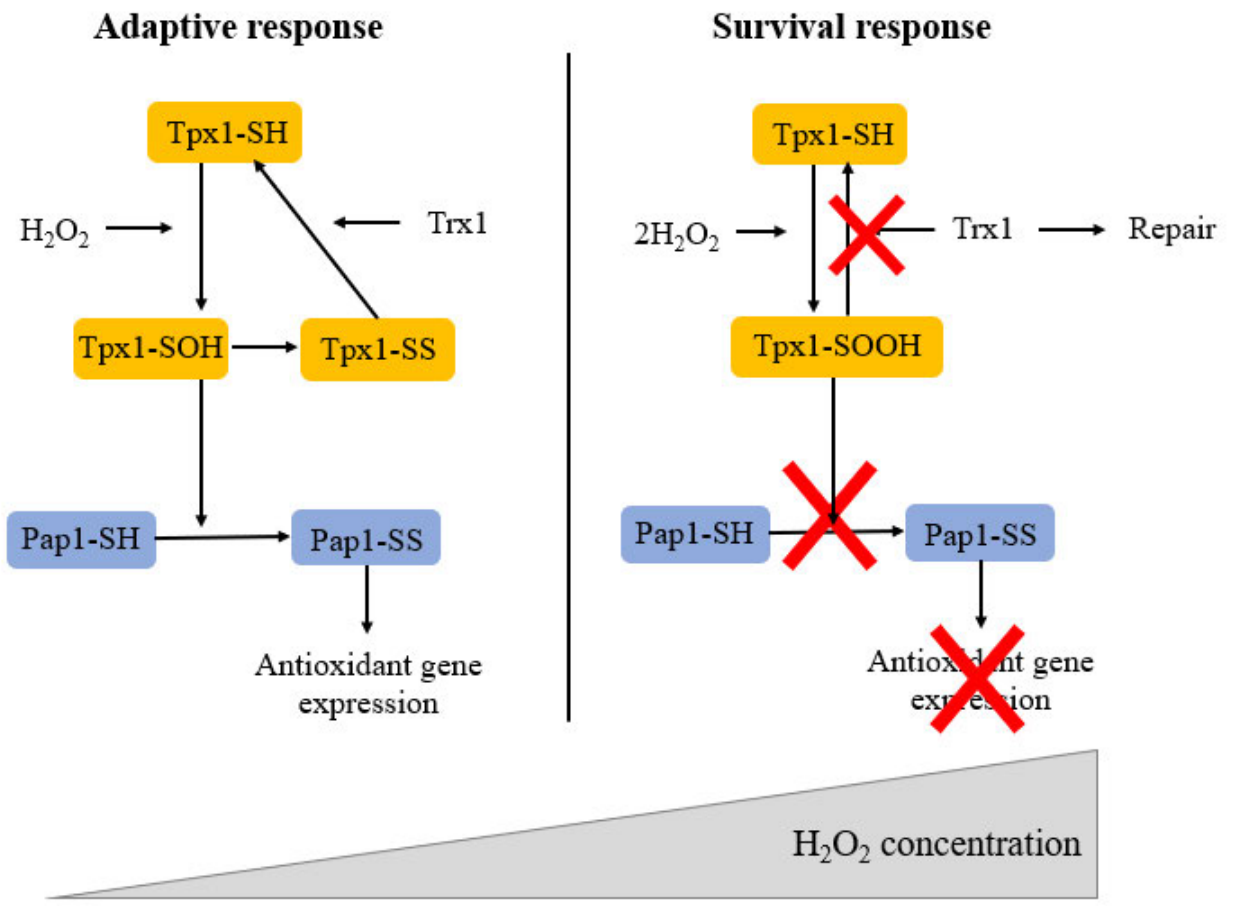

Figure 2.1: Hydrogen peroxide concentration can elicit an adaptive or survival response in *S. pombe* based on Tpx1 reactivity. At lower concentrations of hydrogen peroxide, reduced Tpx1 (SH) becomes oxidized, which oxidizes Pap1. Once activated, Pap1 evokes a transcriptional response of antioxidant genes known as the adaptive response. Under these conditions, Tpx1 oxidation is reversed by Trx1. Following exposure to much higher concentrations of hydrogen peroxide, Tpx1 becomes hyperoxidized (SOOH). While hyperoxidized, Tpx1 cannot oxidize Pap1, shutting down the signalling pathway. Trx1 can also not reduce hyperoxidized Tpx1 and therefore can become involved in repair processes. This figure was developed from literature sources (Day *et al.*, 2012; Veal *et al.*, 2014).

The work reported in this chapter focused on chemically perturbing the Tpx1/Pap1 pathway to determine if an incoherent feedforward loop was responsible for the Pap1 dynamic profile. For these experiments, the stress was limited to the *S. pombe* adaptive response phase. *S. pombe* SB3 cells were treated with various oxidants, and the resultant oxidation profiles were used to determine the signalling parameters, namely signalling time, duration and amplitude for these profiles (Heinrich *et al.*, 2002; Pillay *et al.*, 2016). The signalling parameters will be determined using mathematical equations (Heinrich *et al*., 2002; Pillay *et al*., 2016) and oxidation data obtained from western blots.

2.2. Materials and Methods

2.2.1. Materials

Tert-butyl hydroperoxide, diamide, acrylamide, N, N' methylene-bisacrylamide, iodoacetamide, and anti-mouse (rabbit) IgG peroxidase antibody were all purchased from Sigma Aldrich (Capital Labs, Johannesburg, South Africa). Ammonium persulfate, dithiothreitol (DTT), TEMED, and Coomassie Brilliant Blue R-250 were also obtained from Capital Labs (Johannesburg, South Africa). The Pierce BCA protein assay kit was purchased from ThermoFisher Scientific (Johannesburg, South Africa). Bovine serum albumin (BSA) was purchased from Celtic molecular diagnostics (Cape Town, South Africa). Clarity^{TM} Western ECL substrate and monoclonal (mouse) anti-v5 antibody (α-Pk) (lot number: 1709) were obtained from Bio-Rad (Lasec, Johannesburg, South Africa). The PCR primers were acquired from Integrated DNA Technologies (WhiteSci, South Africa), and all other PCR reagents were obtained from Bio-Rad (Lasec, Johannesburg, South Africa).

All amino acids and other reagents used were purchased from Sigma Aldrich (Capital Labs, Johannesburg, South Africa) or Saarchem (Merck, Johannesburg, South Africa). The *S. pombe* strains used for this project were a kind gift from Dr Elizabeth Veal (Newcastle University, United Kingdom).

2.2.2. Reagents and Buffers

2.2.2.1. 30% Acrylamide solution

Acrylamide solution composed of a 29:1 ratio of acrylamide and N, N' methylene-bisacrylamide dissolved in distilled water. Once dissolved, the acrylamide solution was filtered into an amber bottle through Whatman paper and stored at 4°C.

2.2.2.2. Coomassie blue dye

Coomassie blue dye was prepared using 0.125% Brilliant Blue R-250, 10% (v/v) acetic acid and 50% (v/v) methanol.

2.2.2.3. Destain solution 1

Destain solution 1 was made using distilled water and a final concentration of 10% (v/V) acetic acid and 50% (v/v) methanol.

2.2.2.4. Destain solution 2

Destain solution 2 was also made using distilled water with a final concentration of 7% (v/v) acetic acid and 5% (v/v) methanol.

2.2.2.5. IAM buffer

1% (w/v) SDS and 1.4% (w/v) iodoacetamide were dissolved in 100 mM Tris-HCl (pH 8.0). New IAM buffer was prepared just before use.

2.2.2.6. Loading dye

Loading dye was made by dissolving 0.25% (w/v) bromophenol blue into 30% (v/v) of glycerol.

2.2.2.7. Ponceau S staining solution

A 0.01% (w/v) Ponceau S solution was prepared in 1% (v/v) acetic acid.

2.2.2.8. Primary and Secondary antibody dilution

Mouse anti-Pk monoclonal IgG and rabbit anti-mouse IgG horseradish peroxidase conjugate antibodies were stored at -20°C and diluted to 1 000 X and 50 000 X respectively in 5% (w/v) BSA in TBST when needed.

2.2.2.9. SDS-PAGE (non-reducing) loading dye

The loading dye consisted of 0.8% (w/v) SDS, 0.005% (w/v) bromophenol blue, 10% glycerol (v/v) and 500 mM Tris-HCl (pH 6.7) and was stored at 4°C.

2.2.2.10. SDS-PAGE tank buffer

A final concentration of 1.9 M glycine, 250 mM Tris (pH 8.0), and 1% (w/v) SDS was added to distilled water to prepare SDS tank buffer.

2.2.4.11. TAE buffer

A final concentration of 40 mM Tris-acetate and 1 mM EDTA was used to make 1X TAE buffer. The pH was then adjusted to 8.0.

2.2.2.12. Transfer buffer

The transfer buffer was composed of 50 mM Tris (pH 8.0), 192 mM glycine, 1% (w/v) SDS, and 20% (v/v) methanol in distilled water and was stored at 4°C.

2.2.2.13. Tris Buffered Saline with Tween (TBST)

A final concentration of 20 mM Tris and 150 mM NaCl were dissolved in distilled water, and the pH was adjusted to 6.7. Tween 20 (0.1% (v/v)) was then added to the solution.

2.2.2.14. Tris Lower Buffer (Resolving buffer)

The Lower Buffer was prepared using 3.0 M Tris-HCl and adjusted to pH 8.8. 0.8% (w/v) SDS was then added to the buffer.

2.2.2.15. Tris Upper Buffer

The Upper Buffer consisted of 0.5 M Tris-HCl, adjusted to pH 6.8, and 0.4% (w/v) SDS was then added.

2.2.3. Culture media preparation

2.2.3.1. Edinburgh Minimal Media (EMM)

EMM contained 14.7 mM potassium hydrogen phthalate ($C_8H_5O_4K$), 15.5 mM di-sodium hydrogen orthophosphate (Na_2HPO_4), 93.5 mM ammonium chloride (NH_4CL_2), 2% (w/v) glucose, 0.26 M magnesium chloride ($MgCl_2.6H_2O$), 4.99 mM calcium chloride ($CaCl_2.2H_2O$), 0.67 M potassium chloride (KCl), 14.1 mM di-sodium sulfate (Na_2SO_4), 80.9 mM boric acid, 23.7 mM manganese sulfate ($MnSO_4$), 13.9 mM zinc sulfate ($ZnSO_4.7H_2O$), 7.4 mM ferric chloride ($FeCl_3.6H_2O$), 2.47 mM molybdic acid ($MoO_4.2H_2O$), 6.02 mM potassium iodide (KI), 1.6 mM copper sulfate ($CuSO_4.5H_2O$), 47.6 mM citric acid, 81.2 mM nicotinic acid, 55.5 mM myo-inositol, 40.8 µM biotin, 4.20 mM pantothenic acid, 225 mg/L adenine, 225mg/L lysine, 225 mg/L histidine, 225 mg/L uracil and 250 mg/L leucine and 2% (w/v) agar was added for solid growth.

2.2.3.2. Yeast Extract Supplemented with five Amino Acids (YE5S)

YE5S media contained 3% (w/v) Glucose, 0.5% (w/v) Yeast extract, 225 mg/L adenine, 225mg/L lysine, 225 mg/L histidine, 225 mg/L uracil and 250 mg/L leucine and 2% (w/v) agar included for solid growth.

2.2.4. Methods

2.2.4.1. *Schizosaccharomyces pombe* strain and cultivation

The *S. pombe* SB3 (H–ade6-M216 pap1+(3Pk)::ura4+his7-366) and SB4 (H+ade6 pap1+(3Pk)::ura4+tpx1::ura4+his7-366) strains used in this study was a kind gift from Dr Elizabeth Veal (Newcastle University, United Kingdom) (Bozonet *et al.*, 2005). Both strains

contained a Pk-tag epitope of 14 amino acids (GKPIPNPLLGLDST) on Pap1 (Gadaleta *et al.*, 2013) and a ura4 marker (Bozonet *et al*., 2005). The Pk-tag allowed the identification of the Pap1 protein using an antibody that recognizes the tag (Gadaleta *et al*., 2013), while the ura4 marker, of approximately 200 bp that was inserted utilizing a disruption cassette, was used to identify the cells which contained the Pk-tag (Bozonet *et al*., 2005). The strains were plated from frozen stocks (-80ºC in 50% (v/v) glycerol) onto YE5S agar plates and grown at 30ºC for two days. The plates were stored at 4ºC, and the cultures streaked weekly onto fresh plates. Liquid cultures were grown in EMM by inoculating with a single colony from the agar plate. These cultures were grown overnight (180 rpm at 30ºC), then used to inoculate fresh media, and allowed to grow to an OD~0.5.

2.2.4.2. Preparation of colony DNA

A single *S. pombe* SB3 and SB4 colony was added to 0.2% SDS (w/v) and vortexed for 15 seconds. The colony was then boiled at 100°C for 2 minutes and centrifuged (13 000 x *g*, 1 minute, 25°C). The supernatant was moved to a new tube and used as template DNA for PCR amplification.

2.2.4.3. PCR amplification of the *ura4* marker

Each PCR reaction consisted of 1X GC buffer, 0.2 µM of forward and reverse ura4 primers, 2 mM $MgCl_2$, 0.2 mM dNTPs, 0.4U Phusion high fidelity DNA polymerase, and distilled water to a final volume of 20 µl. Cycling conditions consisted of an initial denaturation at 95°C for 30 seconds, 30 cycles of denaturation at 95°C for 15 seconds, annealing at 50°C for 30 seconds, extension at 68°C for 90 seconds, and a final extension at 68°C for 5 minutes. The annealing temperature of the ura4 primers (Table 2.1) was determined to be 50°C using Oligoanalyser (https://eu.idtdna.com/calc/analyzer) and Primer3 (https://primer3.ut.ee/).

Table 2.1: Sequences of the ura4 oligonucleotide primers.

Primer name	Sequence (5' to 3')
Forward ura4 primer	ACC AGT AGC CAA AGA GCC TT
Reverse ura4 primer	TGA GGA TCG CAA ATT CGC AG

2.2.4.4. Agarose gel electrophoresis

1% (w/v) agarose was dissolved in 50 ml of 1X TAE and allowed to cool. Once cooled, ethidium bromide was added to a final concentration of 0.5 µg/ml before being poured into a gel casting tray to polymerize. 5 µl of loading dye was mixed with 2 µl of PCR product and underwent electrophoreses at 80V for 90 minutes. DNA on the agarose gel was analyzed under UV light using the DNR Bio-Imaging Systems MiniBIS Pro.

2.2.4.5. Sensitivity test of *S. pombe* SB3 cells to the different oxidants

S. pombe SB3 cells were cultured in EMM to an OD~0.5 and used to inoculate YE5S agar plates. Cells were pipetted in a line towards sterile disks of Whatman filter paper, placed on agar plates, which were soaked in 10 µl of each oxidant at differing concentrations, i.e., hydrogen peroxide (0.1-1 mM) (Vivancos *et al.*, 2004; Chen *et al.*, 2008), tert-butyl hydroperoxide (*t*BOOH) (0.1-1 mM) (Chen *et al.*, 2008), and diamide (1-4 mM) (He *et al.*, 2017b; Chen *et al.*, 2018b). The plates were incubated (2 days, 30°C) then imaged under white light. Each sensitivity test was done in triplicate.

2.2.4.6. Determining antibody and protein concentration for western blotting via dot blotting

Protein was extracted (see section 2.2.4.8) from a sample taken from an overnight culture of *S. pombe* SB3 cells. The absorbance value of the protein sample was measured and used to dilute the sample into three different absorbance values (0.3, 0.2, and 0.15 a.u), which was later correlated to its corresponding protein concentration using a standard curve from the BCA method (see section 2.2.4.9). The different protein samples (5 µl each) were then directly pipetted onto nitrocellulose membrane. The membranes were blocked for 30 minutes in 10% (w/v) BSA before being incubated in different concentrations of primary antibody (0.25-1 µg/ml) overnight (50 rpm, 4°C). Afterwards, the nitrocellulose membranes were removed from the primary antibody and washed four times with TBST for five minutes each. The membranes were then incubated in varying concentrations of rabbit anti-mouse IgG horseradish peroxidase conjuage (secondary)

antibody (1:25 000-1:120 000) for an hour (50 rpm, RT) and lastly washed four more times with TBST for five minutes each. The membranes were allowed to dry before adding ECL reagent and viewing using the G-BOX Chemi-X5R Gene*Sys* imagining system. ImageJ was used to analyze each dot blot to determine which protein absorbance (and later concentration) and primary and secondary antibody concentrations work best together.

2.2.4.7. Oxidant challenges to *S. pombe* SB3 cells

S. pombe SB3 cells from a single colony were grown overnight (180 rpm, 30°C) in 10 ml of EMM. The following morning 100 µl of culture is diluted into 900 µl of EMM to measure the optical density (OD) at 595 nm. The OD value obtained is multiplied by 10 to account for the dilution factor and is used to determine the amount of culture needed to inoculate 50 ml of fresh EMM to OD~0.15. Cells were cultured (180 rpm, 30°C) until the mid-log phase (OD~0.4-0.5). Once the desired OD is reached, a 2 ml sample was taken and added to a Falcon tube containing 2 ml of ice-cold 20% trichloroacetic acid (TCA). Immediately after, a predetermined concentration of a specific oxidant was added to the culture, and 2 ml samples were taken, as described, at different time points over a one or two-hour time course. The cells were pelleted by centrifugation (2000 x *g*, 5 minutes, 4°C), and the supernatant was discarded. Pellets were snap-frozen in liquid nitrogen and stored at -80°C until protein extraction.

2.2.4.8. Protein isolation from *S. pombe* SB3 cells

Frozen pellets were thawed on ice and resuspended in 200 µl of 10% TCA before being transferred to 2 ml Ribolyzer tubes. Glass beads (0.5 mm, *ca.* 750 µl) were added, and cells were lysed using a bead beater (maximum speed, 15 seconds, 21°C), then placed on ice for one minute and lysed again. 500 µl of 10% TCA was added to the lysed cells, and the sample was briefly vortexed. A hot needle was used to pierce the bottom of the Ribolyzer tube before it was placed into a sterile 1.5 ml tube. Both tubes were then placed into a sterile 50 ml Falcon tube and centrifuged (2000 x *g*, 1 minute, 21°C) to drain the solution into the 1.5 ml tube. The protein was then pelleted by centrifugation (13 000 x *g*, 10 minutes, 4°C), and the supernatant was discarded. The protein pellet was washed three times by centrifugation (13 000 x *g*, 1 minute, 4°C) using 100% acetone and then allowed to air dry for 10 minutes to remove any excess acetone. For alkylation to occur, the pellet was resuspended in 35 µl of IAA buffer and incubated for 20 minutes at 25°C. Afterwards, the sample was centrifuged (13 000 x *g*, 3 minutes, 21°C), and the supernatant

was transferred to a new tube and stored at -20°C until ready to use. Protein samples were prepared essentially as previously described (Delaunay *et al*., 2000).

2.2.4.9. BCA protein assay to determine the absorbance of protein samples

Fresh BCA working solution was prepared by mixing solutions A and B according to the number of samples, i.e., solution A = (number of samples + buffer control + negative control) x 3 x 200 µl while solution B = (number of samples + buffer control + negative control) x 3 x 4 µl. 200 µl of BCA working solution was pipetted into a 96-well plate followed by 1 µl of each protein sample in triplicate. The buffer control wells had 1 µl of IAA buffer added in triplicate while an extra microlitre of BCA working solution was added to the negative control wells to ensure a constant volume. The 96-well plate was incubated at 37°C for one hour, and afterwards, the absorbance was measured at 562 nm using the Versamax ELISA microplate reader (Molecular Devices, San Jose, California, USA). The absorbance values allowed dilution correction to ensure equal protein concentrations across all samples when loading onto an SDS-PAGE gel. This method was performed as per the Pierce BCA protein assay kit (Thermo Fisher).

2.2.4.10. SDS-PAGE electrophoresis

The 8% SDS-PAGE gel consists of the resolving and stacking solutions made with Tris lower and upper buffer, respectively. Both solutions also contained 30% acrylamide solution, water, TEMED, and 10% ammonium persulfate (APS), which was freshly prepared each time. The protocol for making both solutions for the non-reducing SDS-PAGE gels was based on the Laemmli method (Laemmli, 1970) can be found in table 2.2. Before loading the samples onto the gel, 10µl of SDS loading dye was added to each sample before it was boiled at 100°C for five minutes and allowed to cool to 4°C. Electrophoresis was run at 200 V for 50 minutes in a 1 X SDS tank buffer.

Table 2.2: Mixture used to prepare the resolving and stacking gels in the SDS-PAGE gel.

Reagent	Resolving gel (ml)	Stacking gel (ml)
30% acrylamide solution	4	0.65
Tris lower buffer	3.75	-
Tris upper buffer	-	1.25
Water	7.25	3.05
APS (10%)	0.1	0.05
TEMED	0.03	0.001

2.2.4.11. Transfer of protein to nitrocellulose membrane

Following completion of the SDS-PAGE electrophoresis, a transfer sandwich was made while submerged in ice-cold transfer buffer. The sandwich was made by layering a transfer stack at the bottom, followed by the SDS-PAGE gel, the nitrocellulose membrane (0.2 µm), and another transfer stack. The transfer ran for three hours at 200 V in ice-cold transfer buffer. Ice packs were also placed into the Mini-PROTEAN Tetra Cell tank (Bio-Rad Laboratories, Hercules, California, USA) and changed at 90 minutes to ensure the transfer buffer remained cold. To ensure the transfer occurred efficiently, the SDS-PAGE gel was stained overnight in Coomassie blue (50 rpm, 21°C) and destained the following day using Destain solutions 1 and 2.

2.2.4.12. Western blot development and visualization

Upon completion of the transfer, the nitrocellulose membrane was stained with Ponceau S stain for five minutes to allow total protein quantification (see section 2.2.4.13). The Ponceau S stain was removed using 0.1 M NaOH diluted in distilled water. Afterwards, the unoccupied sites on the membrane was blocked for 30 minutes in 10% (w/v) BSA dissolved in TBST and then incubated in 1 µg/ml mouse anti-Pk monoclonal IgG antibody overnight (50 rpm, 4°C). The following day, the membrane was washed four times for five minutes each in TBST. Afterwards, it was incubated for 1 hour (50 rpm, RT) in 1:50 000 of rabbit anti-mouse IgG horseradish peroxidase conjugate antibody and then washed again as described before being air-dried. Once dry, ECL reagent was added to the membrane for imaging using the G-BOX Chemi-X5R Gene*Sys* imaging system. Precision Plus Protein^{TM} WesternC^{TM} standard (Bio-rad) were separated on the SDS-PAGE gel for molecular mass determination.

2.2.4.13. Analysis of Pap1 protein bands using ImageJ

The intensity of the respective protein bands in the western blot was quantified using the gel analysis function on ImageJ (https://imagej.nih.gov) by selecting the relevant bands. The resultant intensity of both reduced and oxidized Pap1 bands was added together to obtain $Pap1_{total}$. Oxidized Pap1 ($Pap1_{ox}$) was then divided by $Pap1_{total}$ to get the fractional Pap1 oxidation (Pap1 oxidation charge) (Padayachee *et al*., 2020). These values were plotted against the relevant time points resulting in the graph for Pap1 activation. The signalling parameters were then calculated from the area under the curve of the graph (see section 2.3.4).

ImageJ was also used to quantify the intensity of the reduced Pap1 bands from the DTT control blots. The $Pap1_{ox}$ values were then divided by the reduced Pap1 values for each time point. These values ($Pap1_{ox}$/Reduced Pap1 control) were plotted against the Pap1 oxidation charge ($Pap1_{ox}/Pap1_{total}$) value in a linear regression plot to determine their relationship.

As a second control, the Ponceau S stained blots were also analyzed with ImageJ to determine the amount of total protein ($Protein_{total}$) per lane (Sander *et al.*, 2019; Pillai-Kastoori *et al.*, 2020). $Pap1_{ox}$ was then divided by $Protein_{total}$ values for each time point. The $Pap1_{ox}/Protein_{total}$ values were plotted in a linear regression plot against $Pap1_{ox}/Pap1_{total}$ values. Once again, a linear relationship between these values indicated equal loading in each lane.

2.2.4.14. Signal quantification of Pap1 activation

The signalling parameters were calculated from the signal profile graphs. First, the total amount of activated target protein (I_i) was determined using equation (1). Signalling time (τ_i) was calculated using equations (2) and (3), while signalling duration (ϑ_i) and signalling amplitude (S_i) can be calculated using equations (4) and (5), respectively (Heinrich *et al.*, 2002; Pillay *et al.*, 2016).

$$I_i = \int_0^\infty P_i(t)dt \qquad (1)$$

$$\tau_i = \frac{T_i}{I_i} \qquad (2)$$

$$T_i = \int_0^\infty t \cdot P_i(t)dt \qquad (3)$$

$$\vartheta = \sqrt{\frac{\int_0^\infty t^2 P_i(t)dt}{I_i} - \tau_i^2} \qquad (4)$$

$$S_i = \frac{I_i}{2\vartheta_i} \quad (5)$$

P_i represents the amount of activated target protein while t represents a signal interval. The signalling parameter analyses were completed using the Python Anaconda v4.10.3 package (https://www.anaconda.com) with the Pandas, Matplotlib, NumPy, Seaborn, SciPy and Stats modules. A full Jupyter notebook with all relevant code used in this thesis is available in the Appendix.

2.3. Results

2.3.1. Confirmation of the Pk-tag in *S. pombe* SB3 through identification of the *ura4* marker

The *S. pombe* SB3 strain used in this study contained a Pk-tag on Pap1 and a *ura4* marker that was used to select for these cells. Before starting the western blotting experiments, we tested for the presence of this marker on the cells provided by our collaborator. The *S. pombe* SB4 strain also had the *ura4* marker (Bozonet *et al*., 2005) and was used as a positive control. Colony DNA was isolated from *S. pombe* SB3 and SB4 cells (section 2.2.4.2) and used for PCR amplification of *ura4*. The products were run on an agarose gel (Figure 2.2), showing that *S. pombe* SB3 contained the marker.

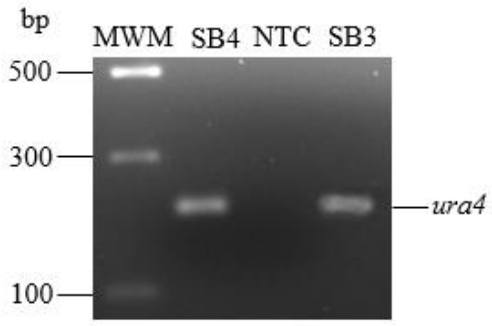

Figure 2.2: Confirmation of the Pk-tagged Pap1 in *S. pombe* SB3. The *ura4* marker (211 bp) was amplified in the *S. pombe* SB3 strain, indicating genetic modification. Amplification of *ura4* in SB4 and a no template control (NTC) was used as a positive and negative control, respectively.

2.3.2. Determining the sensitivity of *S. pombe* SB3 cells to different concentrations of hydrogen peroxide, tert-butyl hydroperoxide, and diamide

Although *S. pombe* can survive comparatively high concentrations of ROS (Day *et al.*, 2012; Veal *et al.*, 2014; Tomalin *et al.*, 2016), we confirmed that the concentrations of oxidants used in this study were not lethal using halo sensitivity tests (Song and Roe, 2008; Veal *et al.*, 2014; Chen *et al.*, 2018b). Discs were soaked with the particular oxidant and placed on an agar plate where a fresh liquid culture was pipetted. The plates were incubated at 30°C for two days, and sensitivity was determined by the presence of a halo around the disc. The *S. pombe* SB3 cells showed no sensitivity towards the hydrogen peroxide (Figure 2.3A-D) or tert-butyl hydroperoxide concentrations used in this study (Figure 2.3E-H) in agreement with previous studies (Chen *et al.*, 2008; Song and Roe, 2008; Brown *et al.*, 2013). Further, *S. pombe* SB3 cells exposed to 1-2.5 mM of diamide also showed no sensitivity to the oxidant at these concentrations (Figure 2.3I-L), which was expected (Song and Roe, 2008; Chen *et al.*, 2018b). These images were taken two days following incubation to prevent overgrowth of the streak. Consequently, although some colonies are harder to discern (Figure 2.3K and L), they are present.

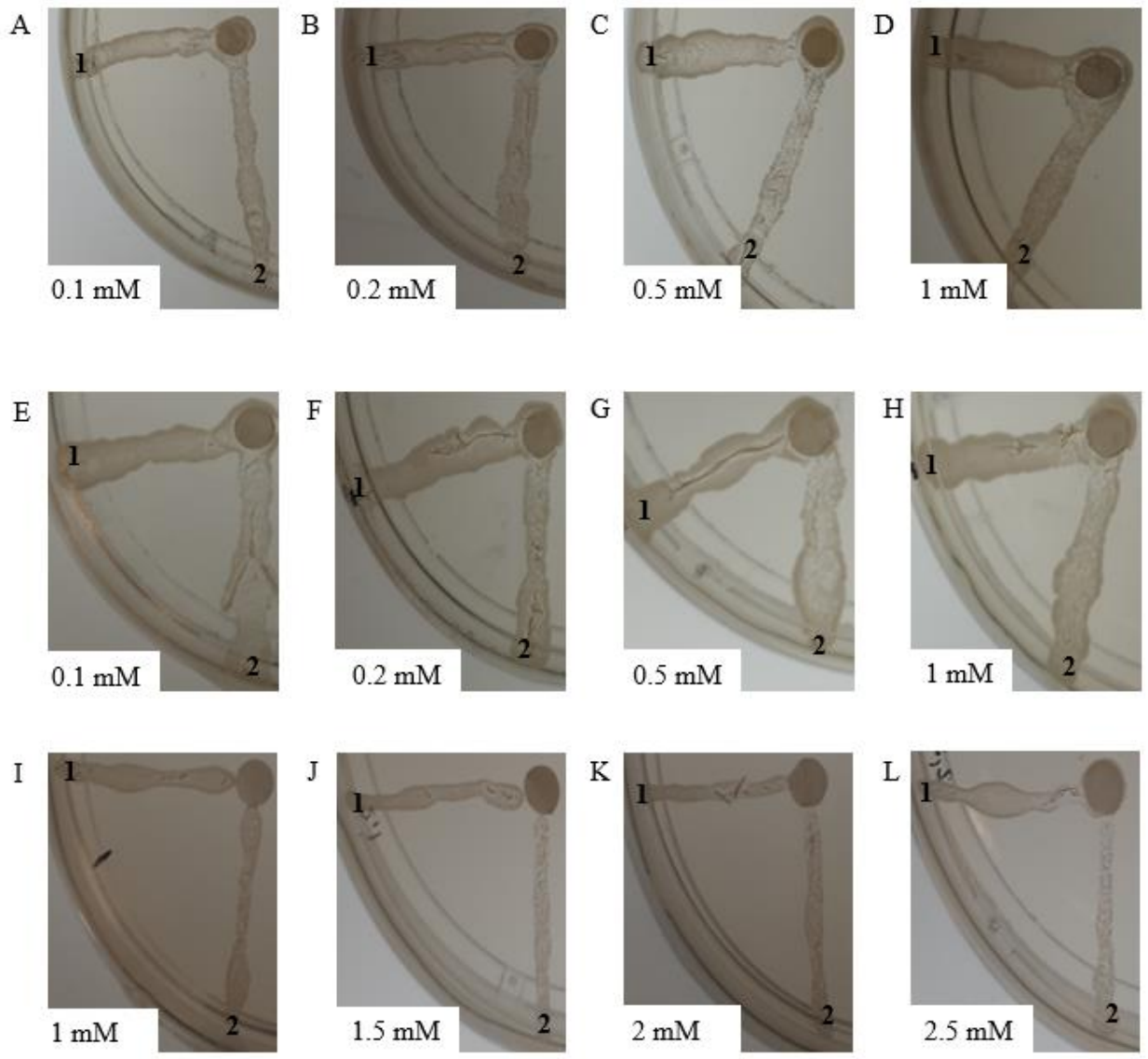

Figure 2.3: *S. pombe* SB3 sensitivity tests using a range of hydrogen peroxide and tert-butyl hydroperoxide. Undiluted (1) or 10-fold diluted (2) *S. pombe* SB3 cells were exposed to 0.1-1 mM of hydrogen peroxide (A-D), 0.1-1 mM tert-butyl hydroperoxide (E-H), and 1-2.5 mM diamide (I-L) and no halos were observed around the discs. These tests were conducted in triplicate.

2.3.3. Validation of the western blotting method of Pk-tagged Pap1 *in vivo*

To ensure the specificity of the antibody to the Pk-tag on Pap1, total protein was extracted from *S. pombe* SB3 cells exposed to 100 µM of hydrogen peroxide. Western blot analysis without the mouse anti-Pk monoclonal IgG antibody revealed no proteins (Figure 2.4), confirming the specificity of the secondary antibody.

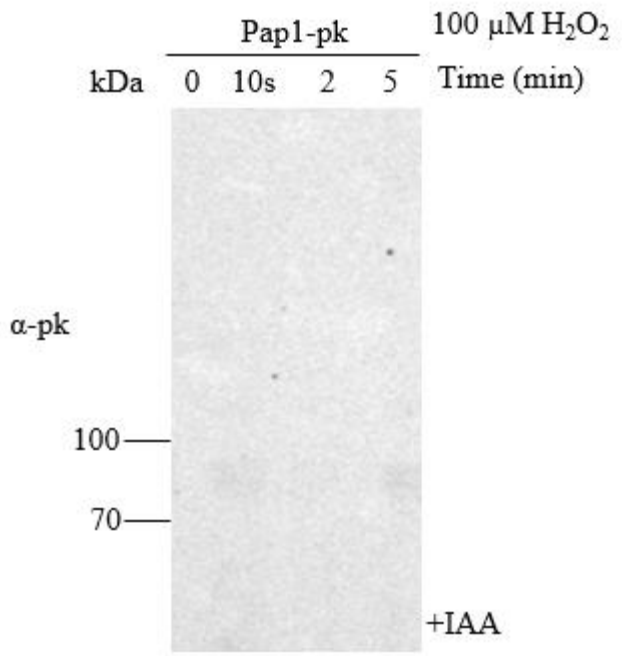

Figure 2.4: Analysis of the secondary antibody's specificity to the Pk-tagged Pap1 protein. *S. pombe* SB3 cells were exposed to 100 µM hydrogen peroxide for 5 minutes. The protein extracted was treated with IAA and subjected to western blotting without the primary antibody.

Another western blot analysis was done to ensure that the primary antibody identified the expected protein bands. *S. pombe* SB3 cells were exposed to 100 µM hydrogen peroxide, and samples were taken. As expected, western blot analysis revealed two distinct bands, which were reduced Pap1 (upper band) and oxidized Pap1 (lower band) (Figure 2.5). Reduced Pap1 ran at ~90 kDa while the oxidized band ran at ~70 kDa due to the intramolecular disulfide bonds within the protein structure (Bozonet *et al.*, 2005). An oxidation band at time zero (before addition of the oxidant) could be seen on this blot and was also observed on some later blots, but this was considered to be due to normal cellular peroxide metabolism and has been noted in previous studies (Vivancos *et al.*, 2004; Vivancos *et al.*, 2005; Brown *et al.*, 2013). Some non-specific bands were identified as indicated by an asterisk (*), but their pattern did not differ from the zero time point, suggesting that these proteins were redox-insensitive. To save space in the thesis, all other blots in the thesis were cropped to show the Pap1 bands, but full blots are available in the Appendix

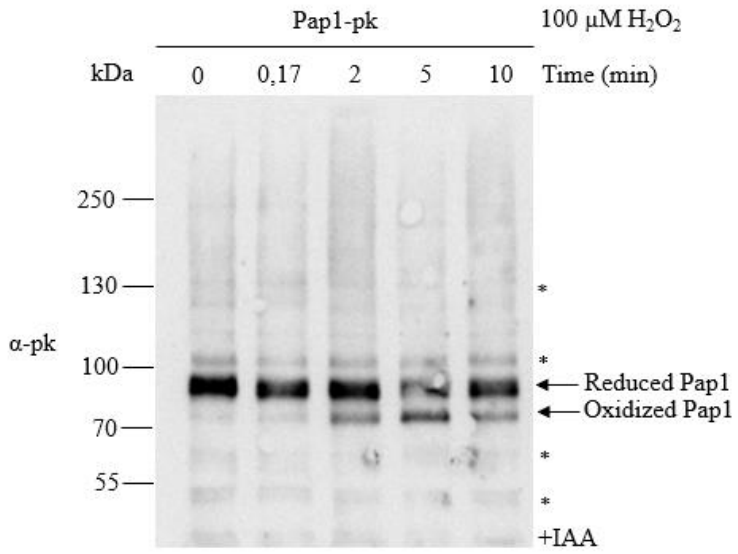

Figure 2.5: Reduced and oxidized Pk-tagged Pap1 were identified using the α-Pk monoclonal and secondary antibodies. *S. pombe* SB3 was exposed to 100 µM hydrogen peroxide and analyzed via western blotting. The antibodies successfully identified both reduced and oxidized Pap1 at ~90 and ~70 kDa, respectively. Non-specific binding is shown by an asterisk (*). Full blot available in Appendix 1 (Figure S1).

For the next step, we determined the appropriate combination of protein and antibody concentrations for western blot analysis. Protein samples extracted from unstressed *S. pombe* SB3 cells were diluted into three different absorbance values (0.15, 0.2 and 0.3 a.u) obtained from a BCA assay, pipetted directly onto the nitrocellulose membrane and then incubated in various combinations of antibody concentrations (Figure S2, Appendix 1). The dot blots were analyzed using ImageJ, which revealed that the combination of 375 µg/ml protein, which correlated to 0.15 a.u (Figure 2.6B), 1 µg/ml primary antibody, and 1:50 000 secondary antibody produced the most suitable signal in our hands (Figure 2.6A). One more set of dot blots was done using protein concentration values spanning 0-655 µg/ml (absorbance range equivalent to 0-0.3 a.u) with the antibody concentrations mentioned above (Figure S3, Appendix 1). These dot blots were then analyzed to determine whether the chosen concentration of 375 µg/ml was within the linear range for signal intensity. These results show that the range of protein and antibody concentrations used in this assay were sufficient for quantification (Figure 2.6C).

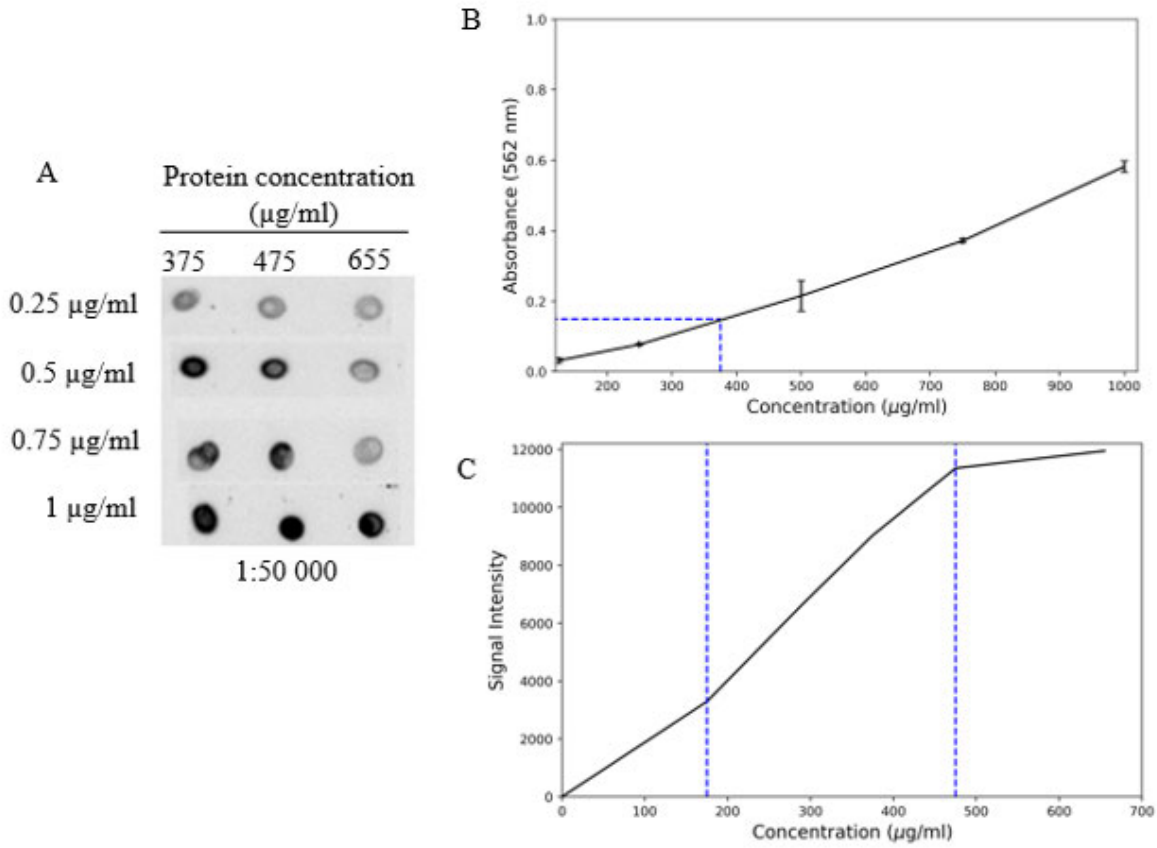

Figure 2.6: Determination of the protein and antibody concentrations for western blot analysis. Three different protein concentrations were inoculated in a range of 0.25-1 µg/ml of primary antibody and 1:50 000 secondary antibody to determine which combination will result in the best outcome (A). A standard curve was produced using the Pierce BCA protein assay kit. The absorbance value of 0.15 was extrapolated, resulting in a protein concentration of 365 µg/ml (blue lines) (B). The signal intensities were plotted against concentration to ensure the combination of protein and antibody used fell within the linear range (C).

Diamide can cause oxidative stress by interacting with glutathione and the thiol groups on proteins (Chen *et al.*, 2018b) and would therefore be a valuable oxidant to modulate the pathway in addition to the well-known oxidants hydrogen peroxide and tert-butyl hydroperoxide (Vivancos *et al.*, 2005; Chen *et al.*, 2018b; Domènech *et al.*, 2018). Therefore, the next step was to check if diamide caused Pap1 oxidation. Although *S. pombe* SB3 cells did not show sensitivity up to 2.5 mM of diamide, cells were exposed to a maximum of 2 mM as published data has tended to use a range of 1-2 mM (Song and Roe, 2008; Chen *et al.*, 2018b). Samples were taken over 10 minutes, and the protein was extracted and subjected to western blot analysis. However, there were no

significant changes in the amount of oxidized Pap1 over a truncated time-course (Figure 2.7) and this oxidant was not used further.

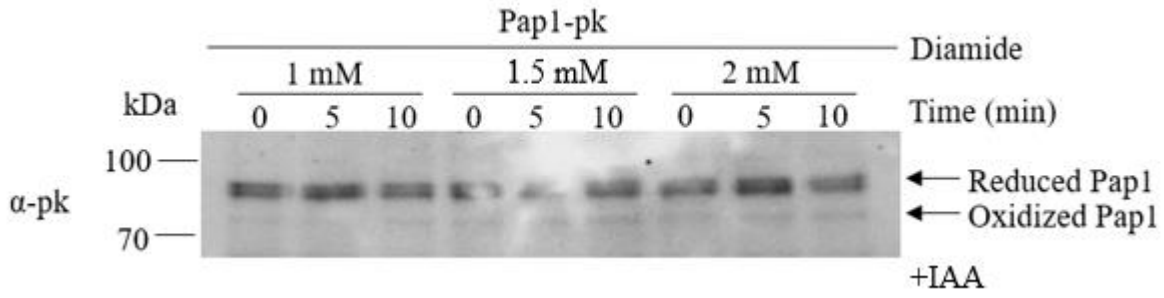

Figure 2.7: Western blot analysis of diamide treated *S. pombe* SB3 cells to determine if Pap1 oxidation occurs. Protein was extracted from *S. pombe* SB3 cells treated with 1, 1.5, and 2 mM of diamide and Pap1 oxidation was analyzed over ten minutes (Figure S4, Appendix 1).

2.3.4. Oxidation profiles of Pk-tagged Pap1 in response to exposure to 0.1-1 mM hydrogen peroxide

Hydrogen peroxide was the first oxidant used to modulate the Tpx1/Pap1 pathway. Protein isolates from *S. pombe* SB3 cells exposed to 100 µM of hydrogen peroxide for 60 minutes were subjected to western blot analysis to track the oxidation and subsequent reduction of Pap1-Pk (Figure 2.8A). Pap1 oxidation could be observed within just ten seconds after hydrogen peroxide exposure, but Pap1 was fully reduced over the time course. These experiments were carried out in triplicate, and a similar oxidation pattern was obtained in all cases (Figure S5, Appendix 1). The protocol for measuring protein from the cells using the BCA protein assay ensured that equal protein concentrations were used for each time point. However, to confirm this, the samples were treated with DTT to reduce the oxidized Pap1, resulting in a single band on the western blot (Figure 2.8B). This control showed that equivalent Pap1 concentrations were loaded onto the gel, Pap1 was reducible and further confirmed the antibody specificity (Tomalin *et al.*, 2016).

Analogous to the thioredoxin redox charge (Padayachee *et al.*, 2020), the Pap1 oxidation charge ($Pap1_{ox}/Pap1_{total}$) was determined for each time point. As the total Pap1 concentration (reduced and oxidized Pap1) does not change over the time course, it acts as an internal loading control. The oxidation profile of Pap1 at 100 µM hydrogen peroxide displayed rapid oxidation, reaching the peak of oxidation at ten minutes followed by a slow, prolonged decline in oxidation from just after ten minutes to 60 minutes (Figure 2.8C).

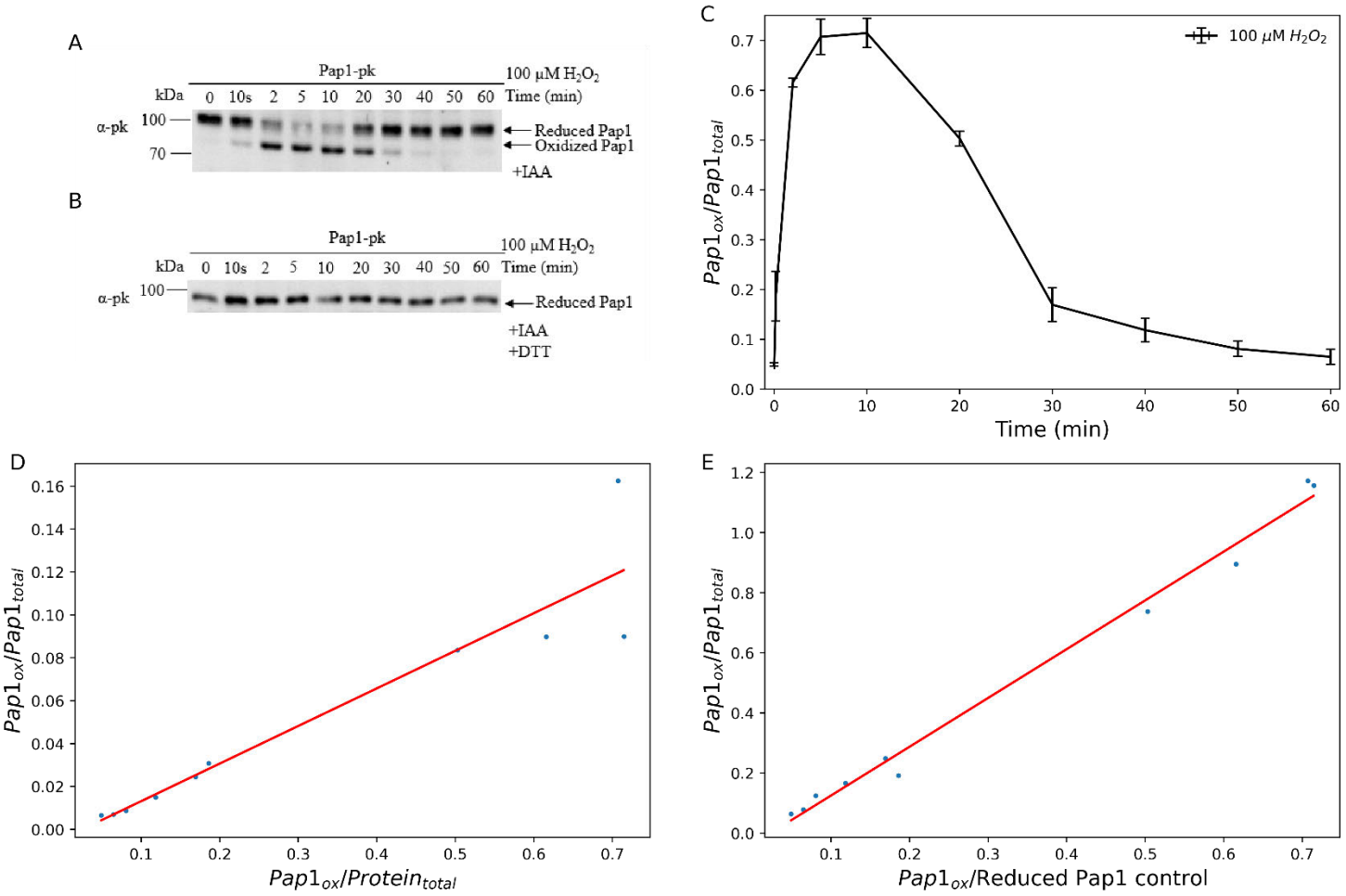

Figure 2.8: Western blot analysis of Pap1 from *S. pombe* SB3 cells exposed to 100 µM of hydrogen peroxide. Protein was extracted from these cells and visualized via western blotting. The oxidation of Pap1 was monitored over a 60 minute time course (A), and the same protein was DTT treated and used as a loading control (B). The oxidation profile of Pap1 was obtained by utilizing the signal intensity of the bands on the western blot (C). Linear regression plots of the fraction of oxidized Pap1 against the total protein (D) and reduced Pap1 control (E) values acted as controls. The means and standard errors of three separate experiments (Table S1, Appendix 1) are shown.

Two additional loading control methods were used to quantify the signals from these experiments. First, the signal intensity of oxidized Pap1 was normalized against the total protein concentration ($Protein_{total}$) per lane on Ponceau S stained blots. This method has been shown to be superior to loading controls with house-keeping proteins (Sander *et al.*, 2019; Pillai-Kastoori *et al.*, 2020). As a second loading control, oxidized Pap1 was divided by reduced Pap1 control (Tomalin *et al.*, 2016). A linear correlation was obtained between the Pap1 oxidation charge and total protein and reduced Pap1 controls showing the Pap1 oxidation charge was a comparable loading control to previously published methods (Figures 2.8D-E).

The *S. pombe* SB3 cells were challenged to an increased hydrogen peroxide concentration of 200 µM (Figure 2.9A-B), which is still within the adaptive range for the fission yeast (Figure 2.1) (Veal *et al.*, 2014). The oxidation profile of Pap1 at 200 µM showed a rapid increase in oxidation by ten seconds that peaked at two minutes (Figure 2.9C). Interestingly a second peak was obtained at 40 minutes, followed by a slow decrease in oxidation. These experiments were done in triplicate and a similar banding pattern was observed across the blots (Figure S6, Appendix 1). Once again, the loading controls appeared to show a linear correlation with each other (Figure 2.9D-E).

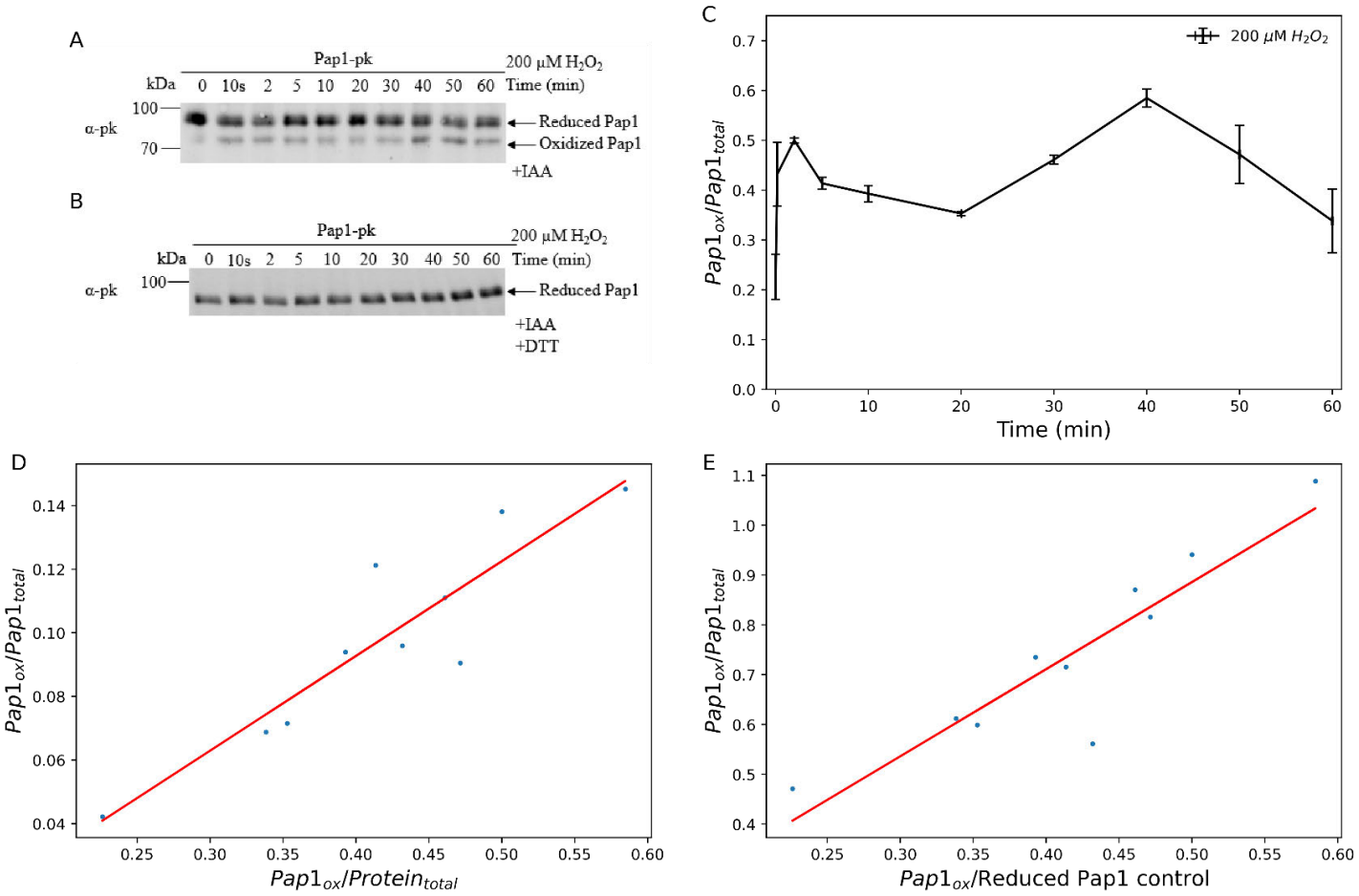

Figure 2.9: Analysis of Pk-tagged Pap1 following exposure to 200 µM of hydrogen peroxide. The oxidation of Pap1 was tracked over a 60 minute time course (A), and DDT treated samples were used as a loading control (B). The oxidation profile of Pap1 displayed a double peak in oxidation as well as a rapid increase and slow decrease in oxidation (C). Linear regression plots utilizing total protein (D) and reduced Pap1 control (E) values were used as controls. Standard errors of three separate experiments are shown (Table S2, Appendix 1).

Next, the *S. pombe* SB3 cells were exposed to 500 µM of hydrogen peroxide (Figure 2.10). Most published studies do not track Pap1 oxidation beyond 60 minutes as the doubling time of fission yeast is between two to four hours (Vivancos *et al.*, 2004; Calvo *et al.*, 2013; Domènech *et al.*, 2018). However, as a higher concentration of hydrogen peroxide was used in this assay, a longer time course of 120 minutes was utilized as an extended oxidation period was expected. The oxidation profile of Pap1 also showed two oxidation peaks (Figure 2.10A, C). The first peak occurred at ten seconds, followed by a decrease in oxidation. The oxidation gradually increased again from 20 minutes until it peaked for the second time at 50 minutes just ten minutes after the second oxidation peak in cells treated with 200 µM of hydrogen peroxide. A similar band pattern was obtained across three independent replicates (Figure S7, Appendix 1). Although an extended time course was used in this assay, Pap1 was still oxidized beyond 120 minutes. The standard loading controls for this assay revealed a linear relationship between the Pap1 oxidation charge and total protein control (Figure 2.10D), although some nonlinearity was observed with the reduced Pap1 control (Figure 2.10E).

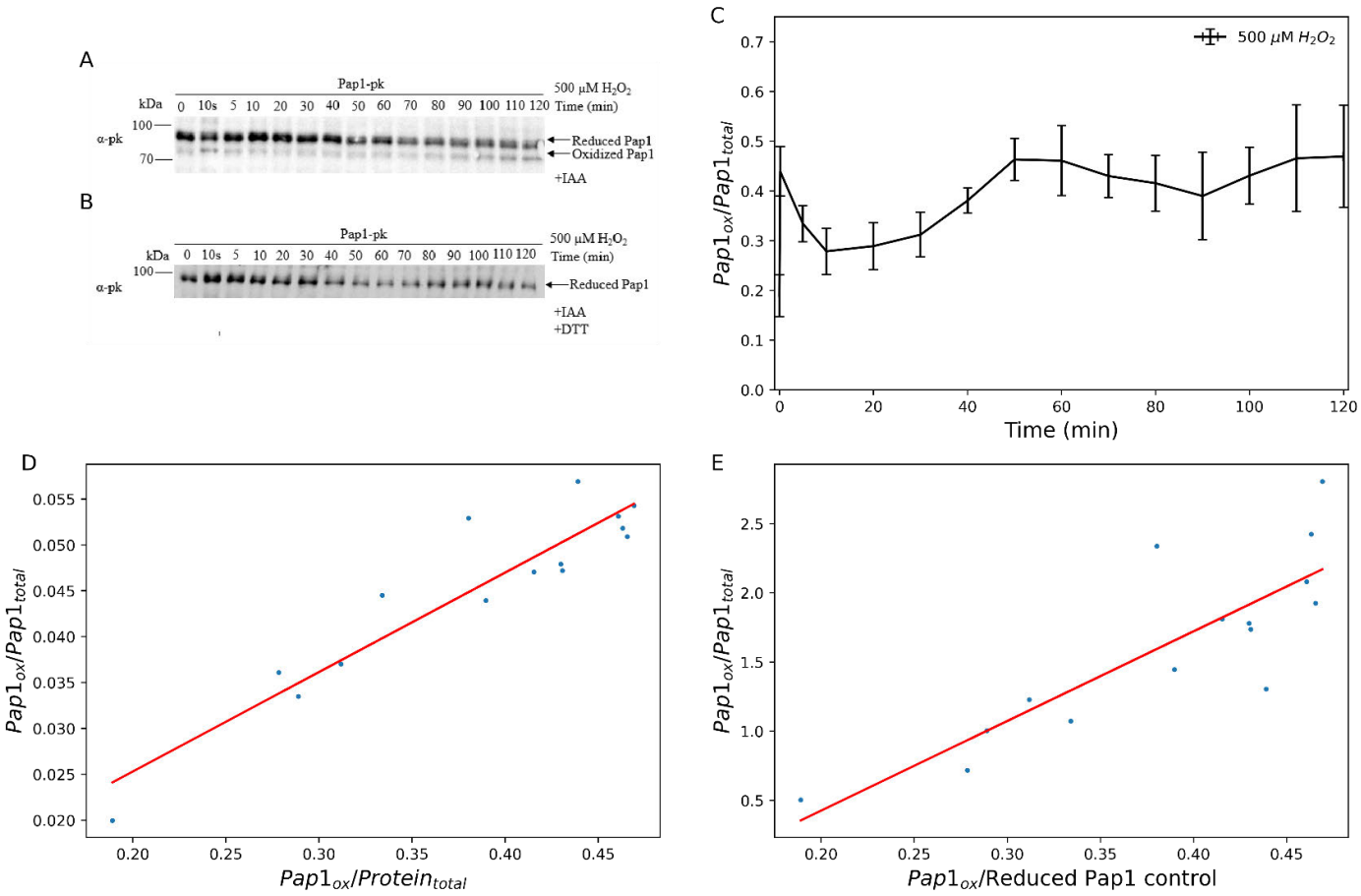

Figure 2.10: Western blot analysis of Pap1-Pk from *S. pombe* SB3 cells challenged with 500 μM of hydrogen peroxide. The oxidation of Pk-tagged Pap1 was monitored over a 120-minute time course, showing prolonged oxidation (A), and samples treated with DTT were used as a loading control (B). The resultant oxidation profile of Pap1 also exhibited two peaks in oxidation at ten seconds and 50 minutes (C). Regression plots were plotted using total protein (D) and reduced Pap1 control (E) values. The standard errors shown were obtained from three independent replicates (Table S3, Appendix 1).

The final concentration of hydrogen peroxide that *S. pombe* SB3 cells were exposed to was 1 mM which is considered a medium-range value that still evokes an adaptive response within *S. pombe* (Veal *et al.*, 2014). As with 500 μM of hydrogen peroxide, an extended time course of 120 minutes was also used for this experiment (Figure 2.11). Similarly, to the previous oxidation profiles, Pap1 showed an almost immediate increase in oxidation at ten seconds (Figure 2.11A, C) with additional peaks over the time course. The first oxidation peak was seen at ten seconds, and a second peak occurred at 40 minutes and the third peak at 110 minutes. These experiments were carried out in triplicate with a similar banding pattern obtained across all blots (Figure S8,

Appendix 1). However, unlike previous experiments, a linear correlation was not obtained with the loading controls (Figure 2.11B, D-E).

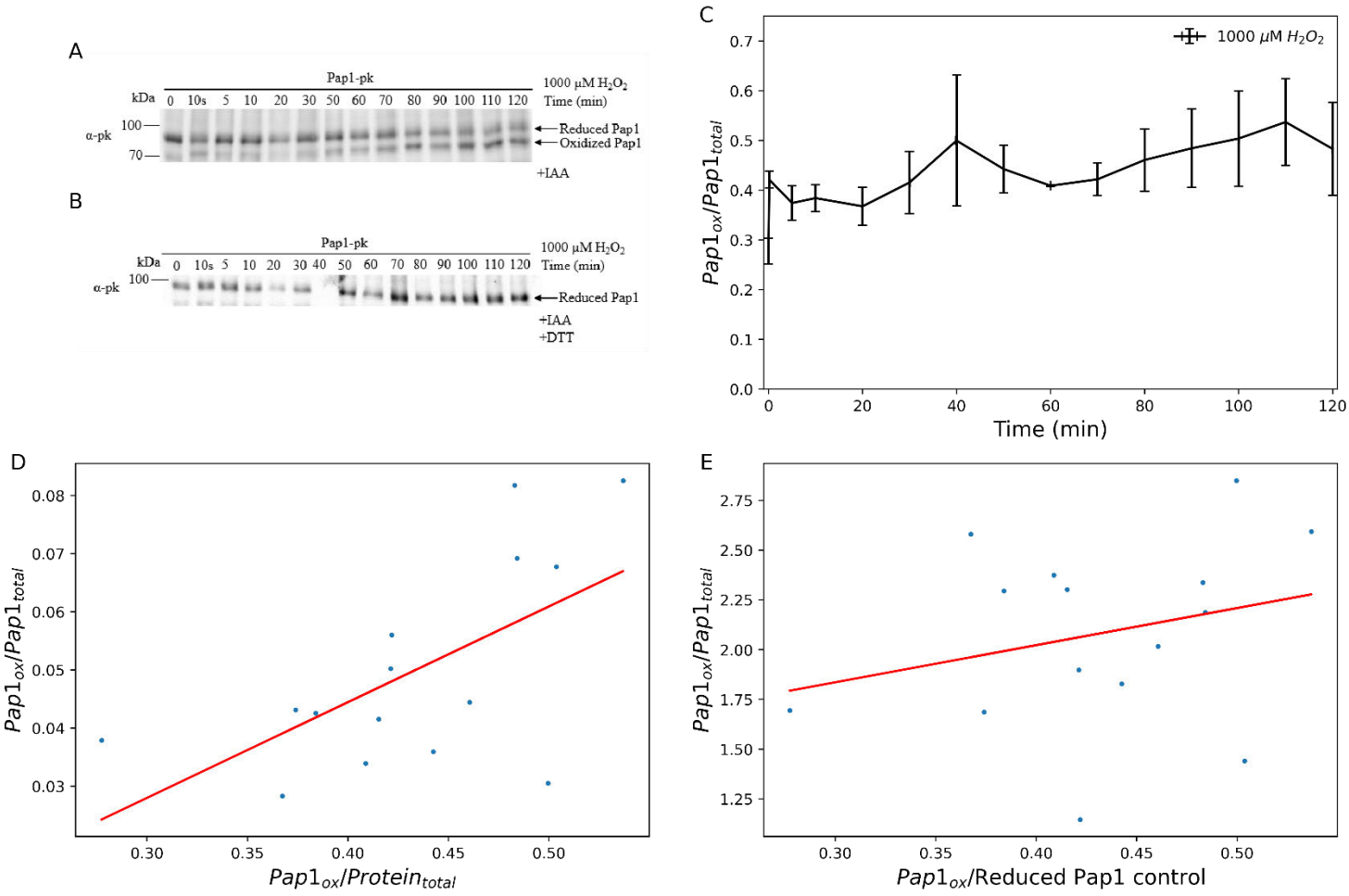

Figure 2.11: Analysis of Pap1-Pk from *S. pombe* SB3 cells treated with 1000 µM of hydrogen peroxide. The oxidation of Pk-tagged Pap1 was tracked over a 120 minute time course and showed a significant amount of oxidation still occurring at 120 minutes (A). Samples treated with DTT were used as a loading control (B). The oxidation profile of Pap1 after exposure to 1000 µM of hydrogen peroxide displayed a double peak in oxidation and a rapid increase and a slow decrease in oxidation(C). Regression plots were produced using total protein (D) and reduced Pap1 control (E) values as controls. The standard errors shown were calculated from three independent replicates (Table S4, Appendix 1).

The Pap1 oxidation profiles for 100, 200, 500, and 1000 µM of hydrogen peroxide were plotted on the same graph (Figure 2.12). Only at 100 µM of hydrogen peroxide does Pap1 show a single peak in oxidation followed by a reduction. At the other concentrations, Pap1 is rapidly

oxidized at ten seconds, followed by reduction and a gradual oxidation increase. The complete reduction of Pap1 for 100 µM of hydrogen peroxide was completed in 60 minutes, but for the 500 and 1000 µM experiments, Pap1 remained oxidized for longer than 120 minutes. Reduction of Pap1 at 200 µM hydrogen peroxide seemed to continue past 60 minutes.

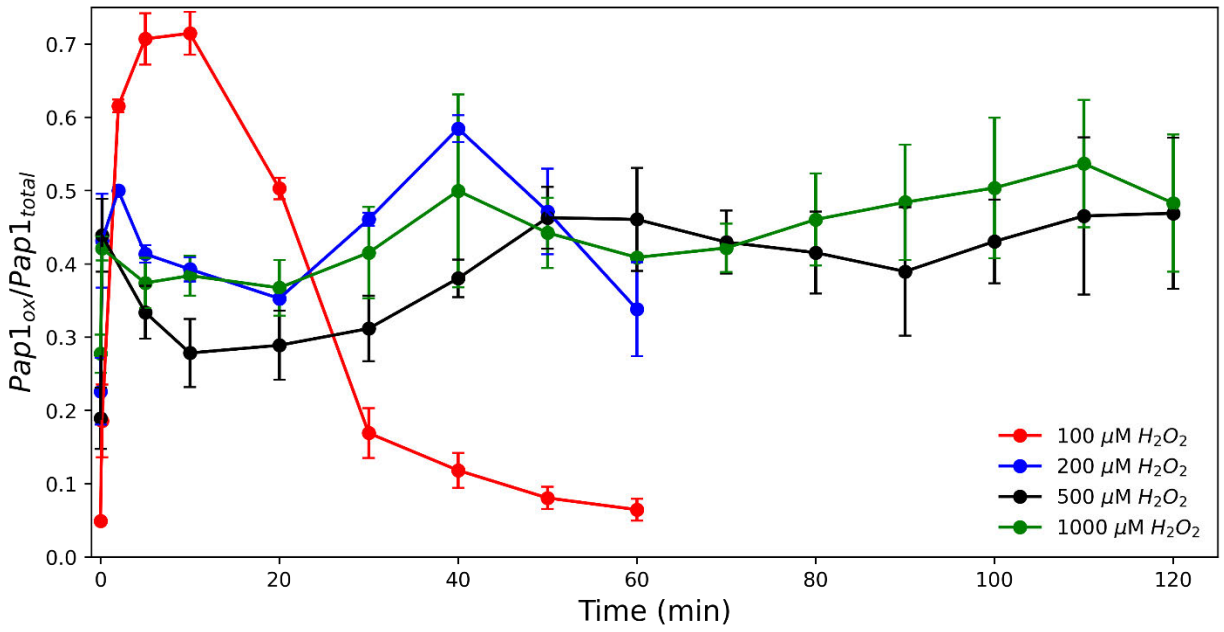

Figure 2.12: Comparison of the Pap1 oxidation profiles after treatment with 100, 200 500, and 1000 µM of hydrogen peroxide. Western blotting data were analyzed to produce the oxidation profiles of 100 and 200 µM hydrogen peroxide for 60 minutes and 500 and 1000 µM hydrogen peroxide for 120 minutes. Standard error bars represent samples taken for each time point for three independent experiments.

The oxidation profile graphs (Figure 2.12) were then used to calculate the three signalling parameters for Pap1 oxidation, viz. signalling time, signalling duration, and signalling amplitude (Table 2.3). Signalling time is the average time taken to activate (oxidize) Pap1, while signalling duration is the average time that Pap1 is activated. Signalling time is the average time taken to activate (oxidize) Pap1, while signalling duration is the average time that Pap1 is activated. Lastly, signalling amplitude is the average concentration of activated Pap1 over the signal interval (time course) (Heinrich *et al.*, 2002; Pillay *et al.*, 2016).

Table 2.3: The signalling parameter values for Pap1 from *S. pombe* SB3 cells challenged by different oxidants at different concentrations for 60 and 120-minute time courses. Values for signalling time, signalling duration, and signalling amplitude after exposure to 100-1000 µM hydrogen peroxide, 100-200 µM tert-butyl hydroperoxide, and 70-100 µM combination of both oxidants.

Type of Oxidant	Concentration (µM) of oxidant	Signalling amplitude	Signalling time (min)	Signalling duration (min)
Hydrogen Peroxide	100	0.70±0.01	17.34±0.53	13.47±0.43
	200	0.78±0.01	30.74±0.57	17.16±0.24
	500	0.71±0.04	63.91±2.43	33.71±0.83
	1000	0.77±0.01	63.10±3.36	34.38±0.46
Tert-butyl hydroperoxide[1]	100	0.56±0.05	26.16±0.19	16.53±0.04
	200	0.63±0.01	23.05±0.86	16.01±0.47
Hydrogen peroxide & tert-butyl hydroperoxide[2]	70	0.67±0.004	58.98±0.37	34.55±0.22
	100	0.60±0.03	57.47±0.17	35.09±0.13

[1] Data discussed in section 2.3.5
[2] Data discussed in section 2.3.6

A significant increase in the signalling amplitude between 100 µM and 200 µM hydrogen peroxide was noted (Figure 2.13A) while changes between 100 µM to 500 µM and 200 µM to 1000 µM hydrogen peroxide were non-significant (Table S5). Note that the signalling amplitude does not necessarily refer to the maximal output of the signalling profile but rather the average concentration of oxidized Pap1 over the time course. Increasing the hydrogen peroxide concentration from 100-500 µM resulted in dose-dependent significant increases in the signalling time and signalling duration (Figure 2.13B-C), which was expected from the signal profiles (Figure 2.12).

Thus, our results show that signalling time and duration appear to be more important indicators than signalling amplitude in these hydrogen peroxide challenge experiments. Most

studies simply use changes in oxidation on blots to characterize redox signalling (Vivancos *et al.*, 2005; Brown *et al.*, 2013). These results show that such qualitative assessments of Pap1 oxidation may be missing the vital contribution of signalling time and duration to Pap1 signalling.

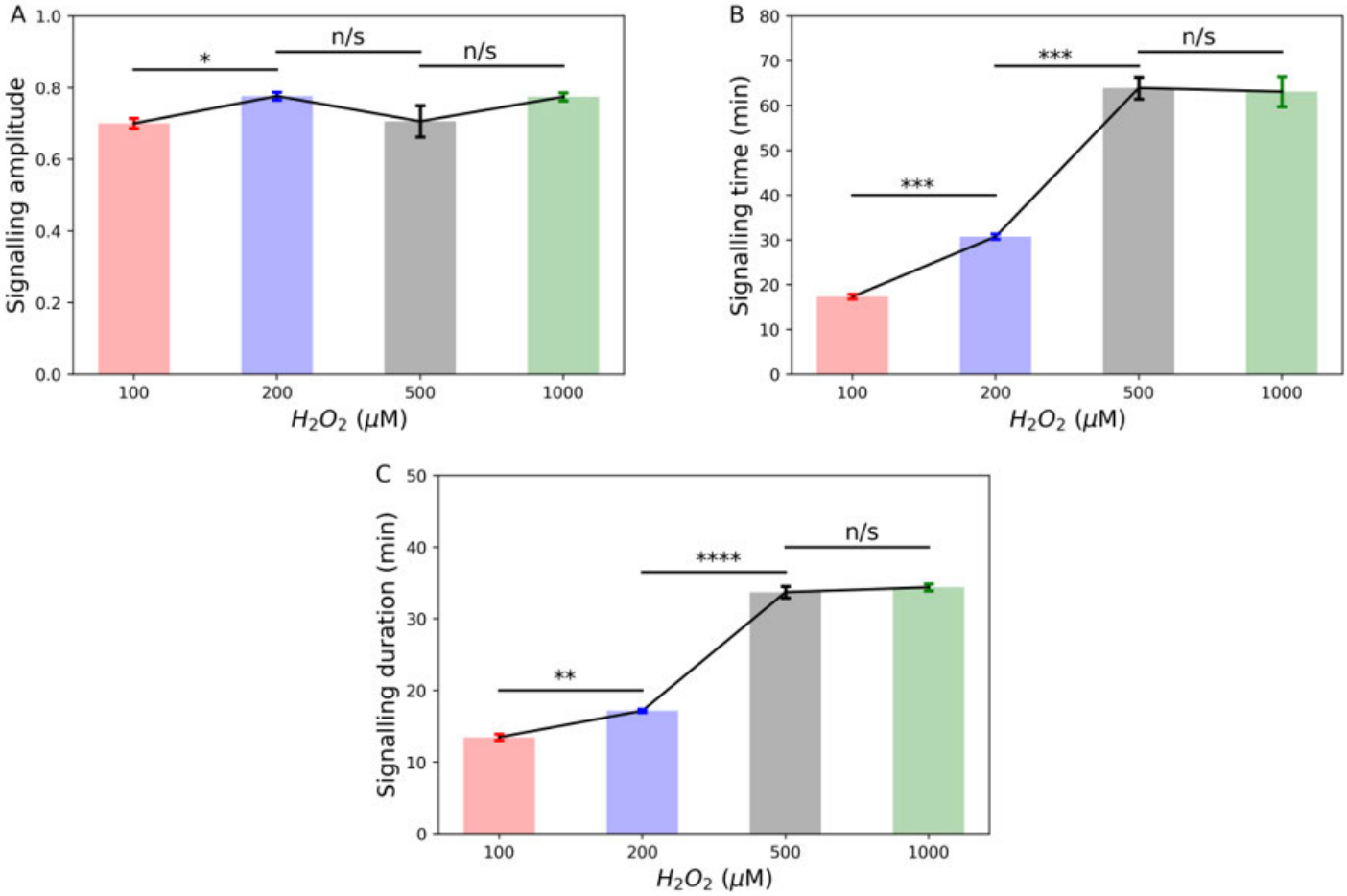

Figure 2.13: The changes in signalling parameters of Pap1 oxidation when exposed to various hydrogen peroxide concentrations. The signalling parameters viz. signalling amplitude (A), signalling time (B), and signalling duration (C) were calculated and plotted as bar graphs to visualize the data better. Significance was determined by conducting a t-test with unequal variance and one-tailed distribution, where *p<0.05, **p<0.01, ***p<0.001, ****p<0.0001 and n/s is non-significant.

As mentioned above, Pap1 oxidation was tracked over a 120-minute time course at higher oxidant concentrations to account for extended oxidation periods. Although this choice provided insight, it is also important to note that *S. pombe*'s generation time is 2.5-3 hours depending on the media and growth conditions (Petersen and Russell, 2016), and the oxidant was added to the cells when they were in the mid-log phase. This means that during the time course, the cells were

actively dividing, and by the two-hour mark, there would have been an increase in the number of cells in the culture. As the time course proceeds, the amount of oxidant would subsequently be diluted across the new cells compared to the beginning of the time course. Therefore, the datasets were trimmed to 60 minutes and the signalling parameters recalculated (Table 2.4).

Table 2.4: Signalling parameters of Pap1 oxidation limited to a 60 minutes time course. Values for the signalling parameters from cells treated with hydrogen peroxide only or a combination of hydrogen peroxide and tert-butyl hydroperoxide were recalculated to only include data up to 60 minutes.

Type of Oxidant	Concentration (µM) of oxidant	Signalling amplitude	Signalling time (min)	Signalling duration (min)
Hydrogen Peroxide	100	0.70±0.01	17.34±0.53	13.47±0.43
	200	0.78±0.01	30.74±0.57	17.16±0.24
	500	0.59±0.04	32.74±0.79	18.44±0.17
	1000	0.7±0.08	30.95±0.28	17.85±0.4
Tert-butyl hydroperoxide[1]	100	0.56±0.05	26.16±0.19	16.53±0.04
	200	0.63±0.01	23.05±0.86	16.01±0.47
Hydrogen peroxide & tert-butyl hydroperoxide[2]	70	0.63±0.01	29.83±0.18	18.62±0.19
	100	0.61±0.03	28.74±0.13	18.19±0.11

[1] Data discussed in section 2.3.5
[2] Data discussed in section 2.3.6

After reevaluation of the signalling parameters, it was found that the signal amplitude change between 200 µM and 500 µM hydrogen peroxide became significant while the difference from 500 µM to 1000 µM remained non-significant (Figure 2.14A). The difference in signalling time between 200 µM and 500 µM of hydrogen peroxide was no longer significant (Figure 2.14B). Although the signalling time of 500 µM and 1000 µM decreased to 32.74 and 30.95, respectively, this difference remained non-significant (Table 2.4 and Figure 2.14B). The change in signalling duration from 200 µM to 500 µM hydrogen peroxide remained significant but at a lower *p*-value

than previously measured, while the difference between 500 µM and 1000 µM was still non-significant (Figure 2.14C). Nonetheless, the difference in signalling time values when comparing 100 µM to 500 µM and 1000 µM were significant (Table S5). However, in contrast to the full-time course values, the difference between 200 µM and 1000 µM was non-significant. The same pattern was also found for signalling duration, while the signalling amplitude differences were non-significant (Table S5). Overall the signalling time and duration values for hydrogen peroxide concentrations at 500 µM and 1000 µM decreased by almost half of the original values in Table 2.4. Interestingly, in contrast, the signal amplitude values for these two concentrations decreased slightly compared to the initial signal amplitude values. Collectively, this shows that the Tpx1/Pap1 pathway seems to reach its peak signalling time and duration by 500 µM hydrogen peroxide.

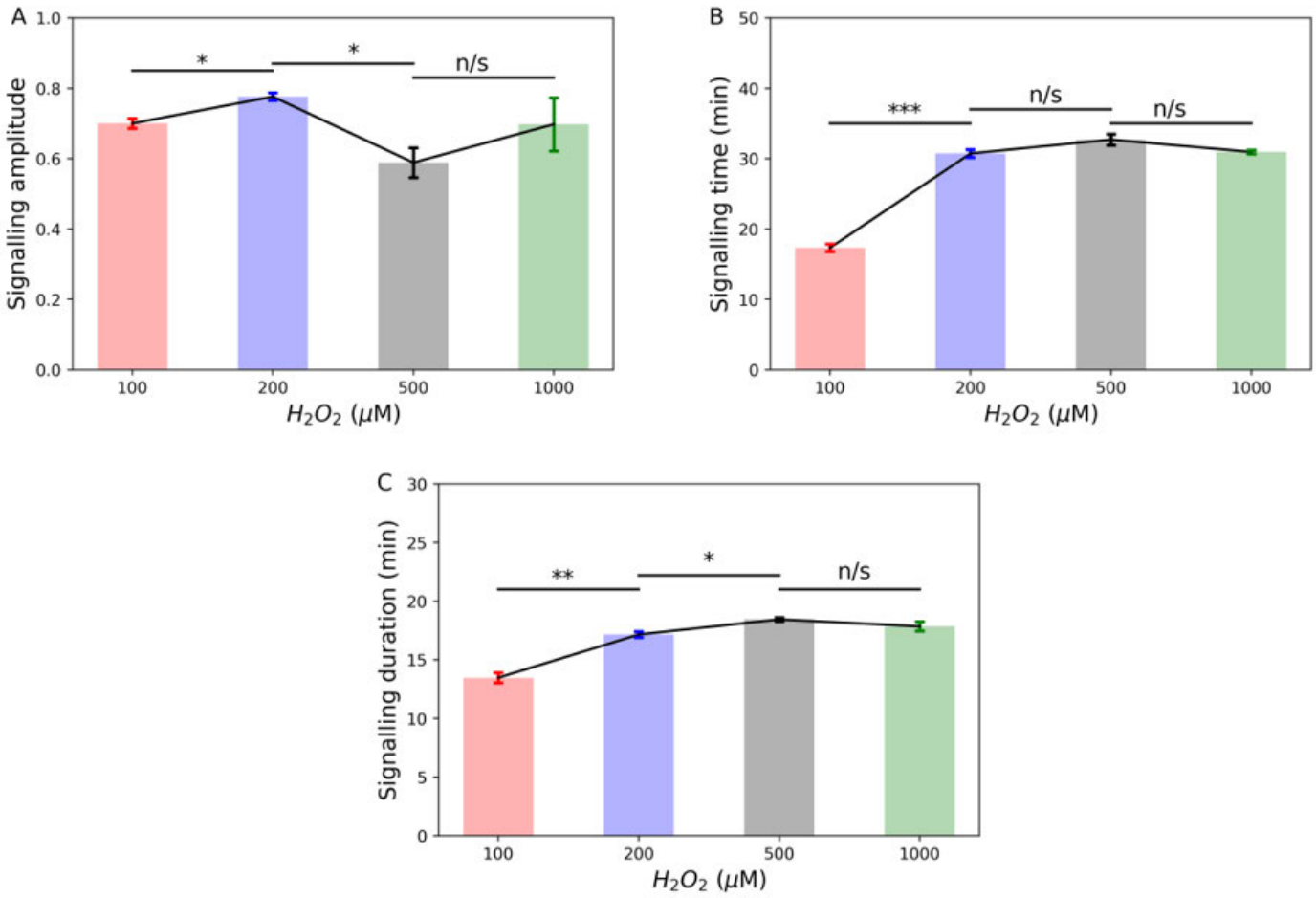

Figure 2.14: Bar graphs showing the differences between signalling parameters at different hydrogen peroxide concentrations for a 60-minute time course. The new signalling amplitude (A), signalling time (B), and signalling duration (C) parameters were produced using only data up to 60 minutes in each

time course. Significance between the parameter values for each concentration were determined by conducting a t-test with unequal variance and one-tailed distribution, where *p<0.05, **p<0.01, ***p<0.001, ****p<0.0001 and n/s is non-significant.

2.3.5. Oxidation profiles of Pk-tagged Pap1 in response to exposure to 100 µM and 200 µM tert-butyl hydroperoxide

S. pombe SB3 cells were treated with tert-butyl hydroperoxide to determine how it would modulate the Pap1 oxidation profile. Tert-butyl hydroperoxide is an organic lipid hydroperoxide analogue that causes oxidative stress as it results in the formation of tert-butoxyl radicals, and fission yeast cells lacking Pap1 showed sensitivity to the oxidant (Toone *et al.*, 1998). *S. pombe* SB3 cells were exposed to a maximum of 200 µM of tert-butyl hydroperoxide as an increase in concentration to 500 µM resulted in no quantifiable oxidation (Figure S9, Appendix 1). This was most likely due to tert-butyl hydroperoxide being able to hyperoxidize Tpx1 at lower concentrations than hydrogen peroxide (Elizabeth Veal, unpublished observations).

S. pombe SB3 cells were exposed to 100 µM tert-butyl hydroperoxide, and samples were taken over a 60-minute time course (Figure 2.15A, B). The oxidation profile showed a single peak at five minutes, which was slightly faster than seen in cells treated with 100 µM of hydrogen peroxide (Figure 2.8C). Pap1 oxidation slowly decreased until 60 minutes (Figure 2.15C), and both loading controls for this assay revealed a linear relationship between the Pap1 oxidation charge and total protein control (Figure 2.15D, E). A similar band pattern was observed across three independent replicates (Figure S10, Appendix 1).

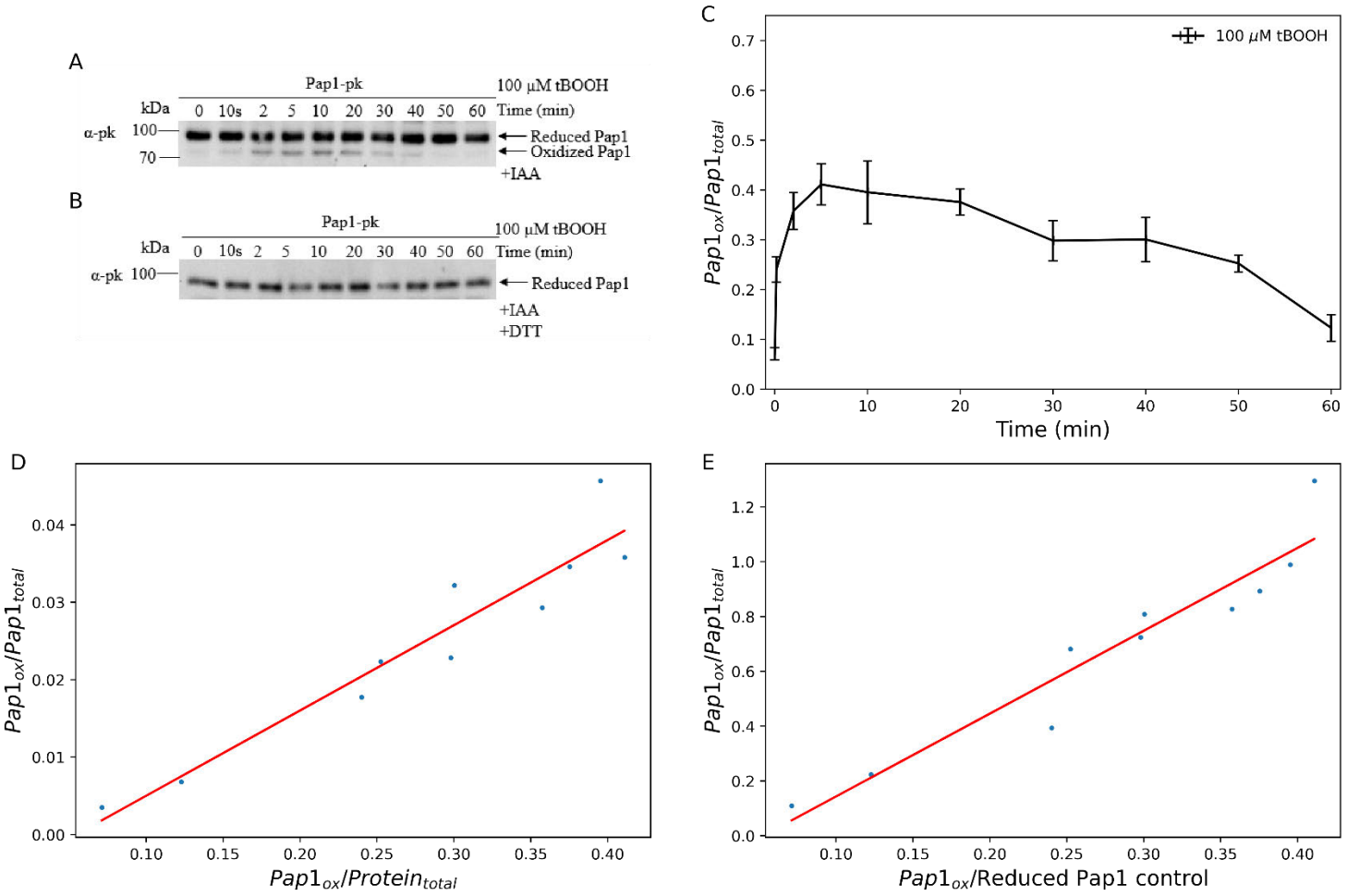

Figure 2.15: Analysis of Pap1-Pk from *S. pombe* SB3 cells exposed to 100 µM of tert-butyl hydroperoxide (tBOOH). The resultant oxidation of Pap1-Pk was tracked over a 60 minutes time course (A). DTT-treated samples were used as a loading control (B). The oxidation profile of Pap1 displayed a rapid increase and extended decrease (C). Total protein (D) and reduced Pap1 control values (E) were used as controls by plotting regression plots. Standard errors shown represent three separate replicates (Table S5, Appendix 1).

The concentration of tert-butyl hydroperoxide was then increased to 200 µM, and the time course was kept at 60 minutes (Figure 2.16A, B). Similarly to that of 100 µM tert-butyl hydroperoxide, an increase in Pap1 oxidation was observed by ten seconds with a peak occurring at five minutes and Pap1 was mostly reduced by 40-50 minutes (Figure 2.16C). Interestingly, the oxidation profile did not have a double peak obtained with the 200 µM hydrogen peroxide treatment showing that different oxidants can have distinct effects on the Pap1 signal profile. These experiments were performed in triplicate with a similar banding pattern obtained across all blots

(Figure S11, Appendix 1). Loading control methods appeared to show a linear correlation with each other (Figure 2.16D-E).

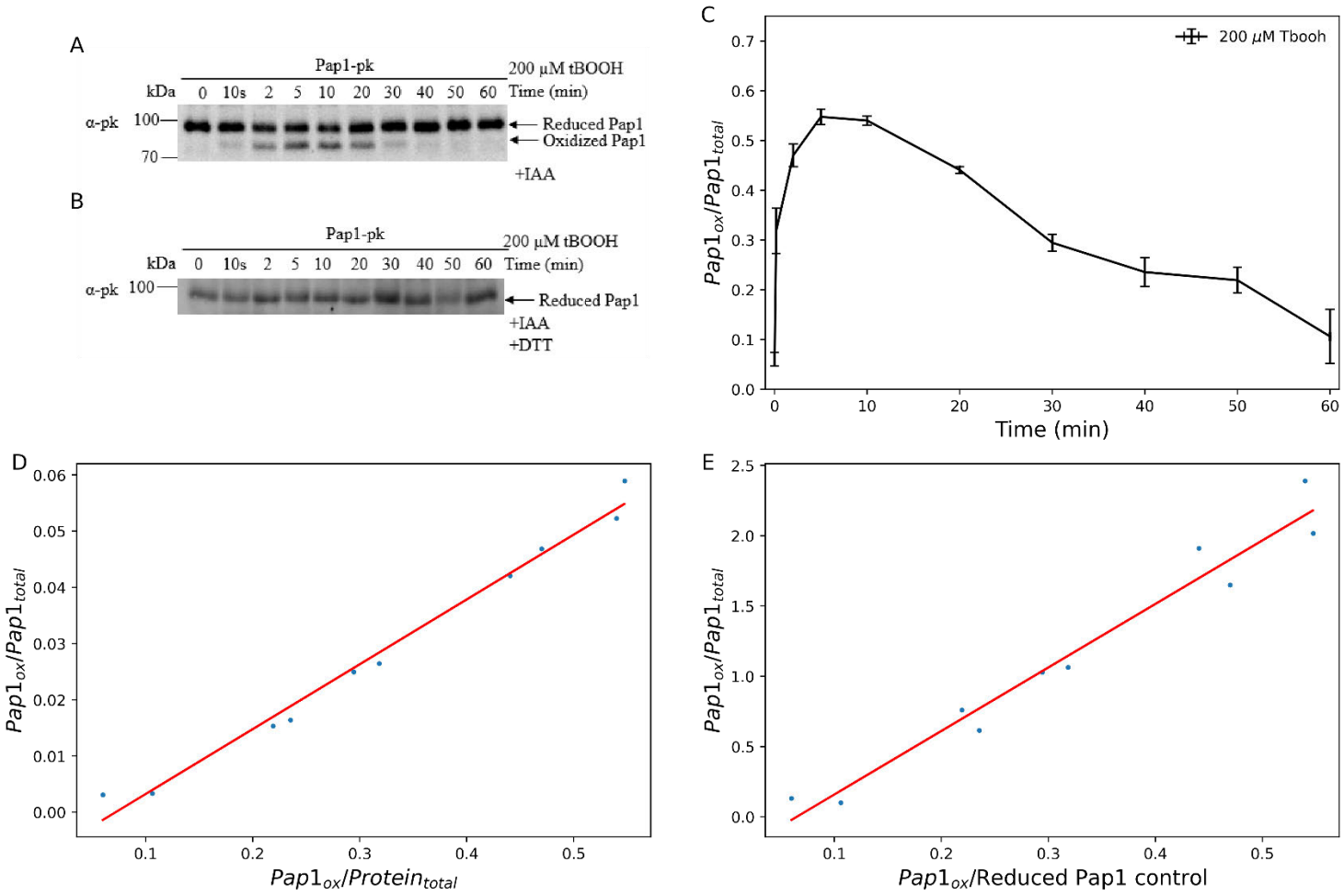

Figure 2.16: Western blotting and analysis of Pap1-Pk from *S. pombe* SB3 cells challenged with 200 µM tert-butyl hydroperoxide. Protein was extracted from samples taken over a 60 minutes time course and subjected to western blotting (A). DTT treated samples were used as a loading control (B). The oxidation profile of Pap1-Pk was produced through ImageJ analysis of the western blot (C). Regression plots utilizing total protein (D) and reduced Pap1 control (E) values were also used as controls. Standard errors shown represent three separate experiments (Table S6, Appendix 1).

When comparing the oxidation profiles of 100 µM and 200 µM tert-butyl hydroperoxide, it was found that both peaked at five minutes and followed a similar pattern (Figure 2.17). However, 200 µM tert-butyl hydroperoxide had a higher peak in oxidation (Figure 2.17).

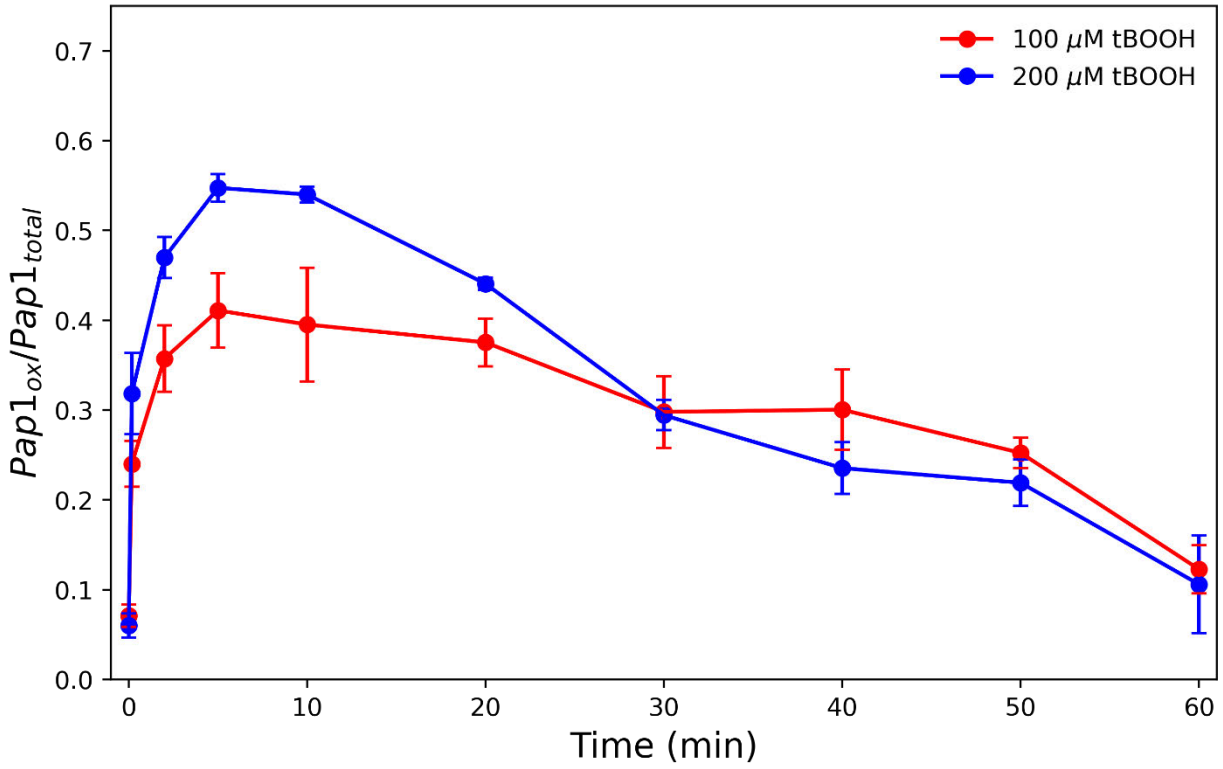

Figure 2.17: Comparison of Pap1 oxidation profiles after treatment with 100 µM and 200 µM of tert-butyl hydroperoxide (tBOOH). Signal intensities from the corresponding western blots were used to produce the oxidation profiles. Standard errors bars represent samples taken for each time point from three independent replicates.

The oxidation profiles of Pap1 treated with tert-butyl hydroperoxide (Figure 2.17) were used to calculate the signalling parameters (Table 2.3). Interestingly, the increase from 100 µM to 200 µM tert-butyl hydroperoxide showed a non-significant difference in signalling amplitude and duration (Figure 2.18A, C). This indicates that the average time that Pap1 is active (signalling duration) is comparable between the 100 µM and 200 µM tert-butyl hydroperoxide treatments. The signalling time also showed a significant decrease between 100 µM and 200 µM tert-butyl hydroperoxide (Figure 2.18B), in contrast to the increase noted between the same concentrations for hydrogen peroxide.

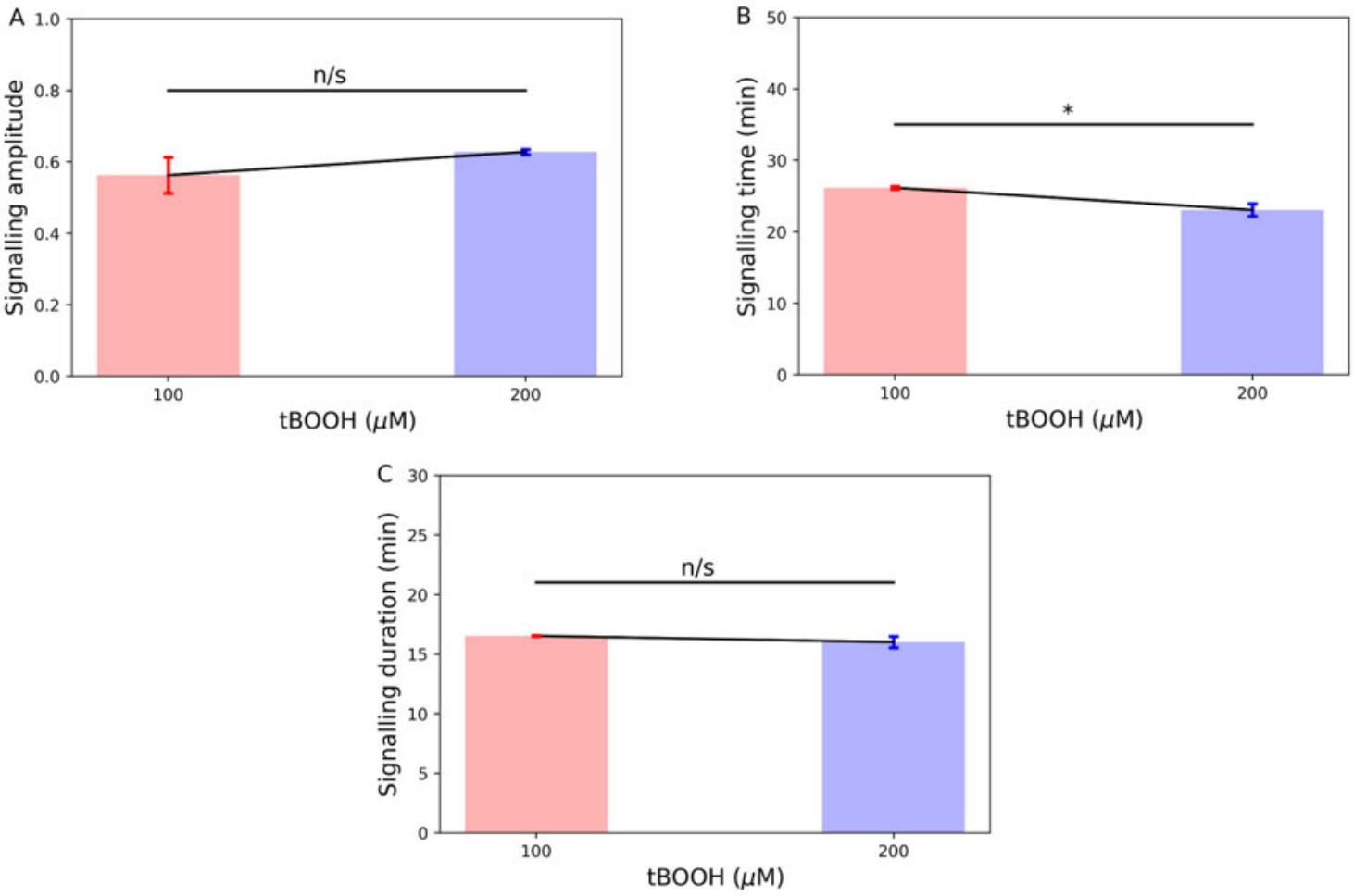

Figure 2.18: Bar graphs showing the differences between signalling parameters of Pap1 oxidation from cells treated with 100 µM and 200 µM tert-butyl hydroperoxide (tBOOH). The signalling amplitude (A), signalling time (B) and signalling duration (C) were calculated from the western blots of Pap1. Significance was determined by conducting a t-test with unequal variance and one-tailed distribution, where *p<0.05, **p<0.01, ***p<0.001, ****p<0.0001 and n/s is non-significant.

2.3.6. Oxidation profiles of Pk-tagged Pap1 in response to exposure to 70 µM and 100 µM of hydrogen peroxide and tert-butyl hydroperoxide

The Pap1 oxidation profile shape following treatment with 100 µM (Figure 2.15C) and 200 µM (Figure 2.16C) tert-butyl hydroperoxide was similar to 100 µM hydrogen peroxide (Figure 2.8C) as shown in Figure 2.19. The tert-butyl hydroperoxide profiles were surprisingly different from 200 µM hydrogen peroxide (Figure 2.9C) and did not contain a second peak. Therefore, an interesting consideration to explore was the effect on Pap1 oxidation profiles and signalling parameters by exposing the cells to a combinational stress of hydrogen peroxide and tert-butyl hydroperoxide.

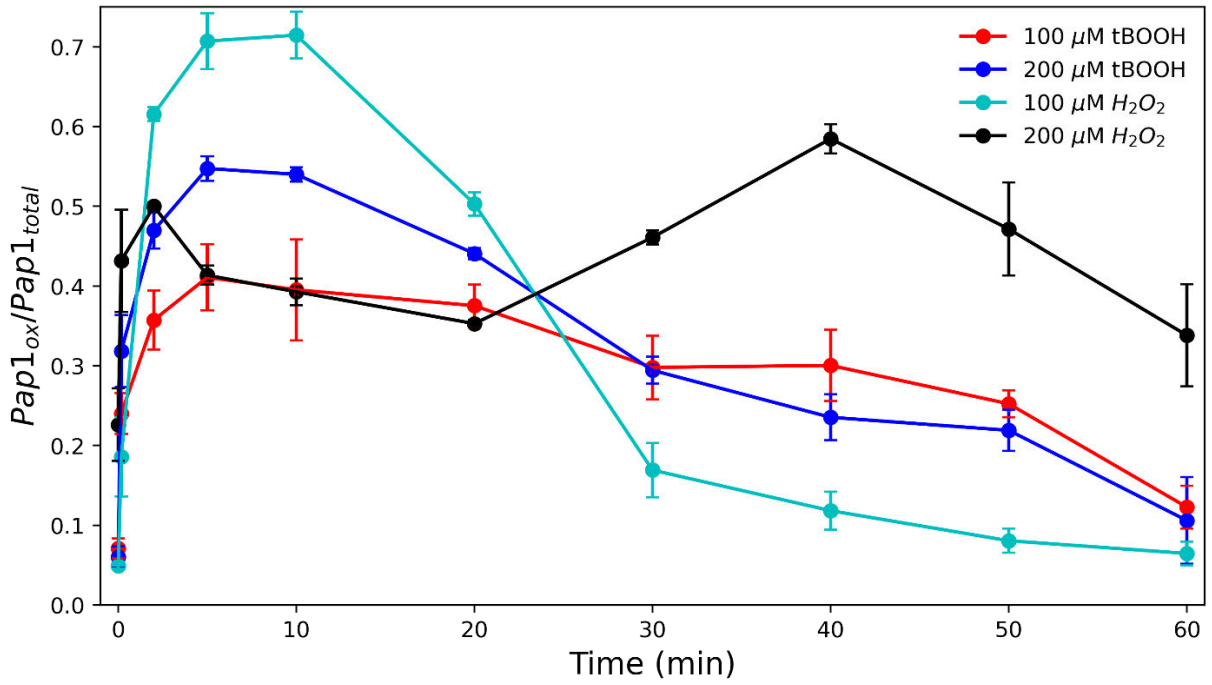

Figure 2.19: Comparison of the Pap1 oxidation profiles obtained from *S. pombe* SB3 cells exposed to 100 µM and 200 µM of hydrogen peroxide and tert-butyl hydroperoxide. Standard error bars represent samples taken from three independent replicates for each time point.

Using 200 µM of each oxidant did not result in any quantifiable change in oxidation over time (Figure S12, Appendix 1). The lowest concentration of hydrogen peroxide that causes oxidation of Pap1 is 70 µM (Veal *et al.*, 2014; Domènech *et al.*, 2018), and it was decided to use this concentration and 100 µM for each oxidant. *S. pombe* SB3 cells were simultaneously exposed to a combination of 70 µM hydrogen peroxide and tert-butyl hydroperoxide (Figure 2.20A-B). As with the higher concentrations of hydrogen peroxide, a 120-minutes time course was used for this experiment. Pap1 oxidation showed two peaks in oxidation which occurred at ten seconds and 60 minutes and were followed by a gradual decrease in oxidation resulting in Pap1 being reduced mainly by 120 minutes (Figure 2.20C). A similar band pattern was observed across three independent replicates (Figure S13, Appendix 1). The loading controls for this assay revealed a partially linear relationship between the Pap1 oxidation charge and total protein control (Figure 2.20D), with a non-linear relationship observed with the reduced Pap1 control (Figure 2.20E)

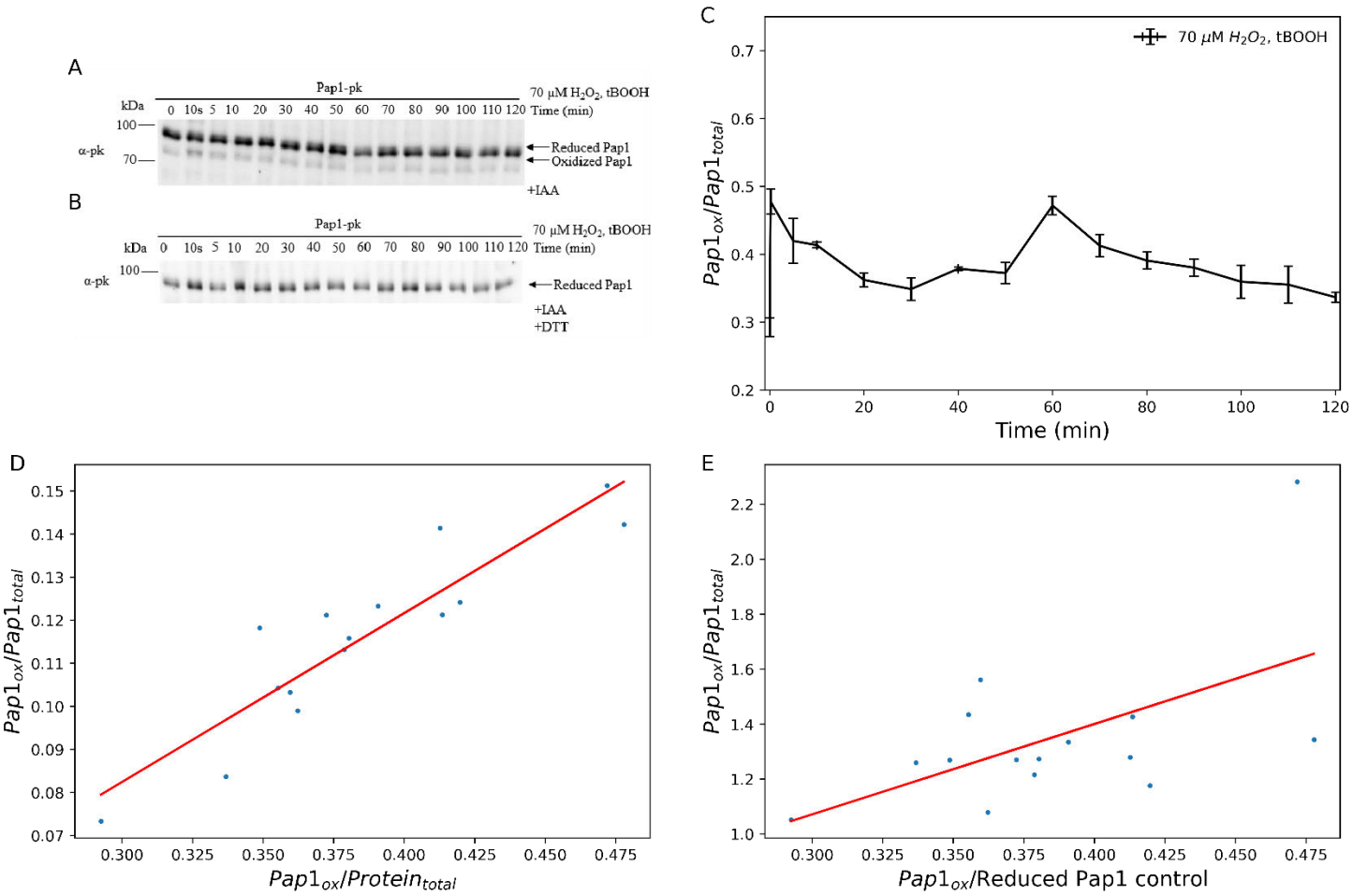

Figure 2.20: Analysis of Pap1 oxidation from *S. pombe* SB3 cells after treatment of a combination of 70 µM hydrogen peroxide and tert-butyl hydroperoxide. Protein samples from a 120-minute time course were run on a western blot to visualize the oxidation pattern (A). DTT treated samples were used as a loading control (B). The oxidation profile produced using signal intensities from the western blot revealed two oxidation peaks occurring at ten seconds and 60 minutes (C). Total protein (D) and reduced Pap1 control (E) values were used as loading controls. Standard errors shown are from three independent experiments (Table S7, Appendix 1).

The concentrations of both oxidants used to challenge *S. pombe* SB3 cells were then increased to 100 µM (Figure 2.21). A rapid increase in Pap1 oxidation was observed at ten seconds, but surprisingly there was no prominent second peak in oxidation as seen with 70 µM hydrogen peroxide and tert-butyl hydroperoxide (Figure 2.21A, C). Instead, after the first peak, small fluctuations in oxidation occurred from 30 minutes until the end of the time course. These experiments were carried out in triplicate and a similar band pattern was observed across all blots (Figure S14, Appendix 1). Some non-linearity was observed between the Pap1 oxidation charge

and total protein control (Figure 2.21D), while a lack of linearity was revealed with the reduced Pap1 control values (Figure 2.21E).

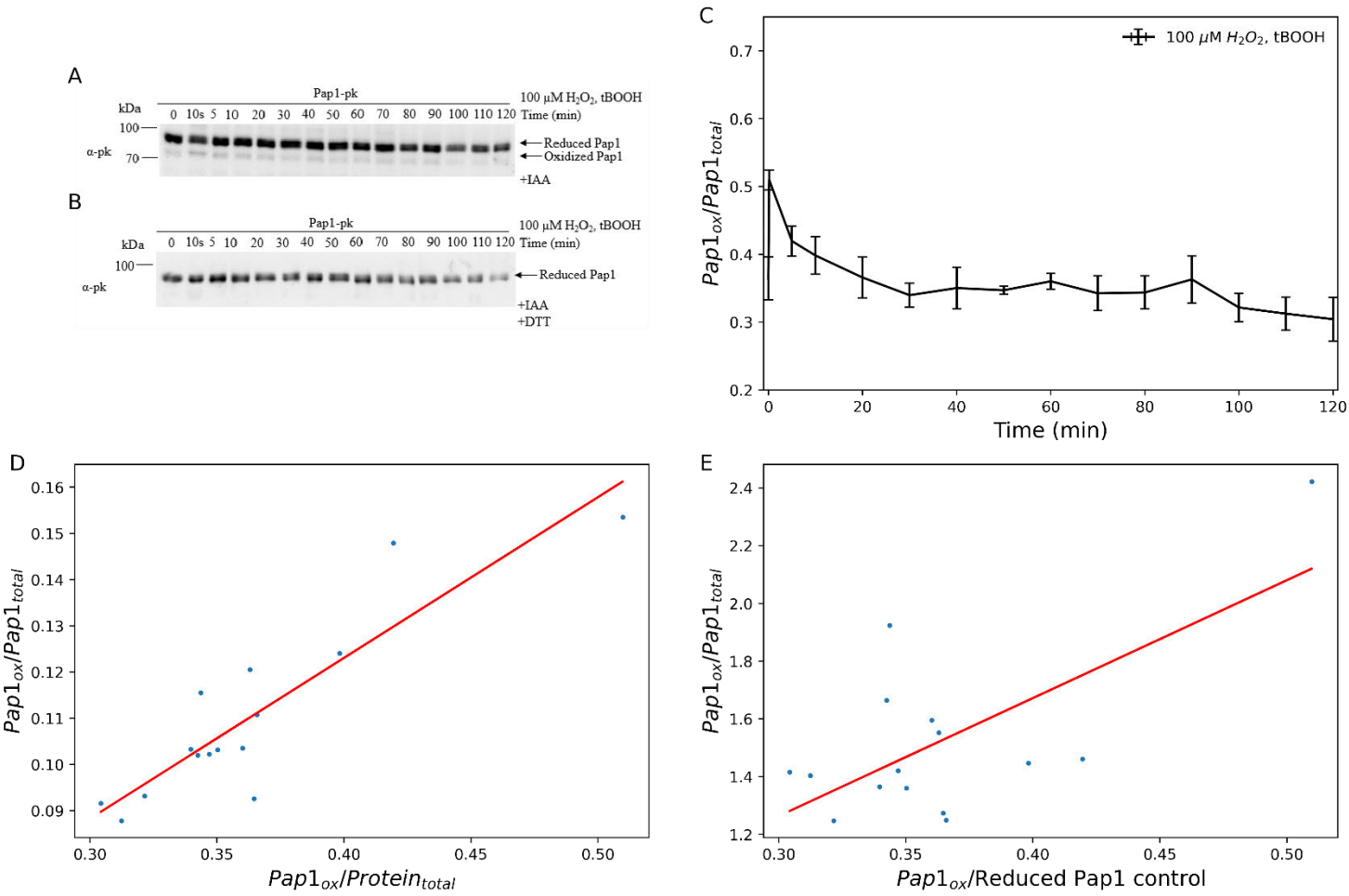

Figure 2.21: Analysis of Pap1 oxidation after exposure to 100 µM of hydrogen peroxide and tert-butyl hydroperoxide. After oxidant addition, protein was extracted from *S. pombe* SB3 cells and analyzed by Western blotting, which showed baseline oxidation at zero seconds that increased by ten seconds (A). Protein samples were treated with DTT and used as a loading control (B). The oxidation profile of Pap1 displayed a single peak in oxidation at ten seconds, thereafter decreasing for the remainder of the time course (C). Total protein (D) and reduced Pap1 control (E) values were used as controls. The standard errors represent three independent experiments (Table S8, Appendix 1).

When comparing the oxidation profiles for both combinational stress experiments, it was found that they both had a similar pattern. Both profiles showed a considerable increase in oxidation at ten seconds, followed by a gradual reduction of Pap1 (Figure 2.22). A second peak in oxidation was seen at 70 µM of hydrogen peroxide and tert-butyl hydroperoxide but was not

observed at 100 µM. Surprisingly the initial stages (0-20 minutes) of the combinational stress oxidation profiles showed a lot of similarity to the 1000 µM hydrogen peroxide profile (Figure 2.22). These oxidation profiles show an initial increase at ten seconds, followed by a slight decrease in oxidation lasting about 20 minutes. In contrast, the oxidation profiles of 100 µM hydrogen peroxide (Figure 2.8C) and both tert-butyl hydroperoxide concentrations (Figure 2.11C and 2.16C) showed a rapid increase until 5-10 minutes followed by a slow decrease until Pap1 is fully reduced.

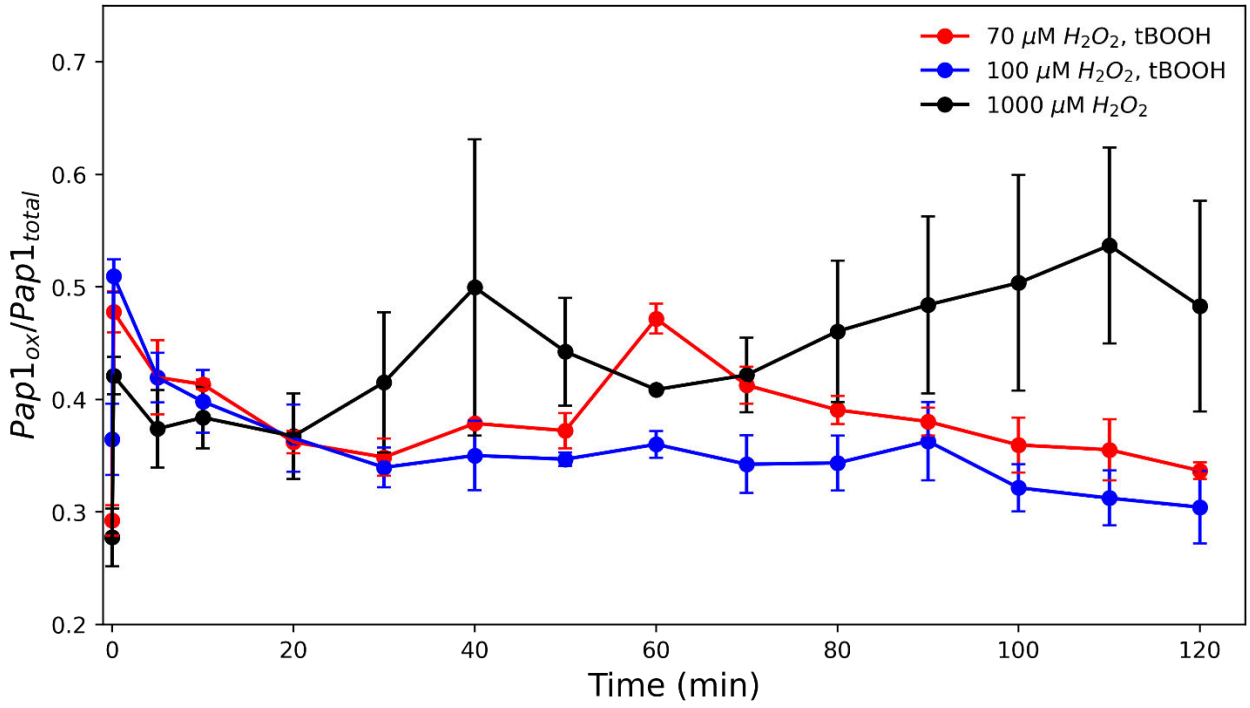

Figure 2.22: Comparison of Pap1 oxidation profiles following treatment with different oxidants. Western blotting data from cells challenged with 70 µM and 100 µM of hydrogen peroxide and tert-butyl hydroperoxide were used to produce the resultant oxidation profiles that were also compared to the profiles obtained from treatment with 500 µM and 1000 µM hydrogen peroxide.

The above oxidation profiles of the combinational stresses (Figure 2.22) were used to determine the signalling parameters for this condition (Table 2.3). Signalling amplitude and duration for 70 µM and 100 µM hydrogen peroxide and tert-butyl hydroperoxide showed no significant difference between the values (Figure 23A, C). In contrast, signalling time did show a significant difference in the change in concentrations (Figure 2.23B). The signalling parameters

for 70 µM combinational stress (signalling time=58.98 and signalling duration=34.55) and 100 µM combinational stress (signalling time=57.47 and signalling duration=35.09) were similar to 1000 µM hydrogen peroxide (signalling time=63.10 and signalling duration=34.38). Further, they were much higher than 100 µM hydrogen peroxide (signalling time=17.34 and signalling duration= 13.47), showing that the combinational stresses led to a profile similar to the higher hydrogen peroxide concentration.

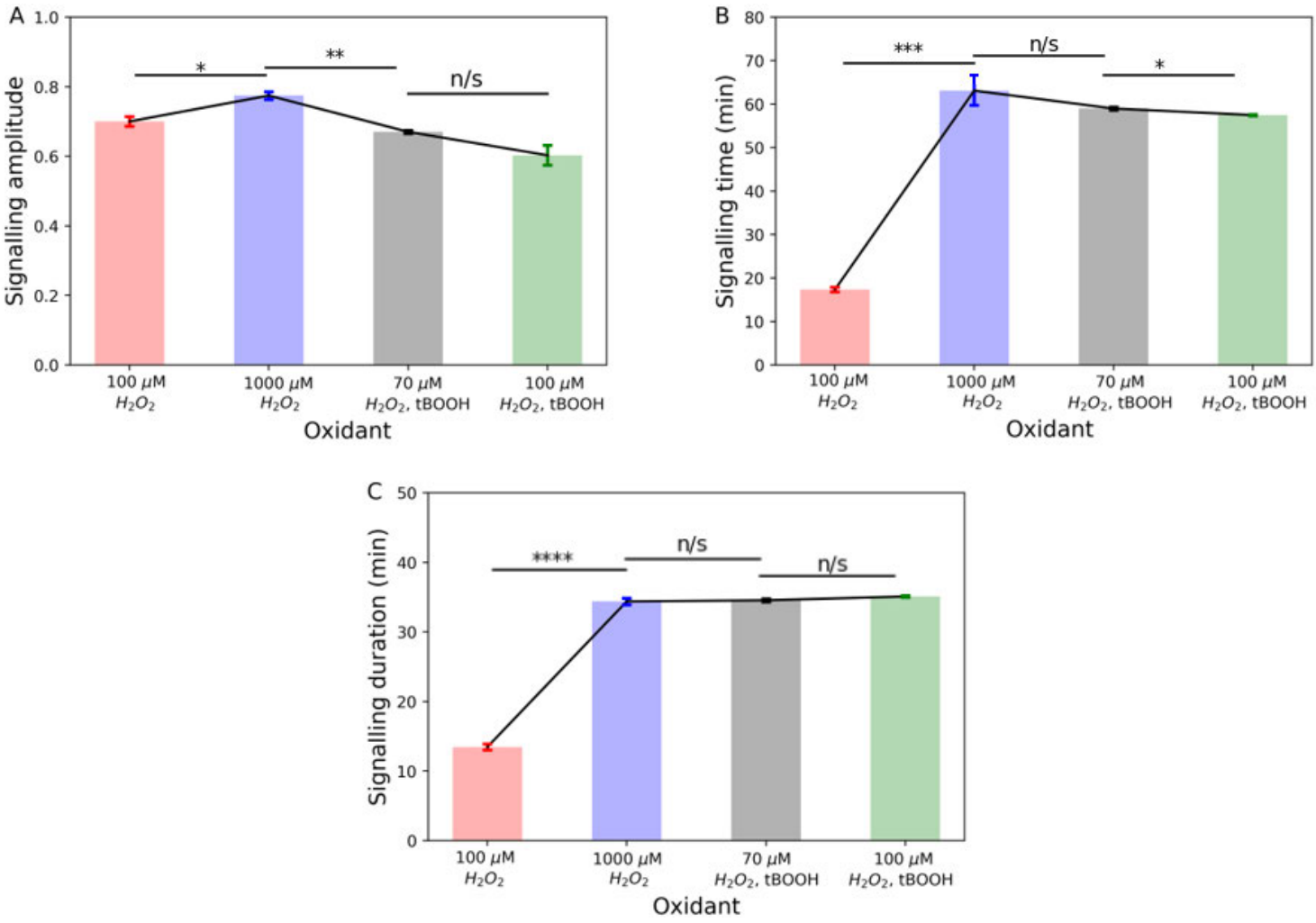

Figure 2.23: Bar graphs comparing the signalling parameters from cells treated with 70 µM and 100 µM of hydrogen peroxide and tert-butyl hydroperoxide as well as 100 µM and 1000 µM hydrogen peroxide. Signalling amplitude (A), signalling time (B) and signalling duration (C) were derived from the oxidation profiles. Significance was determined by conducting a t-test with unequal variance and one-tailed distribution, where *p<0.05, **p<0.01, ***p<0.001, ****p<0.0001 and n/s is non-significant.

Once again, these datasets were trimmed to 60 minutes, and the signalling parameters were recalculated (Table 2.4). The difference between the new combinational stress parameters was not significant for signalling amplitude and duration (Figure 2.24A, C) but remained significant for signalling time (Figure 2.24B). The signalling time and duration for both combinational stresses were again quite similar to 1000 µM hydrogen peroxide parameters but very different from 100 µM hydrogen peroxide parameters.

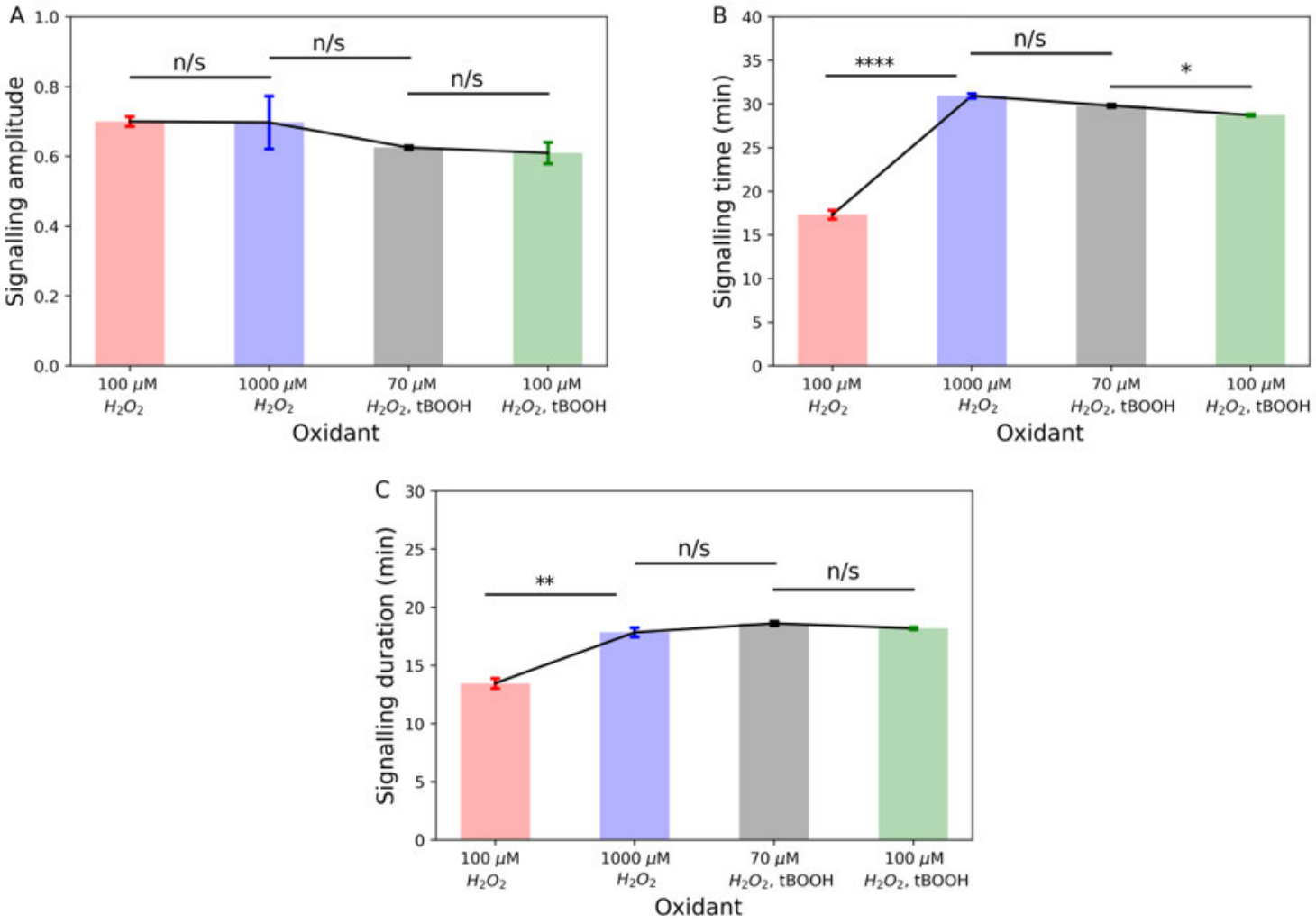

Figures 2.24: The differences between the signalling parameters from cells treated with 70 µM and 100 µM hydrogen peroxide and tert-butyl hydroperoxide combinational stress and 100 µM and 1000 µM hydrogen peroxide for 60 minutes. The signalling amplitude (A), signalling time (B), and signalling duration (C) were recalculated to only include data up to 60 minutes. Significance was determined by conducting a t-test with unequal variance and one-tailed distribution, where *p<0.05, **p<0.01, ***p<0.001, ****p<0.0001 and n/s is non-significant.

2.4. Discussion

The Tpx1/Pap1 pathway has been well studied, but there is still a lack of understanding of Pap1 signal dynamics produced during oxidative stress. Therefore, to determine if an incoherent feedforward loop was responsible for the rapid oxidation and slow reduction of Pap1 when exposed to ROS, the Tpx1/Pap1 pathway was chemically perturbed. Before beginning with the experiments, the redox western blotting method had to be validated to ensure accurate results.

While western blotting has become a valuable and commonly used method, there are multiple steps involved and no single blotting standard for this semiquantitative method, allowing room for variation and error (Gorr and Vogel, 2015; Pillai-Kastoori *et al.*, 2020). Understanding the limitations of this method, it was essential to validate the western blotting method to overcome these drawbacks. Considering that the signalling parameters obtained from analyzing the western blots were vital in this study, it was important to determine the appropriate protein, primary and secondary antibody concentrations. This was also done to ensure consistency across the blots and that results obtained were as accurate as possible to allow for reliable signalling parameter analysis. A protein concentration of 375 µg/ml together with 1 µg/ml and 1:50 000 of primary and secondary antibodies, respectively, fell within the linear range of quantification (Figure 2.6C). After validating the western blotting method, we then had to decide on how long to monitor Pap1 oxidation.

In a study about hydrogen peroxide signalling and toxicity, Pap1 was analysed from *S. pombe* cells treated with 100 µM and 500 µM hydrogen peroxide (Domènech *et al.*, 2018). These experiments were tracked for 50 minutes, and Pap1 exposed to 100 µM hydrogen peroxide was fully reduced by 30 minutes. Pap1 was also exposed to 500 µM hydrogen peroxide in these experiments, and as with our data, a second increase in oxidation at 50 minutes was obtained, which was unfortunately not tracked any further in this study (Domènech *et al.*, 2018). Therefore for the perturbation experiments, we decided to follow Pap1 oxidation over 60 minutes for the lower oxidant concentrations and 120 minutes for the higher oxidant concentrations.

S. pombe cells were exposed to different oxidants at different concentrations, and signalling parameters were calculated (Heinrich *et al.*, 2002; Pillay *et al.*, 2016). Our results showed that the concentrations of 100 µM to 500 µM hydrogen peroxide were able to modulate signalling time and duration significantly. By contrast, tert-butyl hydroperoxide and the combinational stress of

hydrogen peroxide and tert-butyl hydroperoxide resulted in a significant change in signalling time but did not appear to affect signalling amplitude and duration at the concentrations used. A previous transcriptomic study showed that the fission yeast transcriptional response varied depending on the concentration and oxidant used (Chen *et al.*, 2003; Chen *et al.*, 2008). Our results could provide an explanation for this data as our experiments show that different oxidant concentrations and combinations result in distinct Pap1 oxidation profiles and signalling dynamics (Table 2.3).

Unexpectedly, the oxidation profile and signalling parameters obtained after treatment with 70 µM and 100 µM hydrogen peroxide and tert-butyl hydroperoxide were similar to those obtained following treatment with 1000 µM of hydrogen peroxide. This result shows that utilizing two stressors simultaneously at lower concentrations has an additive effect equivalent to the impact of using a single stressor at a much higher concentration. Combinational stresses may be helpful in therapeutic studies, especially in yeast cells that are resistant to high hydrogen peroxide concentrations. For example, a study showed that *S. pombe, S. cerevisiae, Candida albicans* and *Candida glabrata* yeast cells were more easily killed using a combinational stress of hydrogen peroxide and sodium chloride than with either chemical being used individually (Kaloriti *et al.*, 2014).

To conclude, although chemical perturbation provided some insight into the Tpx1/Pap1 pathway, we could not independently modulate the signalling parameters. Therefore, we could not determine whether the Pap1 oxidation profile was due to an incoherent feedforward loop. Consequently, we decided to use computational modelling to gain insights into the system.

Chapter 3: Perturbation of the *S. pombe* Tpx1/Pap1 pathway *in silico*

3.1. Introduction

Computational modelling has become more commonly used in analyzing complex biological systems. This technique involves representing components of a system and their interactions in a mathematical form which allows for precise control over the different parameters and species concentrations within the model (Brodland, 2015; Mooney *et al.*, 2016). Computational modelling is complementary to wetlab experimental work and can allow new insights, determine further experimental investigations, elucidate complex systems, and more (Brodland, 2015). Models have been used to study disease pathogenesis, medication side effects, biological ageing, signalling pathways, redox systems, and more (Smith and Shanley, 2013; Williams *et al.*, 2014; Clegg and Mac Gabhann, 2015; Mooney *et al.*, 2016; Warner *et al.*, 2019).

Computational modelling of redox systems is necessary as these are usually complex networks with proteins that can undergo multiple redox exchanges and can interact with many different targets (Pillay *et al.*, 2013). Numerous models have been developed to study various aspects of redox systems, such as transcription factors, glutaredoxins, peroxiredoxins and redox signalling pathways, amongst others (Pillay *et al.*, 2009; Pronk *et al.*, 2014; Dwivedi *et al.*, 2015; Tomalin *et al.*, 2016). As the chemical perturbation of the Tpx1/Pap1 pathway did not provide sufficient resolution to determine whether an incoherent feedforward loop was responsible for the rapid increase and prolonged decrease in Pap1 oxidation, the next step was to perturb a model of the pathway *in silico*.

To the best of our knowledge, there is only one published model of the fission yeast Tpx1 pathway (Tomalin *et al.*, 2016). The model developed by Tomalin *et al.*, (2016) focused on the different oxidation and reduction reactions Tpx1 undergoes during oxidative stress and revealed the biphasic nature of the relationship between intracellular and extracellular hydrogen peroxide (Tomalin *et al.*, 2016). Although this model was useful, it lacked a few aspects. For example, it did not contain reactions for the oxidation and reduction of Pap1 or the reversal of Tpx1 hyperoxidation by Srx1. Moreover, the oxidation profile of thioredoxin when simulated with

hydrogen peroxide in the model appeared to be unrealistic when compared to in vivo data (Bozonet *et al*., 2005; Day *et al*., 2012).

Due to the lack of data on the Tpx1/Pap1 pathway, we decided to construct a simple core model that would provide an overview of the system rather than a complex and detailed computational model. Core models are not fitted to experimental datasets but offer a reasonable estimate of the behaviour of the system so that the logic of the system can be elucidated (Pillay *et al.*, 2013). Our model contained three reactions for Tpx1 oxidation and reduction, two reactions for Pap1 oxidation and reduction, and a single reaction for Trx1 reduction (Figure 3.1). With this model, we could selectively manipulate different protein concentrations and reaction rates to gain new insights into the Tpx1/Pap1 pathway dynamics.

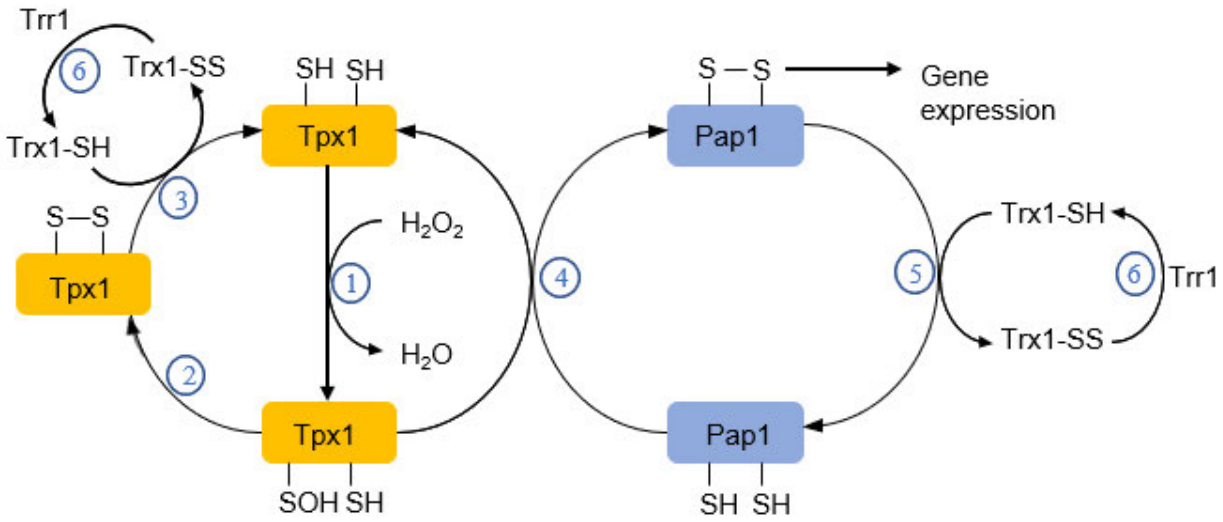

Figure 3.1: Wiring diagram of the Tpx1/Pap1 pathway in *S. pombe*. The kinetic model was built using the above six reactions that show Tpx1 forming a sulfenic acid by breaking down a single hydrogen peroxide molecule (1) which can either form a disulfide bridge (2) or oxidize Pap1 (4). Oxidized Tpx1 and Pap1 are both reduced by thioredoxin (Trx1-SH) (3,5), resulting in its oxidation (Trx1-SS). Oxidized thioredoxin is reduced by thioredoxin reductase (Trr1) (6).

3.2. Methods

The modelling file was written using the Scintilla text editor (https://www.scintilla.org/), and simulations were carried out using Python Simulator for Cellular Systems (PySCeS) (https://pypi.org/project/pysces/) (Olivier *et al.*, 2005) in a Jupyter notebook (https://jupyter.org/).

3.3. Results

3.3.1. Developing the kinetic model of the Tpx1/Pap1 pathway

Prior to developing a kinetic model, data from literature and databases like BRENDA was acquired to parameterize the model (Pillay *et al.*, 2013). This Tpx1/Pap1 pathway model was developed using six reactions (Table 3.1) which correlated to the reactions in Figure 3.1. The corresponding concentrations of the metabolites in these reactions can be found in Table 3.2.

Table 3.1: Reactions, kinetic parameters and their values used to develop the computational model based on the *S. pombe* Tpx1/Pap1 pathway in Figure 3.1.

Reaction	Kinetic Parameter	Value	Unit
R1: Tpx1SH + H2O2 = Tpx1SOH + H2O	k_1	20	$\mu M^{-1}.s^{-1}$
R2: Tpx1SOH = Tpx1SS	k_2	2	s^{-1}
R3: Tpx1SS + Trx1SH = Tpx1SH + Trx1SS	k_3	0.2	$\mu M^{-1}.s^{-1}$
R4: Tpx1SOH + Pap1SH = Tpx1SH + Pap1SS	k_4	0.04	$\mu M^{-1}.s^{-1}$
R5: Pap1SS + Trx1SH = Pap1SH + Trx1SS	k_5	0.001	$\mu M^{-1}.s^{-1}$
R6: NADPH + Trx1SS = NADP + Trx1SH	k_{cat6}	66	s^{-1}

Table 3.2: Concentrations of the different metabolites used in the computational model of the Tpx1/Pap1 pathway.

Metabolites	Concentration (µM)	Reference
Tpx1 total	4	(Marguerat *et al.*, 2012)
Pap1 total	0.0245	(Marguerat *et al.*, 2012)
Trx1 total	0.71	(Marguerat *et al.*, 2012)
H_2O_2	200	Estimated
H_2O	1	Estimated
NADPH total	150	(Lee *et al.*, 1995)

Next, the model was analyzed using the PySCeS computational modelling software, which produced ordinary differential equations (ODE) based on the reactions. The model of the Tpx1/Pap1 pathway resulted in eight ordinary differential equations:

1. $\frac{\partial Tpx1SH}{\delta t} = -1(k_1 * Tpx1SH * H_2O_2) + k_3 * Tpx1SS * Trx1SH + k_4 * Tpx1SOH * Pap1SH$
2. $\frac{\partial H_2O_2}{\delta t} = -1(k_1 * Tpx1SH * H_2O_2)$
3. $\frac{\partial Tpx1SOH}{\delta t} = k_1 * Tpx1SH * H_2O_2 - 1(k_2 * Tpx1SOH) - 1(k_4 Tpx1SOH * Pap1SH)$
4. $\frac{\partial Tpx1SS}{\delta t} = k_2 * Tpx1SOH - 1(k_3 Tpx1SS * Trx1SH)$
5. $\frac{\partial Trx1SH}{\delta t} = -1(k_3 * Tpx1SS * Trx1SH) - 1(k_5 * Pap1SS * Trx1SH) + \frac{\left(k_{cat6} * trr1 * \frac{NADPH}{k_6 nadph} * \frac{Trx1SS}{k_6 trx1ss}\right)}{\left(\frac{1+NADPH}{k_6 nadph} * \frac{1+Trx1SS}{k_6 trx1ss}\right)}$
6. $\frac{\partial Trx1SS}{\delta t} = k_3 * Tpx1SS * Trx1SH + k_5 * Pap1SS * Trx1SH - \frac{\left(k_{cat6} * trr1 * \frac{NADPH}{k_6 nadph} * \frac{Trx1SS}{k_6 trx1ss}\right)}{\left(\frac{1+NADPH}{k_6 nadph} * \frac{1+Trx1SS}{k_6 trx1ss}\right)}$
7. $\frac{\partial Pap1SH}{\delta t} = -1(k_4 * Tpx1SOH * Pap1SH) + k_5 * Pap1SS * Trx1SH$
8. $\frac{\partial Pap1SS}{\delta t} = k_4 * Tpx1SOH * Pap1SH - 1(k_5 * Pap1SS * Trx1SH)$

The software ordered and solved these equations in a stoichiometric matrix with the rows and columns of the matrix representing the species and the reactions involving those species, respectively. Positive and negative signs in the matrix indicated whether the species were produced or consumed in a reaction, and the integers describe the stoichiometry of the reactions in the matrix (Pillay *et al.*, 2013).

The model was simulated to determine whether it produced a Pap1 profile with a rapid increase followed by a slow decrease in oxidation. Consequently, the model was simulated from 100-1000 µM of hydrogen peroxide. The resultant Pap1 oxidation profiles showed an immediate increase and slow reduction in oxidation, with the oxidation profile lasting progressively longer as the hydrogen peroxide concentration increased (Figure 3.2). Hyperoxidation of Tpx1 was not added to the model as all further simulations were carried out at 200 µM, where generally hyperoxidation of Tpx1 does not occur (Domènech *et al.*, 2018).

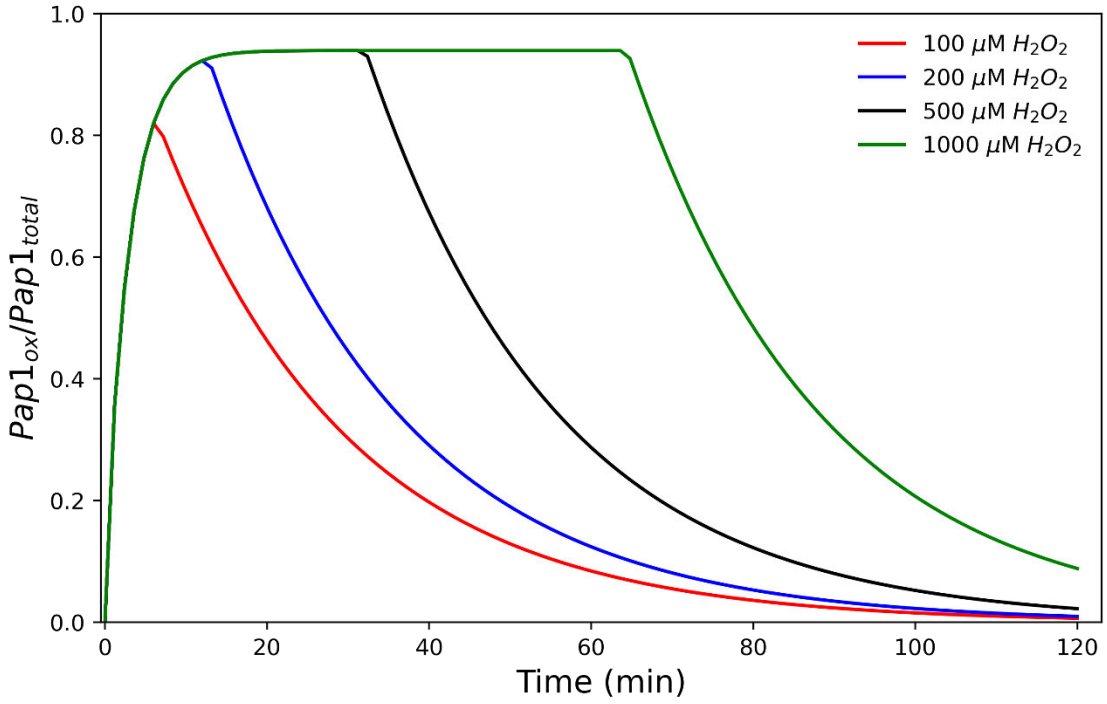

Figure 3.2: The Tpx1/Pap1 model simulated Pap1 oxidation profiles with a rapid increase and slow decrease for 100-1000 µM hydrogen peroxide. Pap1 oxidation increased proportionally over time with the amount of hydrogen peroxide.

3.3.2. Perturbing the thioredoxin activity to modulate incoherence within the Tpx1/Pap1 pathway

As we proposed that the Trx1 protein was responsible for the incoherent characteristic of the Tpx1/Pap1 pathway, the kinetic parameter values for Trx1 reduction of Tpx1SS (k_3) and Pap1SS (k_5) (Figure 3.3A) were altered to determine the effect on the oxidation profile. An increase and decrease in parameter k_3 had minimal impacts on the oxidation profile (Figure 3.3B) and the signalling parameters (Table 3.3). This result was surprising as we expected an increase in parameter k_3 to increase the amount of reduced Tpx1, which should have caused a rise in Pap1 oxidation. However, Tpx1, like other peroxiredoxins, is already present at much higher concentrations than Trx1 (Marguerat *et al.*, 2012) and therefore changing k_3 did not dramatically affect the availability of Pap1.

As expected, decreasing parameter k_5 (Figure 3.3C) and the Trx1SH concentration (Figure 3.3D) resulted in Pap1 reduction occurring slower than in the base condition, causing an increase

in signalling time and duration (Table 3.3). On the other hand, increasing k_5 and the total thioredoxin concentration had the opposite effect. These results show that instead of an incoherent feedforward loop, it is Trx1 limitation that plays a key role in Pap1 signalling time and duration (i.e.), increasing the thioredoxin concentration or increasing the rate of Pap1 reduction decreases the Pap1 signal duration (Table 3.3). Altering the Tpx1 and Trr1 concentrations and k_1, k_2, k_4, and k_{cat6} parameters did not result in considerable changes in the Pap1 oxidation profile (Figure S1-S6, Appendix 2).

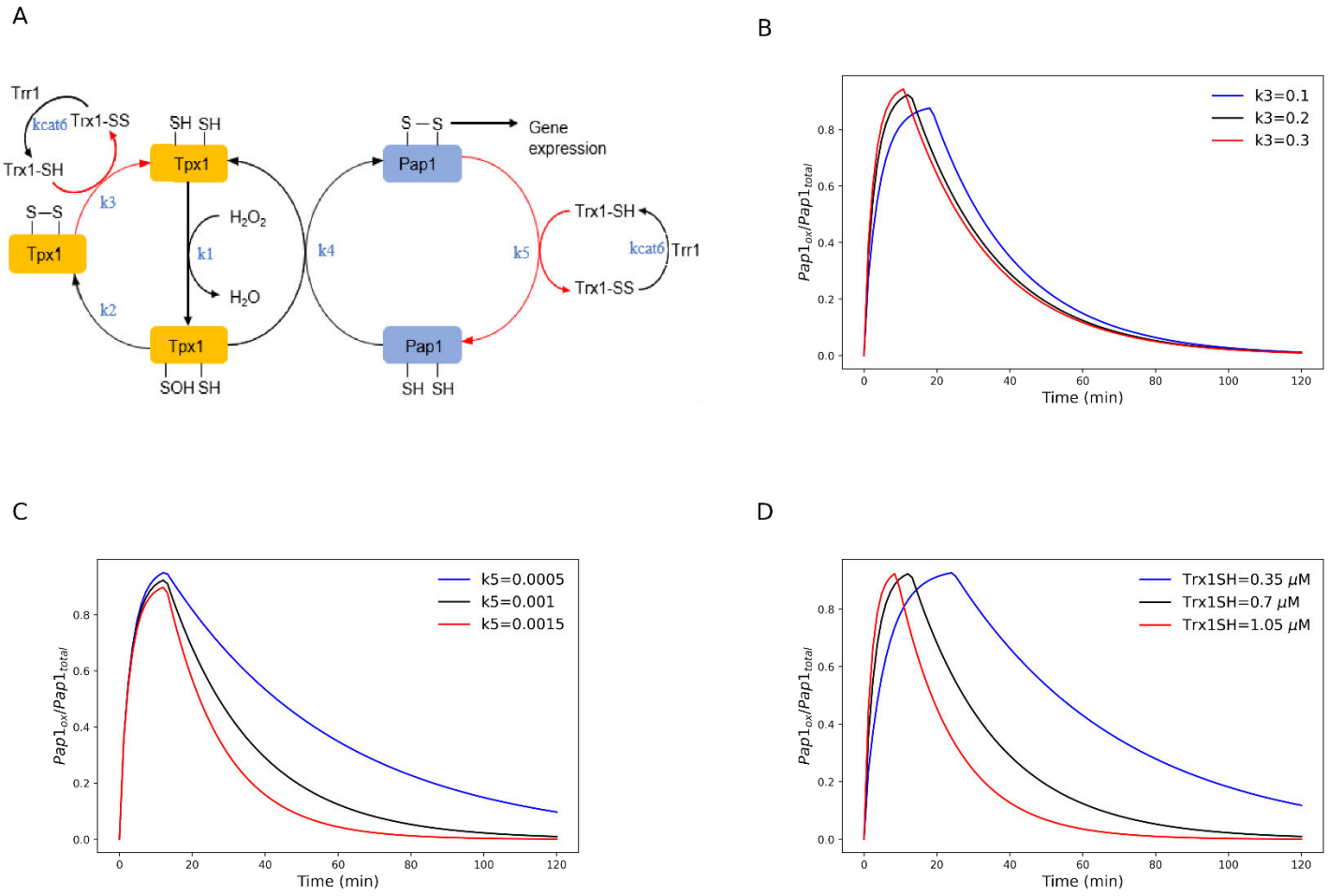

Figure 3.3: Trx1 plays a key role in determining the Pap1 oxidation profile. A Tpx1/Pap1 pathway model depicting the kinetic parameters and the consequent reactions altered during the simulations (red arrows) (A). The effect on Pap1 oxidation profiles during an increase (red) and decrease (blue) of the original model k_3 (B) and k_5 (C) kinetic parameters (black) as well as the concentration of reduced Trx1 (Trx1SH) (D).

Table 3.3: Values for signalling time, duration and amplitude for parameters k_3 and k_5. The kinetic parameter values were altered to a lower and higher value from the original, and the signalling parameters were calculated at these different parameter values.

	Value (μM/s)	Signalling amplitude	Signalling time (min)	Signalling duration (min)
Kinetic Parameter				
	Lower = 0.1	0.77	1734.02	1304.74
k_3	Original = 0.2	0.72	1604.73	1293.21
	Higher = 0.3	0.70	1564.61	1290.86
	Lower = 0.005	0.85	2391.63	1758.80
k_5	Original = 0.01	0.72	1604.73	1293.21
	Higher = 0.015	0.74	1205.37	948.27
Protein				
	Lower = 0.35	0.96	2581.13	1732.25
Trx1SH	Original = 0.7	0.72	1604.73	1293.21
	Higher = 1.05	0.70	1112.83	938.96

3.3.3. The Pap1 oxidation profile during oxidative stress is directly linked to Trx1 oxidation

To confirm the modelling results, it was necessary to track thioredoxin oxidation *in vivo*. Fortunately, the Trx1 oxidation state in response to hydrogen peroxide was obtained by experiments carried out by a colleague in our group (Tejal Bhagwandeen, unpublished data). When comparing the Pap1 and Trx1 oxidation profiles after exposure to hydrogen peroxide, it was found that they had similar profiles across all the concentrations tested (Figure 3.4A-D). Trx1 oxidation appeared to be correlated to the oxidation profile of Pap1. All Trx1 data and subsequent analysis can be found in Appendix 3.

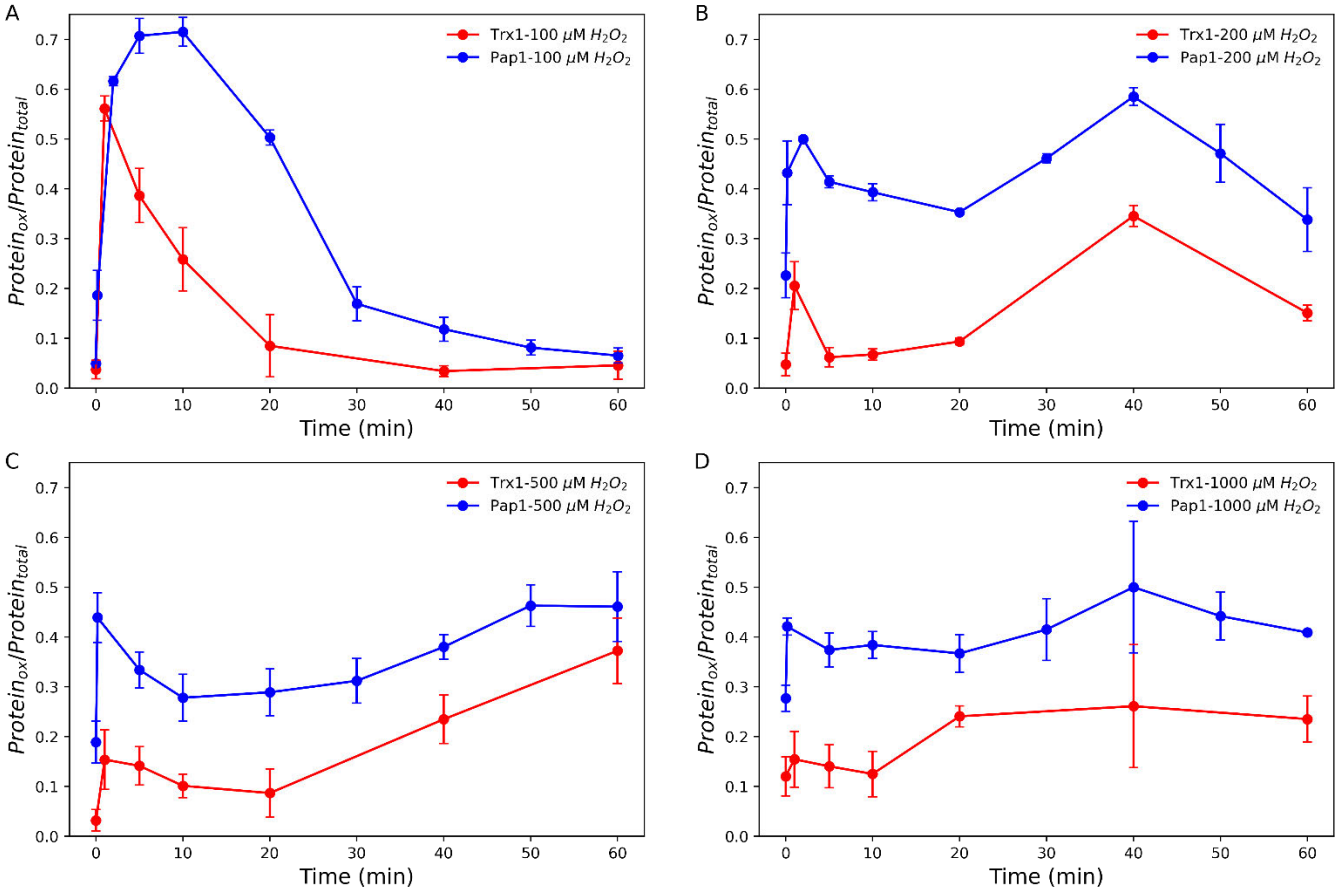

Figure 3.4: Comparison of the oxidation profiles for Pap1 and Trx1 from *S. pombe*. Trx1 oxidation was tracked for 60 minutes after exposure to 100 µM (A), 200 µM (B), 500 µM (C) and 1000 µM (D) hydrogen peroxide and compared to Pap1 oxidation at the same concentrations. Standard errors represent samples taken from three independent samples (Appendix 3).

The Trx1 oxidation profiles were used to determine the Trx1 oxidation signalling amplitude, time and duration and the Pap1 and Trx1 parameters were then compared using biphasic plots (Figure 3.5). Interestingly, it was found that the signalling amplitude did not show any linear correlation between Trx1 and Pap1 oxidation from 100-1000 µM hydrogen peroxide (Figure 3.5A). However, signalling time showed a strong linear correlation between Trx1 and Pap1 oxidation (Figure 3.5B), while signalling duration displayed a linear correlation for all the concentrations of hydrogen peroxide except 200 µM (Figure 3.5C). These results suggest that Trx1 oxidation determines the Pap1 signalling time and duration, which correlate to the average time taken to activate the target protein and the average time the target protein is active, respectively.

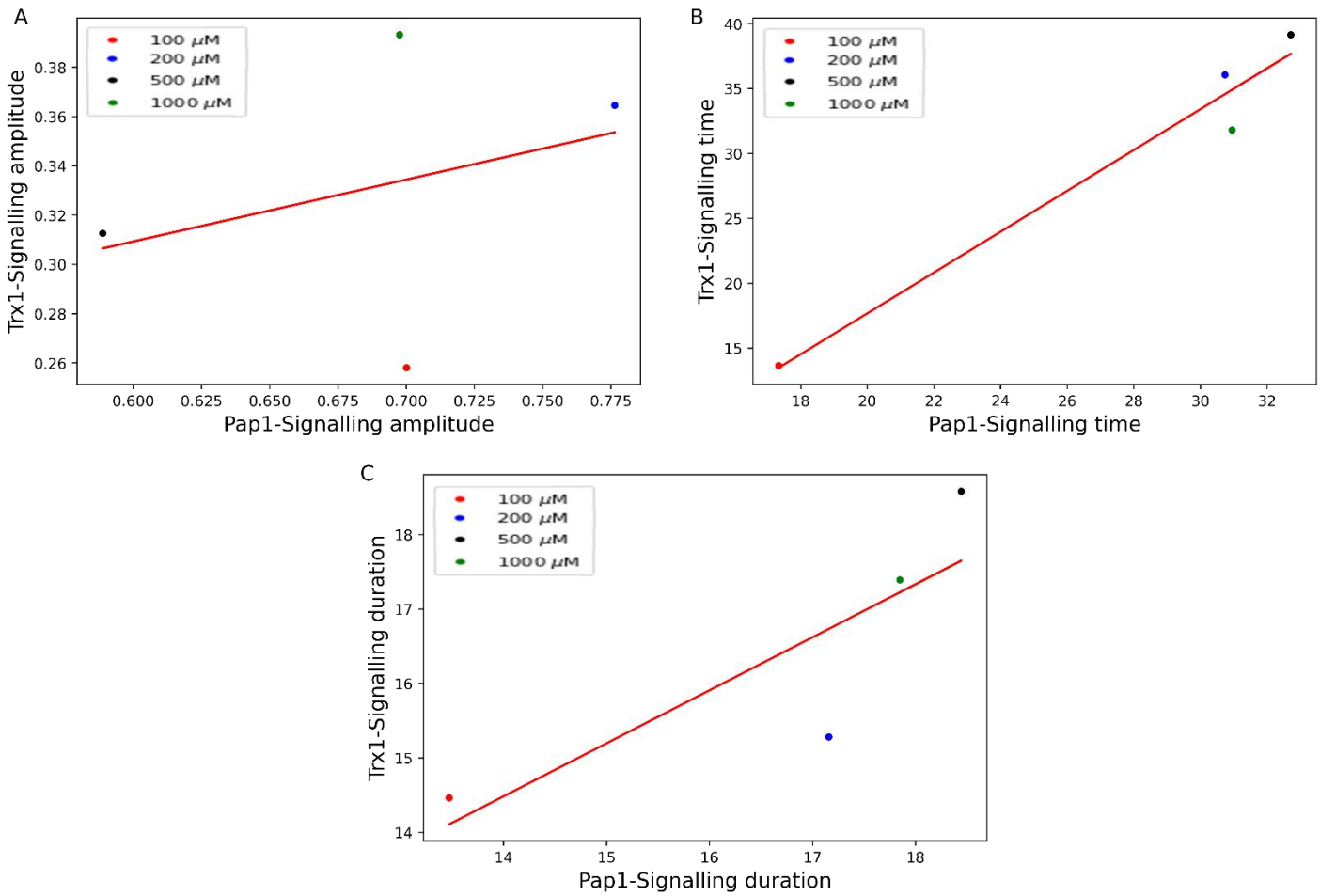

Figure 3.5: Comparison of the signalling parameters from Trx1 and Pap1 oxidation using regression plots. Signalling amplitude (A), signalling time (B) and signalling duration (C) values from Trx1 and Pap1 oxidation were compared for 100-1000 µM hydrogen peroxide.

3.4. Discussion

Computational modelling has become a valuable tool for studying biological systems and was used to understand the mechanism underlying the Pap1 oxidation profile observed during oxidative stress in *S. pombe*. However, although a fission yeast model of the Tpx1 pathway was already available (Tomalin *et al.*, 2016), it did not contain all the necessary reactions and could not simulate Pap1 oxidation as a result. Therefore, another model was developed for analysis to provide new insights into the Tpx1/Pap1 pathway.

Our results show that rather than an incoherent feedforward loop, it was Trx1 oxidation that played a role in determining Pap1 signalling duration (Figure 3.3B-D). Fortunately, *in vivo* Trx1 oxidation results (Tejal Bhagwandeen, unpublished data) were available for comparison to Pap1 oxidation results, which showed that both proteins produced very similar oxidation profiles during oxidative stress occurring at 100-1000 µM hydrogen peroxide. These results show that the redox state of Trx1 determines the oxidation of Pap1 during oxidative stress.

Our data are consistent with a previous study in fission yeast which showed that Trx1 and Pap1 redox changes are entrained over a range of hydrogen peroxide concentrations (Domènech *et al.*, 2018). Similarly, genetic studies have shown that in *S. pombe* thioredoxin reductase mutants (Δ*trr1*), Pap1 is completely oxidized even in the absence of stress, suggesting that Trx1 oxidation is linked to Pap1 oxidation (Brown *et al.*, 2013; Calvo *et al.*, 2013; Paulo *et al.*, 2014).

In conclusion, a simple core model of the Tpx1/Pap1 system was used to gain insight into Pap1 oxidation. This model provided a new hypothesis that thioredoxin oxidation was important for the Pap1 signal profile, which was supported by our *in vivo* results.

Chapter 4: General Discussion

Reactive oxygen species (ROS) cause damage to cellular components and can lead to dysfunction, disease and death when present in excess (Brieger *et al.*, 2012; Zuo *et al.*, 2015; Roy *et al.*, 2017). On the other hand, lower levels of ROS are required for signalling processes and normal cellular functioning (Brieger *et al.*, 2012; Sies and Jones, 2020). This paradoxical role requires cells to manage the amount of ROS present, and in *S. pombe*, this is accomplished by the Tpx1/Pap1 pathway (Day et al., 2012; Garcia-Santamarina et al., 2014; Veal et al., 2014). Following oxidative stress, the *E. coli* transcription factor OxyR showed a rapid increase and decrease in oxidation. On the other hand, Pap1 has a biphasic response with a rapid increase but a prolonged decrease in oxidation. Although the Tpx1/Pap1 pathway has been well-studied, to our knowledge, there is no agreed model on the control of the Pap1 signal dynamics. We hypothesized that Trx1 dual activities in reducing Tpx1 and Pap1 create an incoherent feedforward loop within the Tpx1/Pap1 pathway.

In Chapter 2, the Tpx1/Pap1 pathway was perturbed *in vivo* using different oxidants at different concentrations to modulate the signalling profile of the pathway. The Pap1 oxidation profiles were then used to determine the signalling parameters of the pathway. While different concentrations of hydrogen peroxide were able to modulate signalling time and duration, tert-butyl hydroperoxide and a combination of both oxidants could not do so. Therefore, this method could not be used to answer our hypothesis. Nonetheless, the specific Pap1 oxidation profiles obtained could provide an explanation for the distinct Pap1-dependent transcriptomic responses observed in a previous study (Chen *et al.*, 2008). This study showed that 127 core oxidative stress genes were upregulated when fission yeast cells were exposed to menadione, tert-butyl hydroperoxide, and low (70 µM) and medium (500 µM) doses of hydrogen peroxide. Interestingly, vastly different induction dynamics for ~3500 other genes were obtained for the three different concentrations of hydrogen peroxide and the two other oxidants (Chen *et al.*, 2008). Our study suggests that these distinct transcriptional dynamics are due to the distinct Pap1 activation dynamics induced by different stressors/stressor concentrations. A future study could explore exactly how the different signalling parameters of Pap1 oxidation correlate to the transcriptional responses obtained using various oxidants.

With chemical perturbation providing inconclusive results, computational modelling was used to test our hypothesis. A simple core model of the Tpx1/Pap1 pathway was used to perturb the system *in silico* to determine if an incoherent feedforward loop was responsible for the Pap1 oxidation profile. Unexpectedly it was shown that Trx1 limitation, instead of an incoherent feedforward loop, played a role in the oxidation profile of Pap1 obtained during oxidative stress. Indeed, an intriguing correlation between the Pap1 and Trx1 oxidation profiles at a range of 100-1000 µM hydrogen peroxide concentrations was obtained from our *in vivo* analysis. Although these results indicate that Trx1 plays a significant role in regulating the Tpx1/Pap1 pathway, further *in vivo* experiments will be required to confirm this by directly manipulating the thioredoxin system redox state

S. pombe Δ*trx1* and Δ*trr1* cells result in partial and complete Pap1 oxidation, respectively, before oxidative stress (Day *et al.*, 2012; Brown *et al.*, 2013). Therefore, if Trx1 is constantly oxidized in these mutants, it will not be able to reduce Pap1 or Tpx1 in hydrogen peroxide challenge experiments. In these experiments, we would expect increased Pap1 oxidation, which could be quantified using our signal parameter method.

Our work has led to two additional insights into redox signalling in general. First, prokaryotic transcription factors like OxyR can readily bind to the bacterial genome and induce transcription rapidly (Åslund *et al.*, 1999; Cokus *et al.*, 2006). On the other hand, eukaryotic transcription factors such as Pap1 must traverse the nuclear membrane to induce a transcriptional response (Garcia-Santamarina *et al.*, 2014). Therefore, the sensor-mediated mechanism of Pap1 with its extended period of activation may be a mechanism to allow for sufficient time for transcription factor translocation into the nucleus. Second, distinct Pap1 dynamics may lead to distinct transcriptional responses to various stressors (Chen *et al.*, 2008). Thus, instead of requiring several sensing mechanisms for a range of oxidant stressors, fission yeast cells have a mechanism that can modulate this single transcription factor to give an output that is still relatively specific.

In conclusion, although the *S. pombe* Tpx1/Pap1 pathway has been studied in-depth, there was a lack in understanding what controls the Pap1 oxidation profile obtained during oxidative stress. This work fills part of this knowledge gap and provides an understanding of the design principles of these systems. It remains to be seen whether these design principles can be exploited for the treatment of pathologies involved in dysregulated redox signalling.

References

Alon, U. 2007. Network motifs: theory and experimental approaches. *Nature Reviews Genetics,* 8**,** 450.

Aslani, B. A. & Ghobadi, S. 2016. Studies on oxidants and antioxidants with a brief glance at their relevance to the immune system. *Life Sciences,* 146**,** 163-173.

Åslund, F., Zheng, M., Beckwith, J. & Storz, G. 1999. Regulation of the OxyR transcription factor by hydrogen peroxide and the cellular thiol—disulfide status. *Proceedings of the National Academy of Sciences,* 96**,** 6161-6165.

Beckhauser, T. F., Francis-Oliveira, J. & De Pasquale, R. 2016. Reactive oxygen species: Physiological and physiopathological effects on synaptic plasticity: Supplementary issue: Brain plasticity and repair. *Journal of Experimental Neuroscience,* 10**,** JEN. S39887.

Bersweiler, A., D'autréaux, B., Mazon, H., Kriznik, A., Belli, G., Delaunay-Moisan, A., Toledano, M. B. & Rahuel-Clermont, S. 2017. A scaffold protein that chaperones a cysteine-sulfenic acid in H 2 O 2 signaling. *Nature Chemical Biology,* 13**,** 909.

Bozonet, S. M., Findlay, V. J., Day, A. M., Cameron, J., Veal, E. A. & Morgan, B. A. 2005. Oxidation of a eukaryotic 2-Cys peroxiredoxin is a molecular switch controlling the transcriptional response to increasing levels of hydrogen peroxide. *Journal of Biological Chemistry,* 280**,** 23319-23327.

Brieger, K., Schiavone, S., Miller Jr, F. J. & Krause, K.-H. 2012. Reactive oxygen species: from health to disease. *Swiss Medical Weekly,* 142**,** w13659.

Brodland, G. W. How computational models can help unlock biological systems. Seminars in cell & developmental biology, 2015. Elsevier, 62-73.

Brown, J. D., Day, A. M., Taylor, S. R., Tomalin, L. E., Morgan, B. A. & Veal, E. A. 2013. A peroxiredoxin promotes H2O2 signaling and oxidative stress resistance by oxidizing a thioredoxin family protein. *Cell Reports,* 5**,** 1425-1435.

Calvo, I. A., Boronat, S., Domènech, A., García-Santamarina, S., Ayte, J. & Hidalgo, E. 2013. Dissection of a redox relay: H2O2-dependent activation of the transcription factor Pap1 through the peroxidatic Tpx1-thioredoxin cycle. *Cell Reports,* 5**,** 1413-1424.

Cao, S. S. & Kaufman, R. J. 2014. Endoplasmic reticulum stress and oxidative stress in cell fate decision and human disease. *Antioxidants & Redox Signaling,* 21**,** 396-413.

Cao, Z. & Lindsay, J. G. 2017. The peroxiredoxin family: an unfolding story. *Macromolecular Protein Complexes***,** 127-147.

Chen, D., Toone, W. M., Mata, J., Lyne, R., Burns, G., Kivinen, K., Brazma, A., Jones, N. & BäHler, J. R. 2003. Global transcriptional responses of fission yeast to environmental stress. *Molecular Biology of the Cell,* 14**,** 214-229.

Chen, D., Wilkinson, C. R., Watt, S., Penkett, C. J., Toone, W. M., Jones, N. & Bähler, J. 2008. Multiple pathways differentially regulate global oxidative stress responses in fission yeast. *Molecular Biology of the Cell,* 19**,** 308-317.

Chen, Q., Wang, Q., Zhu, J., Xiao, Q. & Zhang, L. 2018a. Reactive oxygen species: key regulators in vascular health and diseases. *British Journal of Pharmacology,* 175**,** 1279-1292.

Chen, Y., Zhang, Y., Dong, Z. & Ow, D. W. 2018b. Protection from disulfide stress by inhibition of pap1 nuclear export in Schizosaccharomyces pombe. *Genetics,* 210**,** 857-868.

Choi, H.-J., Kim, S.-J., Mukhopadhyay, P., Cho, S., Woo, J.-R., Storz, G. & Ryu, S.-E. 2001. Structural basis of the redox switch in the OxyR transcription factor. *Cell,* 105**,** 103-113.

Clegg, L. E. & Mac Gabhann, F. 2015. Molecular mechanism matters: Benefits of mechanistic computational models for drug development. *Pharmacological Research,* 99**,** 149-154.

Cokus, S., Rose, S., Haynor, D., Grønbech-Jensen, N. & Pellegrini, M. 2006. Modelling the network of cell cycle transcription factors in the yeast *Saccharomyces cerevisiae. BMC Bioinformatics,* 7**,** 1-12.

Commoner, B., Townsend, J. & Pake, G. E. 1954. Free radicals in biological materials. *Nature,* 174**,** 689.

Day, A. M., Brown, J. D., Taylor, S. R., Rand, J. D., Morgan, B. A. & Veal, E. A. 2012. Inactivation of a peroxiredoxin by hydrogen peroxide is critical for thioredoxin-mediated repair of oxidized proteins and cell survival. *Molecular Cell,* 45**,** 398-408.

Delaunay, A., Isnard, A. D. & Toledano, M. B. 2000. H_2O_2 sensing through oxidation of the Yap1 transcription factor. *The EMBO Journal,* 19**,** 5157-5166.

Domènech, A., Ayté, J., Antunes, F. & Hidalgo, E. 2018. Using in vivo oxidation status of one-and two-component redox relays to determine H_2O_2 levels linked to signaling and toxicity. *BMC Biology,* 16**,** 61.

Dwivedi, G., Gran, M. A., Bagchi, P. & Kemp, M. L. 2015. Dynamic redox regulation of IL-4 signaling. *PLoS Computational Biology,* 11**,** e1004582.

Fenton, J. 1894. Oxidation of tartaric acid in presence of iron. *Journal of the Chemical Society, Transactions,* 65**,** 899-910.

Forrester, S. J., Kikuchi, D. S., Hernandes, M. S., Xu, Q. & Griendling, K. K. 2018. Reactive oxygen species in metabolic and inflammatory signaling. *Circulation Research,* 122**,** 877-902.

Gadaleta, M. C., Iwasaki, O., Noguchi, C., Noma, K.-I. & Noguchi, E. 2013. New vectors for epitope tagging and gene disruption in *Schizosaccharomyces pombe*. *Biotechniques,* 55**,** 257-263.

Garcia-Santamarina, S., Boronat, S. & Hidalgo, E. 2014. Reversible cysteine oxidation in hydrogen peroxide sensing and signal transduction. *Biochemistry,* 53**,** 2560-2580.

Gorr, T. A. & Vogel, J. 2015. Western blotting revisited: critical perusal of underappreciated technical issues. *Proteomics–Clinical Applications,* 9**,** 396-405.

Harman, D. 1956. Aging: A Theory Based on Free Radical and Radiation Chemistry. *Journal of Gerontology,* 11**,** 298-300.

He, L., He, T., Farrar, S., Ji, L., Liu, T. & Ma, X. 2017a. Antioxidants maintain cellular redox homeostasis by elimination of reactive oxygen species. *Cellular Physiology and Biochemistry,* 44**,** 532-553.

He, Y., Chen, Y., Song, W., Zhu, L., Dong, Z. & Ow, D. W. 2017b. A Pap1–Oxs1 signaling pathway for disulfide stress in Schizosaccharomyces pombe. *Nucleic Acids Research,* 45**,** 106-114.

Heinrich, R., Neel, B. G. & Rapoport, T. A. 2002. Mathematical models of protein kinase signal transduction. *Molecular Cell,* 9**,** 957-970.

Hong, J., Brandt, N., Abdul-Rahman, F., Yang, A., Hughes, T. & Gresham, D. 2018. An incoherent feedforward loop facilitates adaptive tuning of gene expression. *Elife,* 7**,** e32323.

Kaloriti, D., Jacobsen, M., Yin, Z., Patterson, M., Tillmann, A., Smith, D. A., Cook, E., You, T., Grimm, M. J. & Bohovych, I. 2014. Mechanisms underlying the exquisite sensitivity of Candida albicans to combinatorial cationic and oxidative stress that enhances the potent fungicidal activity of phagocytes. *MBio,* 5**,** e01334-14.

Kausar, S., Wang, F. & Cui, H. 2018. The role of mitochondria in reactive oxygen species generation and its implications for neurodegenerative diseases. *Cells,* 7**,** 274.

Kim, D., Kwon, Y. K. & Cho, K. H. 2008. The biphasic behavior of incoherent feed-forward loops in biomolecular regulatory networks. *Bioessays,* 30**,** 1204-1211.

Krumova, K. & Cosa, G. 2016. Overview of reactive oxygen species.

Laemmli, U.K. 1970. Cleavage of structural proteins during the assembly of the head of the bacteriophage T4. *Nature,* 227 (5259), pp.680-685.

Lee, J., Dawes, I. W. & Roe, J.-H. 1995. Adaptive response of *Schizosaccharomyces pombe* to hydrogen peroxide and menadione. *Microbiology,* 141**,** 3127-3132.

Mailloux, R. J. 2020. An update on mitochondrial reactive oxygen species production. *Antioxidants,* 9**,** 472.

Mangan, S. & Alon, U. 2003. Structure and function of the feed-forward loop network motif. *Proceedings of the National Academy of Sciences,* 100**,** 11980-11985.

Mangan, S., Itzkovitz, S., Zaslaver, A. & Alon, U. 2006. The incoherent feed-forward loop accelerates the response-time of the gal system of Escherichia coli. *Journal of Molecular Biology,* 356**,** 1073-1081.

Marguerat, S., Schmidt, A., Codlin, S., Chen, W., Aebersold, R. & Bähler, J. 2012. Quantitative analysis of fission yeast transcriptomes and proteomes in proliferating and quiescent cells. *Cell,* 151**,** 671-683.

Marinho, H. S., Real, C., Cyrne, L., Soares, H. & Antunes, F. 2014. Hydrogen peroxide sensing, signaling and regulation of transcription factors. *Redox Biology,* 2**,** 535-562.

Massaad, C. A. & Klann, E. 2011. Reactive oxygen species in the regulation of synaptic plasticity and memory. *Antioxidants & Redox Signaling,* 14**,** 2013-2054.

Mccord, J. M. & Fridovich, I. 1969. Superoxide dismutase an enzymic function for erythrocuprein (hemocuprein). *Journal of Biological Chemistry,* 244**,** 6049-6055.

Milo, R., Shen-Orr, S., Itzkovitz, S., Kashtan, N., Chklovskii, D. & Alon, U. 2002. Network motifs: simple building blocks of complex networks. *Science,* 298**,** 824-827.

Mirończuk-Chodakowska, I., Witkowska, A. M. & Zujko, M. E. 2018. Endogenous non-enzymatic antioxidants in the human body. *Advances in Medical Sciences,* 63**,** 68-78.

Mooney, K. M., Morgan, A. E. & Mc Auley, M. T. 2016. Aging and computational systems biology. *Wiley Interdisciplinary Reviews: Systems Biology and Medicine,* 8**,** 123-139.

Neha, K., Haider, M. R., Pathak, A. & Yar, M. S. 2019. Medicinal prospects of antioxidants: A review. *European Journal of Medicinal Chemistry,* 178**,** 687-704.

Nimse, S. B. & Pal, D. 2015. Free radicals, natural antioxidants, and their reaction mechanisms. *RSC Advances,* 5**,** 27986-28006.

Olivier, B. G., Rohwer, J. M. & Hofmeyr, J.-H. S. 2005. Modelling cellular systems with PySCeS. *Bioinformatics,* 21**,** 560-561.

Onukwufor, J. O., Berry, B. J. & Wojtovich, A. P. 2019. Physiologic implications of reactive oxygen species production by mitochondrial complex I reverse electron transport. *Antioxidants,* 8**,** 285.

Padayachee, L., Rohwer, J. M. & Pillay, C. S. 2020. The thioredoxin redox potential and redox charge are surrogate measures for flux in the thioredoxin system. *Archives of Biochemistry and Biophysics,* 680**,** 108231.

Panth, N., Paudel, K. R. & Parajuli, K. 2016. Reactive oxygen species: a key hallmark of cardiovascular disease. *Advances in medicine,* 2016.

Papadakis, M. A. & Workman, C. T. 2015. Oxidative stress response pathways: Fission yeast as archetype. *Critical Reviews in Microbiology,* 41**,** 520-535.

Paulo, E., García-Santamarina, S., Calvo, I. A., Carmona, M., Boronat, S., Domènech, A., Ayté, J. & Hidalgo, E. 2014. A genetic approach to study H 2 O 2 scavenging in fission yeast–distinct roles of peroxiredoxin and catalase. *Molecular Microbiology,* 92**,** 246-257.

Petersen, J. & Russell, P. 2016. Growth and the environment of *Schizosaccharomyces pombe*. *Cold Spring Harbor Protocols,* 2016**,** pdb. top079764.

Phaniendra, A., Jestadi, D. B. & Periyasamy, L. 2015. Free radicals: properties, sources, targets, and their implication in various diseases. *Indian Journal of Clinical Biochemistry,* 30**,** 11-26.

Pillai-Kastoori, L., Heaton, S., Shiflett, S. D., Roberts, A. C., Solache, A. & Schutz-Geschwender, A. R. 2020. Antibody validation for Western blot: by the user, for the user. *Journal of Biological Chemistry,* 295**,** 926-939.

Pillay, C. S., Eagling, B. D., Driscoll, S. R. & Rohwer, J. M. 2016. Quantitative measures for redox signaling. *Free Radical Biology and Medicine,* 96**,** 290-303.

Pillay, C. S., Hofmeyr, J.-H., Mashamaite, L. N. & Rohwer, J. M. 2013. From top-down to bottom-up: computational modeling approaches for cellular redoxin networks. *Antioxidants & Redox Signaling,* 18**,** 2075-2086.

Pillay, C. S., Hofmeyr, J.-H. S., Olivier, B. G., Snoep, J. L. & Rohwer, J. M. 2009. Enzymes or redox couples? The kinetics of thioredoxin and glutaredoxin reactions in a systems biology context. *Biochemical Journal,* 417**,** 269-277.

Pisoschi, A. M. & Pop, A. 2015. The role of antioxidants in the chemistry of oxidative stress: A review. *European Journal of Medicinal Chemistry,* 97**,** 55-74.

Pronk, T. E., Van Der Veen, J. W., Vandebriel, R. J., Van Loveren, H., De Vink, E. P. & Pennings, J. L. 2014. Comparison of the molecular topologies of stress-activated transcription

factors HSF1, AP-1, NRF2, and NF-κB in their induction kinetics of HMOX1. *Biosystems,* 124**,** 75-85.

Rhee, S. G. 2016. Overview on peroxiredoxin. *Molecules and Cells,* 39**,** 1.

Rhee, S. G. & Woo, H. A. 2020. Multiple functions of 2-Cys peroxiredoxins, I and II, and their regulations via post-translational modifications. *Free Radical Biology and Medicine,* 152**,** 107-115.

Roy, J., Galano, J.-M., Durand, T., Le Guennec, J.-Y. & Lee, J. C.-Y. 2017. Physiological role of reactive oxygen species as promoters of natural defenses. *The FASEB Journal,* 31**,** 3729-3745.

Sander, H., Wallace, S., Plouse, R., Tiwari, S. & Gomes, A. V. 2019. Ponceau S waste: Ponceau S staining for total protein normalization. *Analytical Biochemistry,* 575**,** 44-53.

Shen-Orr, S. S., Milo, R., Mangan, S. & Alon, U. 2002. Network motifs in the transcriptional regulation network of *Escherichia coli*. *Nature Genetics,* 31**,** 64.

Sies, H. & Jones, D. P. 2020. Reactive oxygen species (ROS) as pleiotropic physiological signalling agents. *Nature Reviews Molecular Cell Biology,* 21**,** 363-383.

Smith, G. R. & Shanley, D. P. 2013. Computational modelling of the regulation of Insulin signalling by oxidative stress. *BMC Systems Siology,* 7**,** 1-19.

Song, J.-Y. & Roe, J.-H. 2008. The role and regulation of Trxl, a cytosolic thioredoxin in *Schizosaccharomyces pombe*. *The Journal of Microbiology,* 46**,** 408-414.

Tachibana, T., Okazaki, S., Murayama, A., Naganuma, A., Nomoto, A. & Kuge, S. 2009. A major peroxiredoxin-induced activation of Yap1 transcription factor is mediated by reduction-sensitive disulfide bonds and reveals a low level of transcriptional activation. *Journal of Biological Chemistry,* 284**,** 4464-4472.

Tomalin, L. E., Day, A. M., Underwood, Z. E., Smith, G. R., Dalle Pezze, P., Rallis, C., Patel, W., Dickinson, B. C., Bähler, J. & Brewer, T. F. 2016. Increasing extracellular H2O2 produces a bi-phasic response in intracellular H2O2, with peroxiredoxin hyperoxidation only triggered once the cellular H_2O_2-buffering capacity is overwhelmed. *Free Radical Biology and Medicine,* 95**,** 333-348.

Toone, W. M., Kuge, S., Samuels, M., Morgan, B. A., Toda, T. & Jones, N. 1998. Regulation of the fission yeast transcription factor Pap1 by oxidative stress: requirement for the nuclear export factor Crm1 (Exportin) and the stress-activated MAP kinase Sty1/Spc1. *Genes & Development,* 12**,** 1453-1463.

Veal, E. A., Tomalin, L. E., Morgan, B. A. & Day, A. M. 2014. The fission yeast *Schizosaccharomyces pombe* as a model to understand how peroxiredoxins influence cell responses to hydrogen peroxide. Portland Press Limited.

Veal, E. A., Toone, W. M., Jones, N. & Morgan, B. A. 2002. Distinct roles for glutathione S-transferases in the oxidative stress response in *Schizosaccharomyces pombe*. *Journal of Biological Chemistry,* 277**,** 35523-35531.

Veal, E. A., Underwood, Z. E., Tomalin, L. E., Morgan, B. A. & Pillay, C. S. 2018. Hyperoxidation of peroxiredoxins: gain or loss of function? *Antioxidants & Redox Signaling,* 28**,** 574-590.

Vivancos, A. P., Castillo, E. A., Biteau, B., Nicot, C., Ayté, J., Toledano, M. B. & Hidalgo, E. 2005. A cysteine-sulfinic acid in peroxiredoxin regulates H_2O_2-sensing by the antioxidant Pap1 pathway. *Proceedings of the National Academy of Sciences,* 102**,** 8875-8880.

Vivancos, A. P., Castillo, E. A., Jones, N., Ayté, J. & Hidalgo, E. 2004. Activation of the redox sensor Pap1 by hydrogen peroxide requires modulation of the intracellular oxidant concentration. *Molecular Microbiology,* 52**,** 1427-1435.

Vivancos, A. P., Jara, M., Zuin, A., Sansó, M. & Hidalgo, E. 2006. Oxidative stress in Schizosaccharomyces pombe: different H_2O_2 levels, different response pathways. *Molecular Genetics and Genomics,* 276**,** 495-502.

Warner, H. V., Sivakumar, N., Peirce, S. M. & Lazzara, M. J. 2019. Multiscale computational models of cancer. *Current Opinion in Biomedical Engineering,* 11**,** 137-144.

Williams, R. A., Timmis, J. & Qwarnstrom, E. E. 2014. Computational models of the NF-KB signalling pathway. *Computation,* 2**,** 131-158.

Yarosz, E. L. & Chang, C.-H. 2018. The role of reactive oxygen species in regulating T cell-mediated immunity and disease. *Immune Network,* 18.

Zheng, M., Åslund, F. & Storz, G. 1998. Activation of the OxyR transcription factor by reversible disulfide bond formation. *Science,* 279**,** 1718-1722.

Zuo, L., Zhou, T., Pannell, B., Ziegler, A. & Best, T. M. 2015. Biological and physiological role of reactive oxygen species–the good, the bad and the ugly. *Acta Physiologica,* 214**,** 329-348.

Appendix

Appendices can be found at: https://github.com/Chepillay/Kelisa_MSc